Università degli Studi di Padova

Facoltà di Ingegneria

Corso di Dottorato in Ingegneria Dell'Informazione

A Stochastic Geometry approach towards Green Communications in 5G

Dottorando

Atieh Rajabi Khamesi

Supervisore

Prof. Michele Zorzi

Anno Accademico 2017/2018

To my parents,
for their endless love, support and encouragement.

"Inside you there's an artist you don't know about."

-Jalaluddin Rumi

Acknowledgment

First and foremost, I would like to express my sincere gratitude to my advisor Prof. Michele Zorzi for the continuous support of my Ph.D study and life in general, for his patience, understanding, and immense knowledge. His guidance helped me during the time of the research and writing this thesis.

My sincere thanks also goes to Dr. Harpreet S. Dhillon, who provided me with the opportunity to join his research group as a visiting scholar at the Bradley Department of Electrical and Computer Engineering, Virginia Tech, Blacksburg, VA, USA. Without his precious support it would not be possible to make this opportunity happen.

In addition, I would like to express my gratitude to the rest of the thesis committee, specially my thesis evaluators, Dr. Marco Di Renzo and Dr. Harpreet S. Dhillon for their insightful comments and encouragement.

A special thanks to my family, my parents, Mehdi and Narges, my brothers, Ehsan and Amir, and sisters-in-law, Leili and Nasim, for supporting me spiritually throughout writing this thesis and my life in general. I am grateful to all of my friends and fellow labmates with whom I have had pleasurable experience of living and working in Italy and United States. Most importantly, I wish to thank my loving and supportive soulmate , Mohammad, for enlightening my way and his unending inspiration.

This thesis has been financially supported by CARIPARO foundation.

Contents

Abstract

In this dissertation, we investigate two main research directions towards network efficiency and green communications in heterogeneous cellular networks (HetNets) as a promising network structure for the fifth generation of mobile systems. In order to analyze the networks, we use a powerful mathematical tool, named stochastic geometry. In our research, first we study the performance of MIMO technology in single-tier and two-tier HetNets. In this work, we apply a more realistic network model in which the correlation between tiers is taken into account. Comparing the obtained results with the commonly used model shows performance enhancement and greater efficiencies in cellular networks. As the second part of our research, we apply two Cell Zooming (CZ) techniques to HetNets. With focus on green communications, we present a $K-$tier HetNet in which BSs are only powered by energy harvesting. Despite the uncertain nature of energy arrivals, combining two CZ techniques, namely telescopic and ON/OFF scenarios, enables us to achieve higher network performance in terms of the coverage and blocking probabilities while reducing the total power consumption and increasing the energy and spectral efficiencies.

Chapter 1

Introduction

By evolving cellular communication technologies from the analog telecommunications standards in 1G to digital telecommunications and very first steps taken towards data services by introducing Short Message Service (SMS) in 2G Global System for Mobile (GSM), we reached the age of smartphones and 3G Universal Mobile Telecommunication System (UMTS) where real-time video calls can be supported due to higher network bandwidth.

Thereafter, mobile broadband internet access and cloud computing have been supported by 4G Long Term Evolution-Advanced (LTE-A) systems in order to address increasing demand of cellular networks for high data rates and mobility. More recently, the fifth generation of mobile communication systems, 5G, has been introduced to provide more bandwidth and lower latency than previous generations.

Moreover, 5G has emerged not only to enhance the current system performance but also to introduce several new features to the realm of cellular communications [1, 2]. Table 1.1 gives a list of 5G requirements.

On one hand, improving the performance of current systems is always an important motivation to move forward to the new mobile generation while on the other hand, 5G is also expected to introduce several new features. For instance, Internet of Things (IoT) and Machine-to-Machine (M2M) communications which are among the most promising aspects of 5G.

Different methods and technologies have been proposed for 5G in the literature, for example Heterogeneous Networks (HetNet), millimeter-wave (mmWave) and Massive Multiple-Input Multiple-Output (M-MIMO). In Subsection 1.2, we will briefly introduce the proposed methods.

5G requirements and also achievement of new features need to be fulfilled in an affordable and sustainable way. Therefore, considerations regarding the power and energy consumption in 5G are of particular importance from both economic and environmental points of view. Specifically, the abundant number of connected devices expected in 5G has made energy a main concern.

In this chapter, first we will explain our motivations toward this topic. Then, we will summarize the existing works in this area. Presenting the research methodology and providing a list of our contributions and achievements will conclude this chapter.

Table 1.1: 5G Requirements [1].

Requirements	Desired value	Application example
Data rate	1 to 10 Gb/s	Virtual reality office
Data volume	9 Gbytes/h in busy period 500 Gbytes/mo/subscriber	Stadium Dense urban information society
Latency	Less than 5 ms	Traffic efficiency and safety
Battery life	One decade	Massive deployment of sensors and actuators
Connected devices	300,000 devices per AP	Massive deployment of sensors and actuators
Reliability	99.999%	Teleprotection in smart grid network Traffic efficiency and safety

1.1 Motivations

Along with worldwide efforts toward reducing the use of fossil fuels and controlling the emission of carbon dioxide to the atmosphere, the communications community has established a way both in academia and industry to address this issue known as green communications.

The importance of studying green communications comes from at least two main perspectives, namely economic and environmental. On one hand, increasing energy consumption of mobile networks along with the worldwide rise in energy cost, increases the operator expenditure severely. On the other hand, environmental concerns regarding the increase of carbon dioxide level in the atmosphere and its consequent effects on global weather and human health, encourage both academia and industry counterparts to investigate energy efficient methods in information and communication technology (ICT) platforms.

In particular, based on the expected perspectives for 5G, including HetNets, massive MIMO (M-MIMO), D2D, IoT, etc., energy consumption in this system would be inevitably high [3] and therefore it justifies the significance of studying Energy Efficiency (EE) and Spectral Efficiency (SE) in 5G scenarios.

Understanding the performance of the cellular systems requires proper modeling which is at the same time accurate and easy to work with. Modeling HetNets based on independent Poisson Point Processes (PPPs) has been widely used in the literature, however this model fails to capture spatial correlation and inherent repulsion between the network's nodes. Thus, we focus on a more accurate model following Poisson Hole Process (PHP) in a part of our research.

Although numerous advantages of MIMO systems, like spatial diversity and higher data rates, have been proved so far, EE of MIMO systems still needs to be investigated carefully through different network scenarios because of the circuit energy consumption of these systems which is more than Single-Input Single-Output (SISO) systems due to the use of multiple RF chains and requirements for more signal processing.

It is worth mentioning that, following the Shannon capacity bounds and due to the drastic data rate requirements in 5G, the power consumption in the future networks will inevitably grow [3] since the EE methods only based on spectrally efficient technologies are not enough. Therefore, designing a network based on harvesting energy from renewable resources is promising in 5G [4].

Although it has been shown that in current cellular networks about 80% of Base Stations (BSs) work below their estimated peak traffic in 80% of their lifetime, they still consume almost the same as their peak energy because of the energy consumption related to cooling and power amplifying circuits [5–7]. Therefore, the idea of turning off some BSs and offloading the traffic to the neighbor ones, especially in ultra-dense networks, can cause significant energy saving while keeping the quality-of-service (QoS) at an acceptable level. To this aim, the concept of Cell Zooming (CZ) has been introduced which aims to adjust the BSs coverage area and define working modes (ON/OFF) for BSs in the network.

Consequently, in this dissertation, we investigate Energy Efficiency (EE) and Spectral Efficiency (SE) in random cellular networks. To this end, we study two techniques, namely Multiple-Input Multiple-Output (MIMO) and Cell Zooming (CZ), and evaluate their performance and efficiencies in random cellular networks with focus on green 5G. In the next subsection, we will briefly review the related works.

1.2 Literature review

As mentioned earlier in this chapter, 5G is supposed to support up to 1000 times capacity increase, less than 5 ms round-trip latency and at least 100 billion connected devices around the world [8]. As an exciting example, we can mention Tactile Internet which has been expected to establish through 5G. In particular, Tactile Internet (also known as Haptic communications) aims to deliver physical haptic experiences remotely [9]. To this aim, 5G needs to support ultra-low latency communications, ultra-responsive and ultra-reliable network connectivity.

Several paradigms have been proposed to address these stringent requirements, such as mmWave communications, ultra-dense networks (UDNs), D2D communications and M-MIMO. Note that gaining from these techniques is mostly at the cost of complex signal processing and high power consumption. Therefore, it is necessary to design a green 5G network which is energy-efficient without sacrificing the QoS. In this regard, [3] provides an overview on both green 5G techniques and energy harvesting for communication.

In order to support rapidly increasing traffic load and capacity demand, HetNets have been introduced as a promising network architecture. Depend on the path-loss model, shortening the distance between the transmitter and receiver by dense and random deployment of low power small cells is the key to increase network capacity.

Mathematical analysis of large-scale wireless networks using Stochastic Geometry as a powerful tool to model and study random structure networks has attracted extensive attention in recent years [10]. In particular, [11, 12] introduce a general framework for downlink analysis of K-tier HetNets. The key assumption in these networks is to model the BS locations belonging to different tiers as independent Poisson Point Processes (PPPs). Moreover, transmit power, spatial density of BS deployment, supported data rate, etc., vary across the tiers. Leveraging the independent PPP assumption, closed-form expressions of the outage probability and the ergodic data rate have been derived.

Due to the analytical tractability of independent PPP distributed BSs, the majority of the HetNet works use this model, called Homogeneous Independent PPP (HIP) [11–15].

Although modeling the cellular network as a HIP is suitable in terms of the random placing of the network elements and gives tractable first-order results, it underestimates the performance of the actual deployment of cellular network [13]. As a matter of fact, in practical network deployments, the locations of the BSs are determined in a way to avoid close proximity and thus intense interference.

Accordingly, several studies have focused on modeling the cellular networks considering the correlation between the nodes. For example, [16] studied Ginibre point process (GPP) which is a repulsive point process. Besides, downlink performance of cellular networks, where BSs are located following Determinantal Point Processes (DPPs), has been investigated in [17].

Recently, Poisson Hole Process (PHP) have received a lot of attention in order to accurately model interference field in wireless networks, such as cognitive radio networks [18], HetNets [19], and D2D communications [20,21].

As a fundamental work on the characterization of PHP, [22] developed upper and lower bounds on the Laplace transform of interference experienced by a typical node in the PHP. Besides, the contact distance in the PHP has been investigated in [23].

Although PHP is a generalization of well-known and well-studied PPP, dealing with this process is not straightforward. Thus, some techniques have been used in the literature to analyze PHP-based wireless networks.

One approach is to approximate the PHP by a homogeneous PPP with the same density [10]. In another technique, PHP is approximated by its baseline PPP, i.e., the holes are overlooked [18, 24].

Note that each type of PHP approximations is suitable to analyze specific network parameters accurately while it might be imprecise for other metrics [22]. For example, in [19], the outage performance, the per-user capacity, and the area spectral efficiency for HetNets have been derived while authors proposed a PCP approximation of PHP by matching the first and second

order statistics. Moreover, in [22], tighter upper and lower bounds for the Laplace transform of aggregate interference experienced by the typical node in the PHP have been derived.

Almost all prior works on PHP focused on modeling and characterization of PHP in the context of simple wireless networks. However, we apply PHP model in a MIMO HetNet and study its performance in terms of energy and spectral efficiencies. We compare this model with the commonly used HIP network to highlight the effect of interference management achieved by using PHP. In a recent work, [25] studied the performance of M-MIMO in HetNets while approximating the PHP with its baseline PPP to avoid complexity.

Power saving in cellular networks has been considered in several works previously. However, most of these works only focused on managing high-power BSs, called Macro BSs (MBSs) in conventional hexagonal-shape cellular networks.

As a primary work, [26] introduced the concept of CZ in carefully planned conventional cellular networks where the power consumption of MBSs reduce by adjusting the cell size according to the network parameters, such as traffic load, channel conditions and required QoS. Furthermore, in [27] the authors considered energy saving in the planning phase of cellular networks using the CZ technique. More recently, [28] used a game theoretic approach to optimize the cell coverage based on reduction of area power consumption in the heterogeneous ultra-dense network.

It was shown that under low traffic scenario, reducing the number of active MBSs energy savings in the order of $25 - 30\%$ are achievable [29]. Besides, BS sleeping mode has been introduced as an intermediate level between on and off in order to save energy in cellular networks [30].

In another work, authors in [31] jointly applied stochastic geometry and the Dynamic Programming technique to design dynamic BS active operation. Moreover, several BS on/off algorithms were proposed [32–35].

However, all these studies are different from what we have done in our work in terms of system models, objective functions and/or approaches to solve their problems. Specifically, they mostly focused on energy saving through managing high-power BS tier, Macro tier, and neglected the impact of the other lower power BS tiers on the total power consumption of the HetNets [5]. Note that due to dense deployment of small cells in HetNets, aggregate power consumption of the lower power BS tiers can even exceed the Macro tier.

Promising development of Energy Harvesting (EH) techniques and efficiency along with the low power consumption of small cells in HetNets provide the opportunity of using self-powered small cell BSs with EH. There exist several practical wireless systems which use EH, for instance the Huawei Green Base Station [36].

Although using renewable energy resources, like solar, wind, and kinetic activities, is environmental friendly and also an economical way to prolong the network lifetime and improve the energy efficiency of the system [37, 38], the uncertain and intermittent nature of the energy arrivals brings significant challenges for the system design.

Optimal power allocation in EH systems has been studied under different channel models [39–41]. The impact of the energy arrival rates on the coverage probability have been examined for $K-$tier EH HetNets using stochastic geometry [42]. Downlink analysis of a HetNet with both on-grid and EH BSs has been analyzed in [43].

However, there exist several works on wireless-powered communication, for example [44–49]. Since we focus on green communications, we only consider harvesting energy from renewable resources in our work.

1.3 Methodology

In order to study and analyze the system models adopted in our research, we mainly use two mathematical tools, namely stochastic geometry and Markov Chain (MC).

In recent decades, cellular networks are moving from hexagonal shape cellular networks with high power base stations (BSs), called Macro BSs, to heterogeneous networks that consist of an irregular deployment of BSs overlaid by low power BSs, like Pico and Femto cells. Traditionally, cellular networks have been modeled as the BSs placed on a grid, with mobile users either randomly scattered or located at fixed distances. Although these models have been used extensively, they suffer from some shortages. First, these models are highly idealized and can not capture the characteristics of randomly structured networks. Secondly, the obtained results based on these models are not very tractable, so they mostly rely on complex system-level simulations in order to evaluate coverage/outage probability and rate.

Stochastic geometry gives an approach to define and compute macroscopic properties of randomly structured networks, by averaging over all potential geometrical patterns for the nodes. In this method, the locations of the network components, like BSs, mobile users, relays, etc., are considered as the realizations of some point processes. Accordingly, in the case that the underlying random model is ergodic, the probabilistic analysis also provides a tractable way to estimate spatial averages as functions of a relatively small number of parameters, such as densities of the point processes and other network parameters [50].

On the other hand, wireless networks are fundamentally dealing with the intensity of the desired signal and interference which both depend on the spatial location of the nodes [51]. Accordingly, stochastic geometry enables us to derive communication-theoretic results on the connectivity, the capacity, the outage probability, and other fundamental limits of wireless networks. The authors in [51] and [52] provide the tutorials on stochastic geometry and the theory of random geometric graphs with focus on wireless and cellular networks, respectively.

In this work, since we adopt different point processes, in each chapter first we introduce the system model and then provide the necessary terms and theorems regarding the stochastic geometry techniques used.

As mentioned earlier in this subsection, Markov Chain is the second mathematical tool used in our work. The setting for this model is almost the same

for all system models, so here we present it in detail.

Along the lines of [53], without loss of generality, we focus on a typical cell in the cellular network for MC based modeling and performance analysis. First we assume that the call arrivals to the system follow a Poisson process with rate λ. Furthermore, the channel holding time $\mathbb{T}_H$ is assumed to be the minimum of the user session duration, $\mathbb{T}_S$, and the cell dwelling time, $\mathbb{T}_D$, which is defined as time that the mobile user spends in a cell [54]. Both $\mathbb{T}_S$ and $\mathbb{T}_D$ are random variables with exponential distributions with mean ϑ and $1/T_D$ respectively. Cell dwelling is . Thus we have $\mathbb{T}_H = \min(\mathbb{T}_S, \mathbb{T}_D)$, with mean $\eta = \vartheta + 1/T_D$.

In order to represent the transitions between the available channels and the unavailable channels a continuous Gilbert-Elliott channel model is adopted. Based on definition, a channel is unavailable when its downlink SINR value is less than a predefined threshold. Assume that the number of available channels per BS is determined as the difference of the total number of channels and the number of unavailable channels in a cell. Besides, let the transition rate from the unavailable to the available channel be indicated by α and the transition rate from the available channel to the unavailable one be represented as β.

To denote the states in the MC model, a pair of nonnegative integers (m, n) is used, where m is the number of occupied channels and n is the total number of channels available to be allocated for users in the typical cell, including the channels that have already been allocated (i.e., occupied). Moreover, we define C as the maximum number of available channels in the typical cell. Therefore, we have $m \leq n \leq C$. Fig. 1.1 depicts the Markov Chain transition diagram.

The MC state transitions in Fig. 1.1 are given as follows:

1. $(m, n) \rightarrow (m+1, n)$: By arriving a new call, if there exists a free channel, i.e., $m < n$, the number of occupied channels increments by 1.

2. $(m, n) \rightarrow (m-1, n)$: By terminating a call served successfully, the number of occupied channels decrements by 1.

3. $(m, n) \rightarrow (m, n+1)$: By turning an unavailable channel to an available one, which can be allocated to mobile users, because of the time-varying nature of interference, the number of available channels increments by 1.

4. $(m, n) \rightarrow (m, n-1)$: By turning an available channel to an unavailable one, which can not be allocated to mobile users, because of the time-varying nature of interference, the number of available channels decrements by 1.

A Markov process is reversible and its stationary state distribution exists if its transition rates satisfy [55]

$$\begin{aligned}\Lambda(S_1, S_2) \cdot \Lambda(S_2, S_3) \cdot \ldots \cdot \Lambda(S_{u-1}, S_u) \cdot \Lambda(S_u, S_1) \\ = \Lambda(S_1, S_u) \cdot \Lambda(S_u, S_{u-1}) \cdot \ldots \cdot \Lambda(S_3, S_2) \cdot \Lambda(S_2, S_1)\end{aligned} \tag{1.1}$$

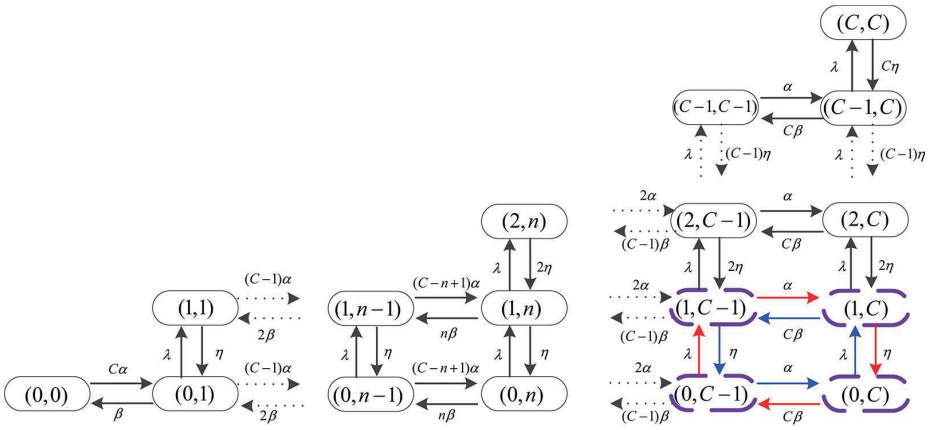

Figure 1.1: Markov chain transition diagram [53]

for any finite sequence of states $S_1, S_2, \ldots, S_u \in \Xi$, where Ξ is the set of all possible states in this Markov process and $\Lambda(S_h, S_k)$ denotes the transition rate from state S_h to state S_k. It can be shown that states in Fig. 1.1 meet Eq. (1.1) Thus, there exists a stationary state distribution.

Fig. 1.1 provides a four-state interpretation of Eq. (1.1) with purple dash line. The left and right side of Eq. (1.1) are shown by the red arrows and blue arrows, respectively. In this way, the product term on the left side of Eq. (1.1) is $\alpha \cdot \eta \cdot C\beta \cdot \lambda$ and $\eta \cdot \alpha\lambda \cdot C\beta$ on the right side. Obviously, these two terms are equal. In a similar way, we can show that Eq. (1.1) holds for any finite number of states in Fig. 1.1.

Moreover, leveraging queuing theory, the stationary state probabilities are given by [53]

$$\pi(m,n) = \frac{1}{\chi}\left(\frac{\lambda}{\eta}\right)^m \frac{1}{m!}\binom{C}{n}\left(\frac{\alpha}{\beta}\right)^n, \tag{1.2}$$

where $\binom{C}{n}$ is the binomial coefficient and gives the number of ways to pick n available channels out of C, maximum number of available ones. To compute the stationary state probabilities, given in Eq. (1.2), the ratio of α over β is required. To find this term, we use the Gilbert-Elliott channel model in which the probability of a channel being unavailable, ϵ, is

$$\epsilon = \frac{\beta}{\alpha + \beta}. \tag{1.3}$$

With a simple manipulation, we have $\frac{\alpha}{\beta} = \frac{(1-\epsilon)}{\epsilon}$.

As mentioned, a channel is unavailable when its downlink SINR value is less than a predefined threshold, therefore ϵ can be interpreted as outage probability, $\mathbb{P}_{\text{out}}$. In the following, with respect to the system model adopted in each chapter, we derive the coverage probability, $\mathbb{P}_{\text{cov}}$, which is the complement of the outage probability i.e., $\mathbb{P}_{\text{cov}} = 1 - \mathbb{P}_{\text{out}}$. We also use the stationary state probability to obtain the blocking probability, and the spatial and energy efficiencies.

1.4 Contributions and main achievements

In this dissertation, we conduct our research in two directions towards green communications in 5G.

First, we study MIMO technology in HetNets. We start with a single tier scenario, called PVT random cellular networks. In this work, we

- study the performance of MIMO in PVT random cellular networks;
- derive the coverage probability and ergodic capacity using stochastic geometry;
- investigate the blocking probability, EE and SSE using MC model;
- highlight the effect of path-loss exponent on noisy and noise-free scenarios;
- compare the obtained results with the SISO scenario under equal sum power constraints.

In this work, we show the effect of path-loss exponent on the coverage and blocking probabilities as well as SSE and EE which implies that a PVT random cellular network with multiple antennas is more sensitive to interference than to noise. We also present the advantage of MIMO systems over SISO scenario in terms of EE and SSE.

Further, we extend our work to a MIMO HetNet scenario. Inspired by the results of the previous work, i.e., higher sensitivity to interference than to noise, unlike most works on HetNets, the dependency between BSs tiers is taken into account. Instead of independently deploying the small cells, we consider an exclusion region around each high power BS and impose the small cells to be active only outside these regions. Therefore, PBS locations form a Poisson Hole Process (PHP). Accordingly, we

- apply more accurate model to study interference field in HetNets, which captures the dependency among tiers;
- derive the the probability density function of the nearest distance to the PHP;
- provide an expression for the ergodic capacity in terms of Laplace transforms of the signal and interference powers;
- investigate the performance of the network and comparison between PHP and HIP in terms of coverage probability, EE and SSE;
- show the tightness of the proposed bounds for different model parameters.
- highlight the EE and SSE improvement in PHP compare to the HIP;

In this work, we show the advantage of using PHP to model HetNets. In particular, considering exclusion region around high power BSs and deployment of the small cells outside these regions improve the performance of the HetNets, such as EE and SSE.

In the second research direction, we study Cell Zooming (CZ) in random cellular networks. To the best of our knowledge, previously, CZ has only been applied in some structured patterns mostly in conventional hexagonal shape cellular networks. We show that CZ can be a viable solution towards green communications in random cellular networks for 5G.

Similar to previous research direction, we start with a simple network model i.e., PVT random cellular networks. We investigate the network performance and the tradeoff between network parameters. In this work, we

- study two CZ techniques in PVT random cellular networks;
- investigate the effect of coverage adjustment and independent thinning process on EE and ASE;
- derive the ergodic capacity per user in PVT random cellular networks;
- investigate the tradeoff between EE and ASE and propose a working region for the network accordingly.

Thereafter, we study a general model of $K-$tier HetNets and focus on green communications and in order to justify some assumptions taken in the previous part, we investigate a green HetNet in which the BSs are off-grid and only supplied by energy harvesting (EH) from renewable resources. In this work, we

- study the idea of drop and play BSs;
- consider the challenge of using EH in HetNets due to the uncertain and intermittent nature of the energy arrivals;
- combine two CZ techniques to improve network performance in terms of the coverage and blocking probabilities;
- compare the performance of EH CZ networks with the non-EH unbiased ones in terms of coverage and blocking probabilities, EE and SE.

Also, we have done some additional research in collaboration with the University of Tehran which is not exactly in the same direction as this dissertation, so we provide it as an appendix.

Chapter 2

Efficiencies in Random MIMO Cellular Networks

In this chapter which is the first technical part of our work, we investigate the performance of Multiple-Input Multiple-Output (MIMO) systems in random cellular networks in terms of Spatial Spectral Efficiency (SSE) and Energy Efficiency (EE). In this model, M-antenna Base Stations (BS) are randomly distributed in $\mathbb{R}^2$ following a Poisson Point Process (PPP). Each BS forms a cell in this Poisson-Voronoi Tessellation (PVT) random cellular network and serves K single-antenna Mobile Users (MUs). Firstly, we provide expressions for the coverage probability and the ergodic capacity using stochastic geometry techniques. Then, using the Markov Chain (MC) model described in Section 1.3, we derive the blocking probability, SSE and EE in this network. Simulation results reveal that a random network with multi-antenna nodes is more susceptible to interference than to noise. Although a higher path-loss exponent degrades the coverage probability in a noisy network, it results in better coverage probability in a noise-free scenario. Besides, our results show a higher SSE and EE of MIMO compared to Single-Input Single-Output (SISO), while an equal sum power constraint is considered at the BSs.

2.1 Introduction

The growth of data traffic demand in mobile communication systems has required to fundamentally re-think the cellular network structure in a totally different way from conventional hexagonal cells. In this scenario, the notion of abundant and almost random Base Station (BS) deployment in terms of micro and femto cells led to the paradigm of Heterogeneous Networks (HetNets) [56, 57]. In this respect, stochastic geometry provides powerful tools and techniques to study this sort of random structures [58].

Moreover, the benefits of MIMO systems over SISO systems have been proved in several aspects, such as Signal-to-Noise Ratio (SNR) enhancement, throughput gain and power saving [59].

Novel features in next generation mobile communication systems, like machine-to-machine (M2M) communications and ubiquitous high data-rate coverage, inevitably require abundant energy and thus massive quantities

of carbon footprint will be produced as a consequence. In this regard, the studies focused on Energy Efficiency (EE) become noteworthy not only to protect the environment but also to reduce the energy-related costs in the mobile communication industry.

A tractable approach toward random networks using stochastic geometry is proposed in [13]. Besides, [53] studied a Markov Chain (MC) channel access model in Poisson-Voronoi tessellation (PVT) random cellular networks. The coverage probability and the impact of channel estimation on the performance of random networks are studied in [60, 61]. Besides, [62] proposed an accurate expression for the uplink outage probability in independent Poisson fields of users and BSs. Note that all these works focused on SISO systems.

In addition, [63] proposed an approximation for the signal and interference power distributions in MIMO systems. The downlink ergodic capacity of the network with randomly distributed BSs cooperating in hexagonal-shape clusters was also derived. In another work, a multi-user spatial multiplexing cellular network was studied and compared with single stream transmission [64]. Besides, [11] introduced a general model for downlink MIMO HetNets and provided the ordering results for the coverage probability for the three considered techniques. Moreover, [65] proposed a tradeoff between the area spectral efficiency and link reliability in MIMO HetNets utilizing a Toeplitz matrix representation.

In this work, we investigate the EE and Spatial Spectral Efficiency (SSE) of a MIMO system in a PVT random cellular network with a MC channel access model. To this aim, the coverage and blocking probability expressions have been derived using stochastic geometry. The rest of the chapter is organized as follows. In Section 2.2, the MIMO system model with imperfect beamforming at the transmitter is introduced. Section 2.3 focuses on the MC transition model. The coverage and blocking probabilities are derived in Section 2.4. The EE and SSE formulation and the simulation results are provided in Sections 2.5 and 2.6, respectively. Finally, Section 2.7 concludes this chapter.

2.2 System Model

We consider a PVT random cellular network as depicted in Fig. 2.1. Assume that the BSs and Mobile Users (MUs) are distributed randomly based on two independent Poisson Point Processes (PPP), Φ_B and Φ_M, with density λ_B and λ_M, respectively.

In this model, every BS is equipped with M antennas, while the MUs are single antenna devices. Each BS serves K MUs in each time slot independently, with $K \leq M$.

Since our focus is on downlink transmission in this work, we perform our analysis for a typical mobile user in the network. We consider the nearest BS association scheme operated by the Control Center in the network. Thus we sort and label the BSs based on their distance to the typical MU. Taking advantage of PPP properties, without loss of generality, we assume that the

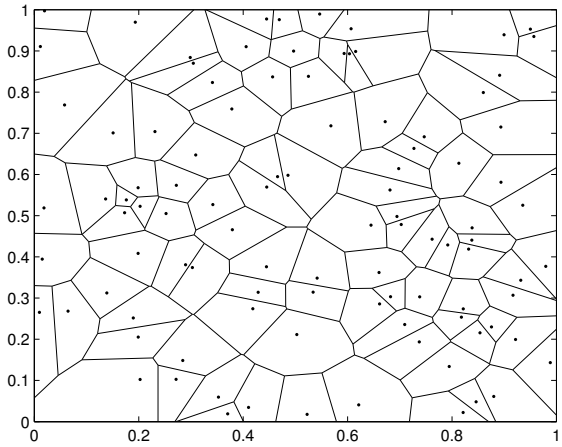

Figure 2.1: An example of PVT Random Cellular Network

typical MU is located at the origin and receives the desired data from BS_j which is the nearest BS to it.

The received signal of the typical user, MS_i, is given by

$$y_i = \mathbf{v}_i \mathbf{g}_{ij}^{\mathsf{H}} \mathbf{u}_j + \sum_{l \in \Phi_B \setminus \{j\}} \sum_{k=1}^{K} \mathbf{v}_i \mathbf{g}_{il}^{\mathsf{H}} \mathbf{u}_l + n, \tag{2.1}$$

where the second term is the aggregate inter-cell interference and $n \sim \mathcal{N}(0, \sigma^2)$ accounts for the noise at the receiver. Furthermore, $\mathbf{g}_{ij} = \sqrt{(1 + x_{ij}/D)^{-\alpha}}\mathbf{h}_{ij}$ is the channel vector between BS_j and MS_i, which captures the small-scale i.i.d. Rayleigh channel fading, $\mathbf{h}_{ij} \sim \mathcal{CN}(\mathbf{0}, \mathbf{1})$, and the non-singular path-loss model, $(1 + x_{ij}/D)^{-\alpha}$ [51, 63]. In this model, x_{ij} indicates the distance of MS_i to BS_j, D denotes a reference distance and $\alpha > 2$ is the path-loss exponent. Note that all the antennas of a specific BS suffer from equal path-loss attenuation. Additionally, $\mathbf{u}_j = \sum_{k=1}^{K} \mathbf{w}_{kj} \cdot m_{kj}$, is composed of the imperfect unit-norm beam alignment vectors, $\mathbf{w}_{kj}$, and the desired data for MS_i transmitted by BS_j. Moreover, $\mathbf{v}_i$ is the unit-norm receive filter at MS_i, which aims to compensate the imperfections of the transmitted beam alignment, so that $\mathbf{v}_i^{\mathsf{H}} \mathbf{g}_{ij} \perp \mathbf{w}_{kj}, \forall k \neq i$.

Note that there is a maximum power constraint P_T for each BS, which is equally divided among the transmitting antennas. Also, x_{ij} is a random variable due to the random locations of the BSs in the network.

2.3 Network Model

We apply the MC process introduced in Section 1.3 to model the transitions between channel states including available and unavailable channels in a typical cell in the PVT random cellular network. In reality, access to a channel to initiate a successful call depends on parameters like the call arrival rate, the maximum number of available channels, etc. As mentioned, in this MC

model, the network state is presented by an (m, n)-tuple in which m is the number of occupied channels and n is the total number of channels, including free and occupied ones.

We re-write Eq. (1.2) here as follows,

$$\pi(m,n) = \frac{1}{\chi}\left(\frac{\mu}{\eta}\right)^m \frac{1}{m!}\binom{C}{n}\left(\frac{1-\epsilon}{\epsilon}\right)^n, \tag{2.2}$$

where μ, η and C are the call arrival rate, the mean channel holding time and the total number of channels, respectively, and χ indicates the normalization factor. And ϵ denotes the probability of a channel being unavailable.

Analogous but complementary to the definition of the coverage probability [13], we assume a channel is "unavailable" if the Signal-to-Interference-plus-Noise Ratio (SINR) of this link falls below predefined threshold, γ. Therefore,

$$\epsilon = \mathbb{P}\left(\text{SINR} < \gamma\right). \tag{2.3}$$

Note that in some works, ϵ is also called the outage probability, which is the complement of the success probability. In the next section, first the SINR of a typical MU and the coverage probability will be derived, and then the blocking probability will be computed.

2.4 Coverage And Blocking Probabilities

Following Eq. (2.1) the SINR of the typical MU after intra-cell interference cancellation is given by

$$\text{SINR} = \frac{(1+r)^{-\alpha}|\mathbf{h}_{ij}^{\mathsf{H}}\mathbf{w}_{ij}|^2}{\sum_{l\in\Phi_B\setminus\{j\}}\sum_{k=1}^{K}|\mathbf{g}_{il}^{\mathsf{H}}\mathbf{w}_{kl}|^2 + K\sigma^2/P_T} \tag{2.4}$$

$$= \frac{(1+r)^{-\alpha}S}{\mathbf{I}(\Phi_B) + K\sigma^2/P_T}, \tag{2.5}$$

where, $\mathbf{I}(\Phi_B)$ is the aggregate inter-cell interference and r is the link length from the typical user, located at the origin, to the nearest BS $\in \Phi_B$ and has probability density function (PDF)

$$f_r(r) = 2\pi\lambda_B r e^{-\pi\lambda_B r^2}. \tag{2.6}$$

Therefore, the coverage probability can be derived along the lines of [13],

$$\mathbb{P}(\text{SINR} > \gamma) = \int_{r>0} 2\pi\lambda_B r e^{-\pi\lambda_B r^2} \cdot \mathbb{P}\left(S > \gamma(1+r)^{\alpha}\left(\mathbf{I}(\Phi_B) + \frac{K\sigma^2}{P_T}\right)\Big| r\right)\mathrm{d}r. \tag{2.7}$$

2.4.1 General Expression

Let $f_y(y)$ be the PDF of $\left(\mathbf{I}(\Phi_B) + \frac{K\sigma^2}{P_T}\right)$. Hence,

$$\begin{aligned}
&\mathbb{P}\left(\mathbf{I}(\Phi_B) + \frac{K\sigma^2}{P_T} < \frac{S}{\gamma(1+r)^{\alpha}}\Big| r\right) \\
&= \mathbb{E}_S\left[\int_0^{S\gamma^{-1}(1+r)^{-\alpha}} f_y(y)\mathrm{d}y\right] \\
&= \mathbb{E}_S\left[\int_{-\infty}^{+\infty} f_y(y)\mathbf{1}(0 \le y \le S\gamma^{-1}(1+r)^{-\alpha})\mathrm{d}y\right] \\
&\overset{(a)}{=} \mathbb{E}_S\left[\int_{-\infty}^{+\infty} e^{-2\pi\frac{K\sigma^2}{P_T}js}\mathcal{L}_{\mathbf{I}}(2\pi js)\right. \\
&\qquad\qquad \left.\cdot\frac{e^{2\pi S\gamma^{-1}(1+r)^{-\alpha}js}-1}{2\pi js}\mathrm{d}s\right] \\
&\overset{(b)}{=} \int_{-\infty}^{+\infty} e^{-2\pi\frac{K\sigma^2}{P_T}js}\mathcal{L}_{\mathbf{I}}(2\pi js) \\
&\qquad\qquad \cdot\frac{\mathcal{L}_S(-2\pi(\gamma(1+r)^{\alpha})js)-1}{2\pi js}\mathrm{d}s. \qquad (2.8)
\end{aligned}$$

where, $\mathbf{1}(\cdot)$ is the indicator function and $j = \sqrt{-1}$. Also, (a), (b) follow from the Plancheral-Parseval and Fubini theorems, respectively. $\mathcal{L}_{\mathbf{I}}(\cdot)$, $\mathcal{L}_S(\cdot)$ denote the Laplace transforms w.r.t. the interference and signal powers, respectively.

Based on the assumptions in Section 2.2 , since $|\mathbf{h}_{ij}|$ is drawn from a Rayleigh distribution and the MIMO beamforming space dimension is $(M - K + 1)$, it can be shown that the signal power follows from the Gamma distribution with the shape and scale parameters as $S \sim \Gamma(M-K+1, 1)$, and therefore we have

$$\mathcal{L}_S(s) = (1+s)^{-(M-K+1)}. \qquad (2.9)$$

Furthermore, [63] proves that

$$\mathbf{I}(\Phi_B) = \sum_{l\in\Phi_B\setminus\{j\}}\sum_{k=1}^{K}|\mathbf{g}_{il}^{\mathsf{H}}\mathbf{w}_{kl}|^2 \overset{d}{=} \sum_{l\in\Phi_B\setminus\{j\}}(1+x_l)^{-\alpha}Z_l, \qquad (2.10)$$

where, $Z_l \sim \Gamma(K, 1)$ and $(\overset{d}{=})$ stands for equality in distribution. Thus, the Laplace transform of the aggregate interference is given by

$$\begin{aligned}
\mathcal{L}_{\mathbf{I}}(s) &= \mathbb{E}_{\Phi_B,\mathbf{g}}\left[e^{-s\mathbf{I}(\Phi_B)}\right] \\
&= \mathbb{E}_{\Phi_B,Z_l}\left[e^{-s\sum_{l\in\Phi_B\setminus\{j\}}(1+x_l)^{-\alpha}Z_l}\right] \\
&\overset{(a)}{=} \mathbb{E}_{\Phi_B}\left[\prod_{l\in\Phi_B\setminus\{j\}}\mathbb{E}_{Z_l}\left[e^{-s(1+x_l)^{-\alpha}Z_l}\right]\right] \\
&= \mathbb{E}_{\Phi_B}\left[\prod_{l\in\Phi_B\setminus\{j\}}\left(1+s(1+x_l)^{-\alpha}\right)^{-K}\right]
\end{aligned}$$

$$\begin{aligned}
&\overset{(b)}{=} \exp\left\{-2\pi\lambda_B \int_r^{+\infty} \left(1-\left(1+s(1+x)^{-\alpha}\right)^{-K}\right) x \, \mathrm{d}x\right\} \\
&= \exp\left\{\pi\lambda_B(1+r)\cdot\left((r-1)\right.\right. \\
&\quad - (1+r)\,{}_2F_1\left(K, \frac{-2}{\alpha}; 1-\frac{2}{\alpha}; -s(1+r)^{-\alpha}\right) \\
&\quad \left.\left. + 2\,{}_2F_1\left(K, \frac{-1}{\alpha}; 1-\frac{1}{\alpha}; -s(1+r)^{-\alpha}\right)\right)\right\} \qquad (2.11)
\end{aligned}$$

where (a) comes from the independence of channel fading and PPP and (b) follows from the probability generating functional of PPP, Φ_B. Moreover, ${}_2F_1(a,b;c;d)$ is the Gaussian hypergeometric function.

2.4.2 Special Case: Fully Loaded Network

In case the network is fully loaded, i.e., $M = K$, we have the following lemma.

***Lemma* 1.** *The coverage probability in a fully loaded MIMO network is*

$$\begin{aligned}
\mathbb{P}(\mathrm{SINR} > \gamma) = &\int_{r>0} 2\pi\lambda_B r e^{-\pi\lambda_B r^2} \cdot e^{-\gamma(1+r)^\alpha \frac{K\sigma^2}{P_T}} \\
&\cdot \exp\left\{\pi\lambda_B(1+r)\cdot\left(r-1-(1+r)\right.\right. \\
&\quad \cdot\ {}_2F_1\left(K, \frac{-2}{\alpha}; 1-\frac{2}{\alpha}; -\gamma\right) \\
&\quad \left.\left. + 2\,{}_2F_1\left(K, \frac{-1}{\alpha}; 1-\frac{1}{\alpha}; -\gamma\right)\right)\right\} \mathrm{d}r. \qquad (2.12)
\end{aligned}$$

Proof. In a fully loaded network, $S \sim \mathrm{Exp}(1)$, and we have

$$\begin{aligned}
&\mathbb{P}\left(S > \gamma(1+r)^\alpha \left(\mathbf{I}(\Phi_B) + \frac{K\sigma^2}{P_T}\right) \middle| r\right) \\
&= \mathbb{E}_{\mathbf{I}}\left[\mathbb{P}\left(S > \gamma(1+r)^\alpha \left(\mathbf{I}(\Phi_B) + \frac{K\sigma^2}{P_T}\right) \middle| r, \mathbf{I}(\Phi_B)\right)\right] \\
&= \mathbb{E}_{\mathbf{I}}\left[\exp\left(-\gamma(1+r)^\alpha \left(\mathbf{I}(\Phi_B) + \frac{K\sigma^2}{P_T}\right)\right)\right]. \qquad (2.13)
\end{aligned}$$

By substituting Eq. (2.13) in Eq. (2.7),

$$\begin{aligned}
\mathbb{P}(\mathrm{SINR} > \gamma) = &\int_{r>0} 2\pi\lambda_B r e^{-\pi\lambda_B r^2} \\
&\cdot e^{-\gamma(1+r)^\alpha \frac{K\sigma^2}{P_T}} \mathcal{L}_{\mathbf{I}}\left(\gamma(1+r)^\alpha\right) \mathrm{d}r, \qquad (2.14)
\end{aligned}$$

where $\mathcal{L}_{\mathbf{I}}(\cdot)$ is given by Eq. (2.11). □

The result of the previous lemma is noteworthy as it results in greatly improved tractability and much shorter simulation time compared to conventional Monte-Carlo simulation.

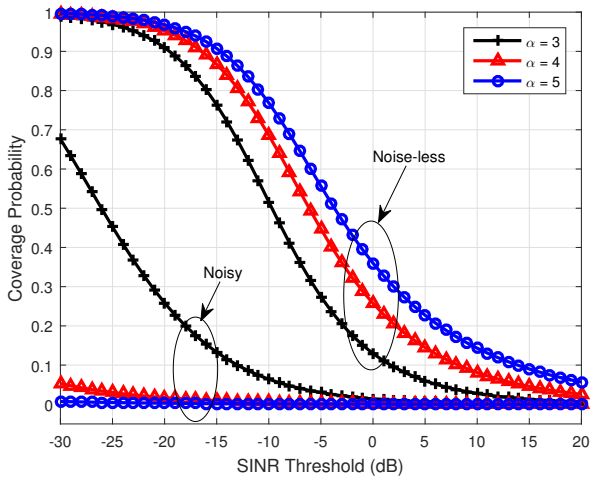

Figure 2.2: Effect of path-loss exponent on coverage probability in noisy and noise-less networks

In the following, we utilize the results obtained above to derive the blocking probability, which is the building block to compute SSE and EE.

By definition [53], a new call arrival will be blocked if all the available network resources in a typical cell are already occupied, which means that the number of active users is equal to the total number of available channels in the cell. Thus, the blocking probability is given by

$$p_{\mathrm{b}} = \sum_{m=n\leq C} \frac{1}{\chi} \left(\frac{\mu}{\eta}\right)^m \frac{1}{m!} \binom{C}{n} \left(\frac{a}{b}\right)^n \tag{2.15}$$

where

$$\frac{a}{b} = \frac{1-\epsilon}{\epsilon}. \tag{2.16}$$

and ϵ is given in Eq. (2.3).

2.5 SSE and EE

In this section, we aim to compute the Spatial Spectral Efficiency (SSE) and the Energy Efficiency (EE) in the system model described in Section 2.2. It is worth mentioning that based on Palm theory, to compute SSE and EE of the whole network, it is sufficient to find SSE and EE for a typical MU and BS, respectively, and then extend the results to the entire PVT random cellular network.

The throughput of any cell with bandwidth W is

$$T_c = (1-p_b)\cdot W \cdot C \cdot \sum_{0\leq m\leq n\leq C} m\cdot \pi(m,n), \tag{2.17}$$

where C is the Ergodic Capacity of a typical MU. Based on Eq. (2.17), cell throughput is a function of the blocking probability, the ergodic capacity and

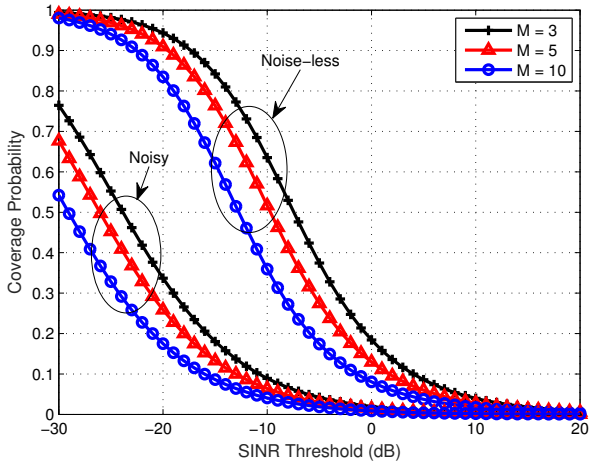

Figure 2.3: Coverage probability of MIMO systems with equal sum power constraint

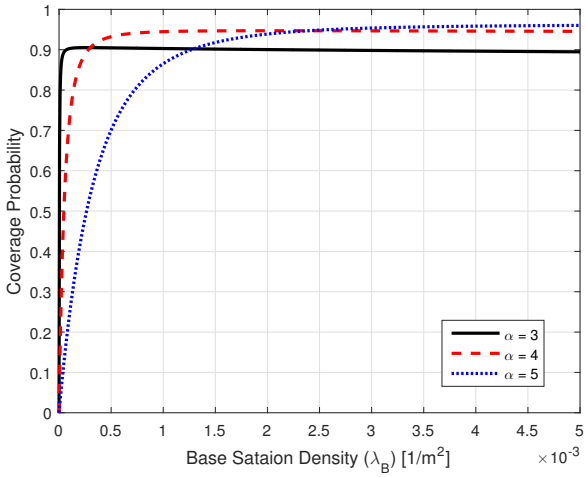

Figure 2.4: Coverage probability for $M = 5$ in a noisy network

the probability of finding an available channel. Accordingly,

$$C = \mathbb{E}\left[\log_2(1+\text{SINR})\right] = \int_0^{+\infty} \mathbb{P}\left(\log_2(1+\text{SINR}) > t\right)\mathrm{d}t$$
$$= \int_0^{+\infty} \mathbb{P}(\text{SINR} > 2^t - 1)\mathrm{d}t \tag{2.18}$$

which follows from positivity of SINR. Therefore, C can be simply obtained in general from Eq. (2.7), and in the special case of fully loaded network from Eq. (2.12). To compute SSE in a PVT random cellular network using cell throughput, we have

$$\text{SSE} = \lambda_B \cdot T_c \tag{2.19}$$
$$= (1-p_b)W\lambda_B \cdot \int_0^{+\infty} \mathbb{P}(\text{SINR} > 2^t - 1)\mathrm{d}t$$

$$\cdot \sum_{0\le m\le n\le C} m \cdot \pi(m,n) \tag{2.20}$$

Moreover, the Energy Efficiency is the total cell throughput, T_{LT}, divided by the lifetime energy consumption of a BS:

$$\mathrm{EE} = \frac{T_{LT}}{E_{LT}} \tag{2.21}$$

where E_{LT} consists of three main parts, namely the consumed energy in factories during the manufacturing phase, the required energy for maintenance and the transmission-related energy, denoted by E_1, E_2 and E_3, respectively. Thus,

$$E_3 = \left(h \cdot P_T \sum_{0\le m\le n\le C} m \cdot \pi(m,n) + k \right) \cdot t_{LT} \tag{2.22}$$

where t_{LT} represents the lifetime of the BS. Also, h and k are the scaling coefficients of the total transmission power, P_T.

Therefore, EE in Eq. (2.21) is given by

$$\mathrm{EE} = \frac{T_c \cdot t_{LT}}{E_1 + E_2 + (h \cdot P_{tr} \sum_{0\le m\le n\le C} m \cdot \pi(m,n) + k) \cdot t_{LT}}. \tag{2.23}$$

2.6 Performance Evaluation and Simulation Results

To investigate the performance of the MIMO scenario in a PVT random cellular network, in this section we provide some simulation results.

Figs. 2.2, 2.3 and 2.4 illustrate the coverage probability of a MIMO system in a fully loaded network. As expected, increasing the noise level degrades the coverage probability. We consider $\sigma^2 = -20$ dBm in our simulations. Moreover, Fig. 2.2 displays the effect of the path-loss exponent on coverage probability. Although α controls the interference level, a higher path-loss exponent degrades the coverage probability in a noisy network as it is multiplied by the noise power in the exponent of Eq. (2.12). On the other hand, in a noise-free scenario, increasing α improves the coverage probability, since it makes the interference decrease.

Fig. 2.3 illustrates the coverage probability in MIMO networks with different numbers of transmit antennas in each BS. With a fixed sum power constraint, P_T, for all types of the BSs, by increasing M, the transmission power of each antenna reduces and thus the coverage probability degrades. Besides, Fig. 2.4 depicts the coverage probability as a function of the BS density, λ_M, for different path-loss exponents. As shown, by increasing the BS density, the network becomes more sensitive to interference, which means that the higher α, the better the coverage probability, due to less aggregate interference.

In Fig. 2.5, the blocking probability for three MIMO systems in noisy and noise-less networks is presented. As expected, the noise-free scenario

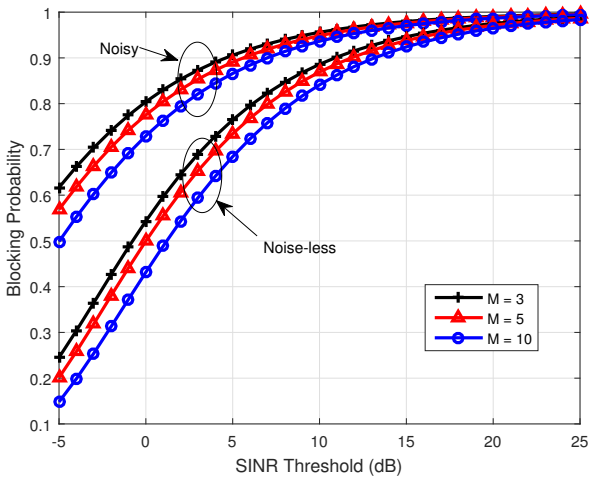

Figure 2.5: Blocking probability in MIMO system with equal sum power constraint

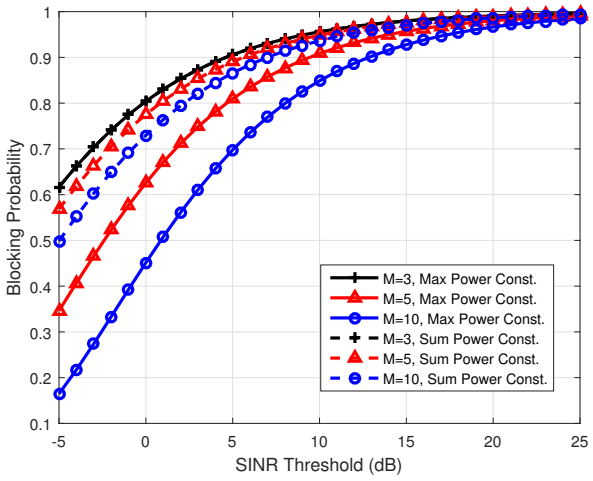

Figure 2.6: Blocking probability in MIMO systems with antenna max power constraint and BS sum power constraint

outperforms the system performance in the presence of noise. Additionally, Fig. 2.6 shows the effect of different power constraints on blocking probability. As depicted, an increasing number of transmit antennas reduces the blocking probability under both max power and sum power constraints, and in the max power constraint scenario the blocking probability improvement is higher as the number of transmit antennas increases. In Figs. 2.7 and 2.8, the spatial spectral efficiencies of MIMO and SISO systems are illustrated as a function of the call arrival rate, μ, in noise-less and noisy networks, respectively. Besides, Figs. 2.9 and 2.10 show the effect of μ on the energy efficiency of MIMO and SISO systems. In noise-less networks, both SSE and EE decrease as the call arrival rate increases. However, there is a μ which maximizes SSE and EE in noisy networks. As a matter of fact, to achieve maximum EE and SSE, it is important to carefully consider the call arrival

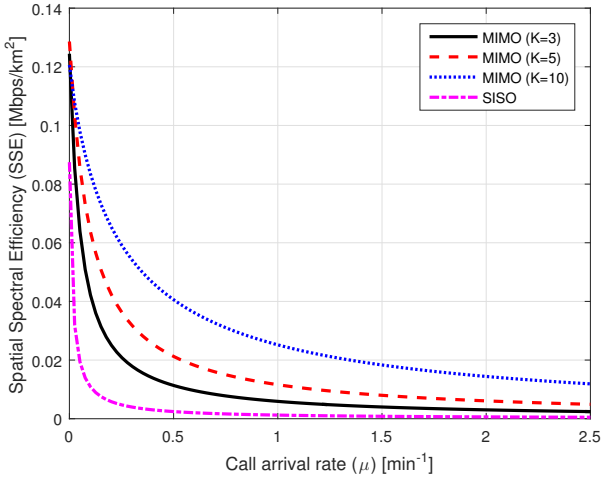

Figure 2.7: Spatial spectral efficiency of MIMO and SISO systems in a noiseless network

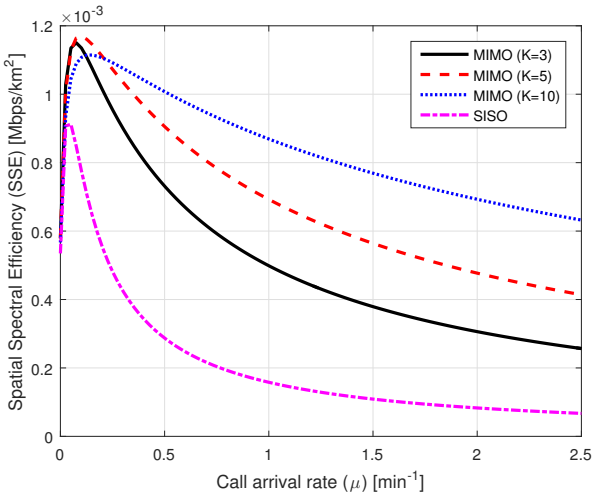

Figure 2.8: Spatial spectral efficiency of MIMO and SISO systems in a noisy network

rate. Moreover, the simulation results reveal the SSE and EE improvement in a MIMO rather than SISO scenario.

Finally, the last two Figs. 2.11 and 2.12 reflect the impact of the path-loss exponent on SSE and EE in MIMO systems. As shown, similar to incrementing the number of transmit antennas in BSs, increasing the path-loss exponent also causes an improvement in SSE and EE, which implies that random MIMO cellular networks are more susceptible to interference than to noise, since α affects and degrades the aggregate interference more than the desired signal.

To sum up, simulation results showed the effect of the path-loss exponent on noisy and noise-free networks. Besides, coverage and blocking probability were depicted in different scenarios. And finally, the performance of random MIMO cellular networks in terms of EE and SSE were presented.

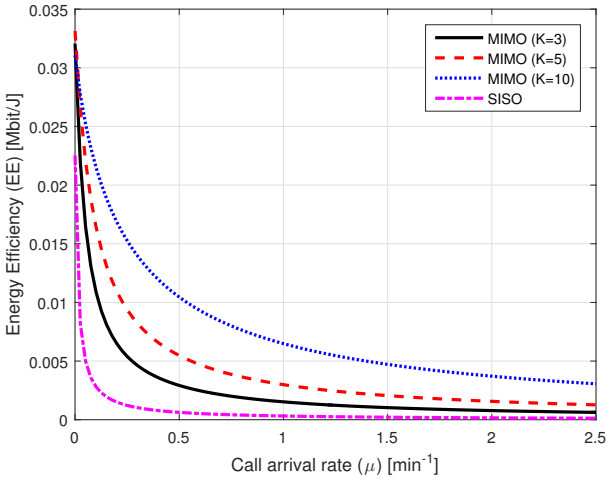

Figure 2.9: Energy efficiency of MIMO and SISO systems in a noise-less network

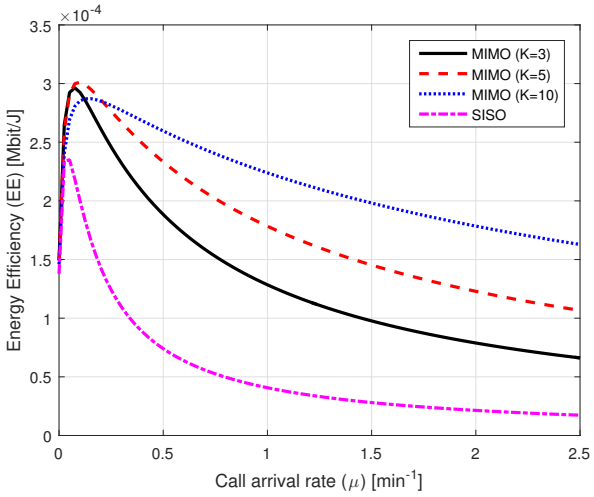

Figure 2.10: Energy efficiency in MIMO and SISO systems in a noisy network

2.7 Conclusion

In this work, we have studied the performance of a MIMO system with imperfect beam alignment in a PVT random cellular network and derived the coverage probability and ergodic capacity. By exploiting a MC transition model for the network, we obtained blocking probability, energy efficiency and spatial spectral efficiency. Our simulation results show that a PVT random cellular network with multiple antennas is more sensitive to interference than to noise. In fact, the higher path-loss exponent degrades the aggregate interference more than the desired signal, and thus has positive impact on the coverage and blocking probabilities as well as SSE and EE. Finally, considering different kinds of network infrastructures, e.g., with macrocells and femtocells, is an interesting direction for future work.

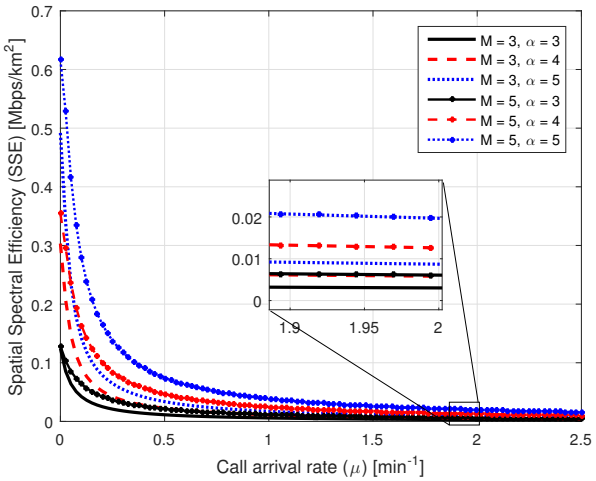

Figure 2.11: Spatial spectral efficiency of MIMO systems in a noise-less network

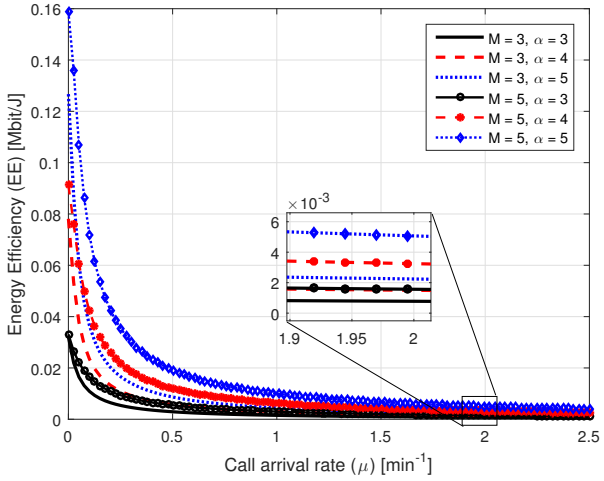

Figure 2.12: Energy efficiency of MIMO systems in a noise-less network

Chapter 3

MIMO HetNets with Inter-Tier Dependence

In this chapter, we study the Energy Efficiency (EE) and Spatial Spectral Efficiency (SSE) of MIMO Heterogeneous Random Cellular Networks (HetNets). To this aim, we consider a 2−tier MIMO cellular network consisting of Macro and Pico tiers whose BS locations follow a Poisson Point Process (PPP) and a Poisson Hole Process (PHP), respectively. The idea come from considering an exclusion region around the high power Macro BSs (MBSs) where there is no active low power Pico BS (PBS), in order to reduce cross tier interference [66]. As the intermediate steps toward our final goal i.e., obtaining EE and SSE, we evaluate the coverage/outage probability of each tier. Moreover, we derive a new expression for the Ergodic capacity in this network as a function of Laplace transform of the signal and interference power. Although using PHP to model Pico BS locations is a more realistic and accurate distribution model, the obtained results are more complex than well-known homogeneous independent process (HIP). Thus, we examine the model through numerical evaluation where we show the advantage of the PHP model over HIP. This observation gives theoretical guidelines for BS deployment for the next generation of mobile communication systems, namely 5G. For example, we show that considering the exclusion regions around high power BSs is more effective than adding a new tier of BSs in order to increase coverage probability.

3.1 Introduction

The fifth generation of mobile communication systems, 5G, is currently being investigated with a number of unprecedented challenges and technical requirements which push researchers and providers to re-think the structure of cellular networks and find the proper solutions to address them. For instance, 5G is expected to offer 1000 times more capacity and to support 7 trillion connected devices [67].

The key requirements of 5G can be listed as follows: high data rate and low end-to-end latency, massive number of connected devices and ubiquitous coverage, compatibility with the existing cellular infrastructures, cost and

energy efficiency, etc. [1,2,8]. To fulfill these requirements, new developments such as massive Multiple-Input Multiple-Output (MIMO) systems and the idea of small cells and random deployment of Base Stations (BSs) in terms of Heterogeneous Network (HetNet) have been proposed and studied [56,57,68].

Hence, as a consequence of network densification due to the growth of data traffic demand and of the enormous number of connected wireless devices, the power consumption of cellular networks rapidly increases, which results in much larger operating cost and CO_2 emission levels [69]. Therefore, the concept of green cellular networking in 5G which addresses Energy Efficiency (EE) and environmental concerns attracts a lot of attentions recently, for example in [35, 70].

In this work, we investigate the performance of MIMO HetNets in terms of EE and patial Spectral Efficiency (SSE). In order to study random networks, some novel tools like stochastic geometry enable us to analyze them efficiently [13, 58, 71]. However, due to tractability and ease of dealing with the Poisson Point Process (PPP), most works on HetNets, e.g., [72–74], consider independent tiers of BSs distributed based on independent PPPs, which is popularly referred to as the Homogeneous Independent Poisson (HIP) model. In reality, within the network planning procedure, the deployment of other tiers of BSs is carefully taken into account. Therefore, considering spatial correlation between different tiers in the network makes the model more realistic, which leads to more reliable results and insights. Note that the spatial correlation of tiers does not contradict the random nature of HetNets. According to the small cell concept, BSs are arbitrarily deployed in order to enhance coverage and satisfy the varying capacity demand [19].

In this work we consider the well-known and studied multiple-input and multiple-output (MIMO) systems whose advantages have been proved in terms of power saving, throughput gain, etc. [59]. Moreover, we study a more accurate model for HetNets based on the Poisson Hole Process (PHP), which will be introduced later. By applying MIMO in this HetNet model, the perspective is to enable 5G to fulfill the throughput and coverage requirements while achieve higher EE and SSE.

Recently, a PHP model has been exploited to characterize inter-tier dependence of the BSs' locations in HetNets [19, 22]. These works analyze the interference and outage probability in 2−tier SISO networks. Besides, [22] proposed a new approach to approximate PHP and derived tighter bounds for the performance of PHP networks compared to the previous approximations in [71].

In this regard, [72] focused on coordinated beamforming techniques in a 2−tier HetNet. Efficiency of these methods was investigated in order to reduce intra-cell and inter-cell interference in this network. In [75], the impact of BS density on the EE in ultra dense HetNets was studied using stochastic geometry. Besides, [76] considered the EE and Spatial Spectral Efficiency (SSE) in a single tier random MIMO network.

A game-theoretic approach is used in MIMO HIP networks in order to study cooperative and non-cooperative energy efficient power control strategies [73]. In addition, [74] studied the effect of the network load on EE in

MIMO HIP networks with wireless backhaul. The results showed a significant EE gain of a 2−tier network over one with a single tier. Moreover, [65] proposed a tradeoff between the area spectral efficiency and link reliability in MIMO HetNets utilizing a Toeplitz matrix representation.

To the best of our knowledge, only [25] has recently considered a PHP model for BS distribution in massive MIMO HetNets. However, authors approximated the signal and interference power with Gamma distributions and avoid complexity by approximating PHP with the baseband PPP. In this work, we show the advantages of this model and provide theoretical guidelines for BS deployment. In particular, [11] introduced a general model for downlink MIMO HetNets and provided the ordering results for the coverage probability for the three considered techniques. It also derived an upper bound for the coverage probability assuming a Poisson BS distribution. However, in this work we derive the lower and upper bounds of the coverage probability for the PHP model. We also show the tightness of these bounds through numerical evaluations. Finally, the ergodic capacity, EE and SSE in a 2−tier MIMO HetNet based on the PHP model are derived.

The rest of the chapter is organized as follows. In Section 3.2, the system model will be introduced. Section 3.3 provides the network metrics including the coverage probability, ergodic capacity, SSE and EE. The lower and upper bounds for the Laplace transform of the aggregate interference will be given in Section 3.4. Moreover in this section, the Laplace transform of the aggregate interference in HIP networks is presented as a benchmark for comparison. Finally, Sections 3.5 and 3.6 provide the numerical evaluations and conclusions of this chapter, respectively.

3.1.1 Motivations and Contributions

In this chapter, we investigate the performance of a 2−tier HetNet in which MBSs are located based on a homogeneous PPP and PBS's locations follow a PHP.

Most works in the field of multi-tier HetNets consider HIP to model the BS locations. Although this assumption is fairly accurate in modeling the irregularity of the BS locations in random networks, it seems inadequate to address the spatial interference management techniques considered during the cellular network planning procedure. This type of interference management methods is based on the spatial interactions among different tiers of the BSs and controls the interference by preventing the BSs from being closer to each other than a predefined minimum distance. Note that both HetNets and MIMO systems are typically interference-limited, therefore any attempt to reduce or control the interference would be noteworthy.

PHP is a generalization of HIP. As will be defined later, in order to obtain PHP, we need to define an exclusion region of radius $\boldsymbol{D}$ around high power BSs in a HIP model. Therefore, in the special case of $\boldsymbol{D} = 0$, PHP degenerates to HIP. So PHP captures all the advantages of HIP and also allows to address more general and more realistic scenarios.

To this aim, in this work we investigate the PHP model, which on one

hand maintains the irregular feature of the BS locations in random networks and on the other hand provides spatial interaction among the transmitters. We will show that this model improves the network performance compared to the HIP model.

In this chapter, we show that the 2−tier PHP model outperforms 2 and 3−tier HIP networks, which implies that instead of deploying a new tier of high density low power BSs to improve the network throughput, interference could be managed by defining an exclusion region around the high power BSs and therefore achieve higher performance.

There are two ways to apply PHP model in real networks. First, consider this model in the network planning phase. Second, in current networks, i.e., HIPs, by imposing small cells to follow PHP. In those networks, only the small cells which are farther than a specific value to the MBSs remain active.

In this work, we first obtain distance distribution to the nearest interferer BS in PHP model. Using this, we derive several metrics including outage/coverage probability and Ergodic capacity. While these metrics are individually important and give useful insights about the network performance, they are adopted to obtain our primary goal in this chapter, i.e., to investigate SSE and EE. A brief explanation of each metric and a discussion of the relations among them are provided in Subsection 3.2.4.

In order to characterize the above mentioned metrics without sacrificing mathematical tractability, we adopt two approximations for the PHP model which respectively overestimate and underestimate the aggregate interference received at a certain point. Therefore, these approximations give lower and upper bounds for the metrics. We will show through numerical evaluations that the proposed bounds are tight.

The proposed analytical framework to study a MIMO HetNet is provable and more reliable than only simulation. Thanks to stochastic geometry, the numerical evaluation of the obtained results is much faster than with Monte Carlo simulation which needs to generate a large number of random variables due to the dense BS deployment of different tiers and the number of MIMO antennas.

In general, the numerical evaluations show that the Pico tier has better performance than the Macro one. At first glance, this observation seems to suggest to offload traffic from the MBSs to the PBSs in order to achieve higher gain. However, considering the call arrival rate and its effects on the EE and SSE seems an interesting topic for the future works.

3.2 System Model

In this section, we describe in detailed the system model used in this work.

3.2.1 Network Model

We consider a HetNet that consists of multiple-antenna Macro and Pico base stations denoted as MBS and PBS, respectively. We assume that MBSs have K_M antennas and are located based on a PPP Φ_M with density λ_M,

over $\mathbb{R}^2$. Furthermore, taking advantage of small cell concepts, K_P-antenna PBSs are distributed randomly following another independent PPP Φ_P with density $\lambda_P > \lambda_M$ in order to enhance Quality of Service (QoS) and coverage. Additionally, we assume that among all PBSs, only those placed outside the exclusion region of radius D around each MBS remain active. Hence, the locations of the active PBSs form a PHP as defined below. Following this assumption, we can have dynamic choice of D in the network which is beyond the scope of this chapter.

Definition 1. *(Poisson Hole Process [71, Example 3.7])*
Let Φ_M be a PPP of density λ_M and Φ_P be a PPP of intensity $\lambda_P > \lambda_M$. For each $x \in \Phi_M$, remove all the points in $\Phi_P \cap C_{x,D}$, where $C_{x,D} = c(x, D)$ is a circle centered at x with radius D . Then, the remaining points of Φ_P form the Poisson hole process, $\tilde{\Phi}_P$.

It can be shown [71] that the density of PHP, $\tilde{\Phi}_P$, is

$$\tilde{\lambda}_P = \lambda_P \exp\left(-\lambda_M \pi D^2\right) \tag{3.1}$$

In this work, the two main purposes in deploying the low power BS tier are offloading traffic and filling coverage holes. The latter is acquired by the higher density of the PBSs, whereas the former is obtained by managing the exclusion region around the MBSs. In the following, MU stands for the Macro User, e.g., a user served by the Macro tier, whereas a Pico User is denoted by PU, which symbolizes the user served by the nearest PBS.

Since working with PHP is not as straightforward as with PPP, some approximations and bounds on PHP have been provided in [19], [22]. Along the lines of [22], we use a model to lower bound the interference. In this model, only the closest hole to the typical user is carved out, thus it avoids the issues arising due to overlap of the holes. In fact, this model maintains a similar level of tractability as that of a PPP due to similar far field effects, while providing the accuracy of local neighborhood near the typical user.

Additionally, in this chapter we assume that the user locations are drawn from an independent PPP, Φ_u, of density λ_u. Focusing on downlink communications, we study a typical user equipped with a single antenna device and located at the origin. Without loss of generality, according to Slivnyak's theorem, the analytical results for an arbitrary point of Φ_u are the same as those at the origin in the point process $\Phi_u \cup \{0\}$ [77]. Thus, the user located at the origin is called *typical* user.

3.2.2 Distance Distribution

Although considering an exclusion region around high power BSs seems an effective way to manage interference, there is not much effort to analyze the system undertaking this assumption and study its different aspects. Therefore, in this part, firstly we derive the distance distribution of a typical Pico user to the nearest interferer MBS while the distance to the serving PBS is given. Due to the intrinsic complexity of exact characterization of PHP, we will derive a lower bound for the probability density function of the distance

Table 3.1: Notation and Network Parameters

Symbol	Description
$\Phi_k, \lambda_k, r_k,$ ρ_k, K_k, K'_k	PPP of the k^{th} tier BS distribution, density, distance to the nearest BS, transmission power, number of the antennas and number of served users, respectively.
$\tilde{\Phi}_P, \tilde{\lambda}_P$	PHP of Pico tier BS distribution, density
M, P	Indicators for the Macro and Pico tiers, respectively.
D	Radius of the exclusion region
$\hat{S}, \hat{I}, \sigma^2$	Signal, interference and noise power, respectively.
α	Path-loss exponent
$\mathbb{P}_{\text{cov}}, \mathbb{P}_{\text{out}}$	Coverage and outage probabilities, respectively.

between a typical Pico user located at the origin and the nearest MBS. To derive the lower bound, we just consider the nearest hole and ignore the rest ones.

As shown in Fig. 3.1, given the distance to the serving BS, here denotes as r_*, the interfering BSs belonging to the cross tier fall in the shaded area. Assume that the typical user is served by the nearest PBS at distance $r_* = r_p$, thus the interfering MBSs should be farther than r_p from the typical Pico user, and also farther than D from the serving PBS, as otherwise the PBS would have been removed according to the definition of the PHP. In fact, we assume that there is a virtual hole of radius D centered at the nearest PBS location. Although this assumption gives a looser bound, we will show in the numerical evaluations that the bounds are tight enough and the gap between the lower and upper bounds is negligible for a wide range of D.

Lemma 2. *The probability density function of the distance between a typical user located at the origin and the nearest cross tier interferer BS is*

$$f_Y(y|r_*) = 2\lambda y \cos^{-1}(a_1) \cdot \exp\left[-\lambda\left(y^2\cos^{-1}(a_1) - D^2\cos^{-1}(a_2) + (D^2 - 2r_*^2)\cos^{-1}(a_3) - \frac{D}{2}\sqrt{a_4} + \frac{1}{2}\sqrt{a_5}\right)\right] \tag{3.2}$$

$$\tag{3.3}$$

where

$$a_1 = \max\left\{-1, -\frac{y^2 + r_*^2 - D^2}{2yr_*}\right\} \tag{3.4}$$

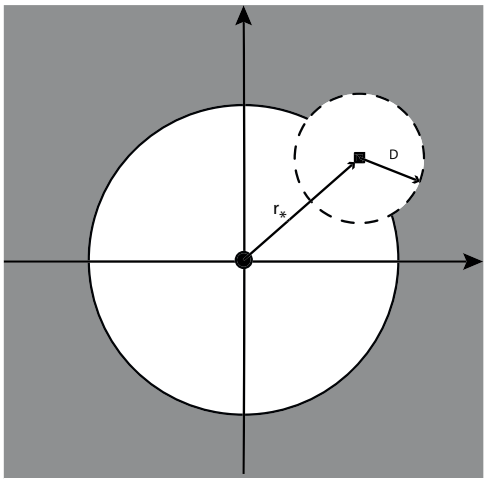

Figure 3.1: A Sketch of the PHP Network

$$a_2 = \max\left\{-1, -\frac{y^2 - r_*^2 - D^2}{2r_* D}\right\} \tag{3.5}$$

$$a_3 = \min\left\{1, \frac{D}{2r_*}\right\} \tag{3.6}$$

$$a_4 = \Big\langle (2r_* - D)(2r_* + D) \Big\rangle^+ \tag{3.7}$$

$$a_5 = \Big\langle (-y + r_* + D)(y - r_* + D)(y + r_* - D)(y + r_* + D) \Big\rangle^+ \tag{3.8}$$

$\langle\cdot\rangle^+$ *is* $\max\{0, \cdot\}$ *and* $y > \max\{r_*, D - r_*\}$.

Proof. See Appendix 3.7.1. □

Note that, in the case of $D = 0$, $f_Y(y|r_*)$ reduces to a truncated Rayleigh, i.e., $f_Y(y|r_*) = 2\pi\lambda y \exp\left[-\pi\lambda\left(y^2 - r_*^2\right)\right]$. On the other hand, for $r_* = 0$ we have $f_Y(y|r_* = 0) = 2\pi\lambda y \exp\left[-\pi\lambda\left(y^2 - D^2\right)\right]$. Furthermore, for $y \gg r_* + D$, an approximate PDF could be $f_Y(y|r_*) = 2\pi\lambda y \exp\left[-\pi\lambda\left(y^2 - \max\{r_*, D\}^2\right)\right]$.

3.2.3 Propagation Model

Under the distance condition mentioned in the previous sub-section, a typical user, MU_i (or PU_i) is associated to the nearest base station, MBS_j (or PBS_j), which is at distance x_{ij}. Similar to [76], a non-singular path-loss model, $\sqrt{(1 + x_{ij})^{-\alpha}}$, with path-loss exponent α, and i.i.d. Rayleigh fading, $\mathbf{h}_{ij} \sim \mathcal{CN}(\mathbf{0}, \mathbf{1})$, have been used in this work. The received signal at the typical Macro User, MU_i, is given by

$$y_{MU_i} = \mathbf{g}_{ij}^{\mathsf{H}} \mathbf{u}_j + \sum_{\eta \in \Phi_M \setminus \{j\}} \mathbf{g}_{i\eta}^{\mathsf{H}} \mathbf{u}_\eta + \sum_{\zeta \in \Phi_P} \mathbf{g}_{i\zeta}^{\mathsf{H}} \mathbf{u}_\zeta + n. \tag{3.9}$$

Besides, (3.10) gives the received signal at the typical Pico User, PU_i,

$$y_{PU_i} = \mathbf{g}_{ij}^{\mathsf{H}} \mathbf{u}_j + \sum_{\eta \in \Phi_M} \mathbf{g}_{i\eta}^{\mathsf{H}} \mathbf{u}_\eta + \sum_{\zeta \in \Phi_P \setminus \{j\}} \mathbf{g}_{i\zeta}^{\mathsf{H}} \mathbf{u}_\zeta + n, \tag{3.10}$$

where $n \sim \mathcal{N}(0, \sigma^2)$ represents the receiver noise with normalized power σ^2, and $\mathbf{g}_{ij} = \sqrt{(1+x_{ij})^{-\alpha}}\mathbf{h}_{ij}$ is the channel vector between BS_j and the typical user. Moreover, $\mathbf{u}_j$ denotes the vector of transmitted symbols by BS_j and is of size either K_M or K_P and of power either ρ_M or ρ_P, according to whether it is transmitted by MBS or PBS. Explicitly, the transmitted symbols in (3.9) are listed below.

$$\mathbf{u}_j = \sqrt{\rho_M} \sum_{n=1}^{K'_M} s_{nj}\mathbf{w}_{nj}, \tag{3.11}$$

$$\mathbf{u}_\eta = \sqrt{\rho_M} \sum_{n=1}^{K'_M} s_{n\eta}\mathbf{w}_{n\eta}, \tag{3.12}$$

$$\mathbf{u}_\zeta = \sqrt{\rho_P} \sum_{n=1}^{K'_P} s_{n\zeta}\mathbf{w}_{n\zeta}. \tag{3.13}$$

While the only difference in (3.10) is

$$\mathbf{u}_j = \sqrt{\rho_P} \sum_{n=1}^{K'_P} s_{nj}\mathbf{w}_{nj}, \tag{3.14}$$

where $K'_M \leq K_M$ and $K'_P \leq K_P$ are the number of served MUs and PUs by each MBS and PBS, respectively. In addition, s and $\mathbf{w}$ are the unit-norm desired data and linear zero-forcing (ZF) precoding vector, respectively. Since ZF-precoding vector is orthogonal to the channel vectors of other users served by the same BS, (3.9) and (3.10) can be re-written as

$$\begin{aligned} y_{MU_i} =& \sqrt{\rho_M} s_{ij}\mathbf{g}_{ij}^{\mathsf{H}}\mathbf{w}_{ij} + \sqrt{\rho_M} \sum_{\eta\in\Phi_M\setminus\{j\}} \sum_{n=1}^{K'_M} s_{n\eta}\mathbf{g}_{i\eta}^{\mathsf{H}}\mathbf{w}_{n\eta} \\ &+ \sqrt{\rho_P} \sum_{\zeta\in\tilde{\Phi}_P} \sum_{n=1}^{K'_P} s_{n\zeta}\mathbf{g}_{i\zeta}^{\mathsf{H}}\mathbf{w}_{n\zeta} + n, \end{aligned} \tag{3.15}$$

$$\begin{aligned} y_{PU_i} =& \sqrt{\rho_P} s_{ij}\mathbf{g}_{ij}^{\mathsf{H}}\mathbf{w}_{ij} + \sqrt{\rho_M} \sum_{\eta\in\Phi_M} \sum_{n=1}^{K'_M} s_{n\eta}\mathbf{g}_{i\eta}^{\mathsf{H}}\mathbf{w}_{n\eta} \\ &+ \sqrt{\rho_P} \sum_{\zeta\in\tilde{\Phi}_P\setminus\{j\}} \sum_{n=1}^{K'_P} s_{n\zeta}\mathbf{g}_{i\zeta}^{\mathsf{H}}\mathbf{w}_{n\zeta} + n. \end{aligned} \tag{3.16}$$

Before moving to the next section, we provide some definitions to simplify the flow of the derivations. Besides, Table 3.1 provides the notation and parameters of the network.

Definition 2. *In the rest of this chapter, the following integral which was*

already calculated in [76], is represented by $\mathcal{G}-$function.

$$
\begin{aligned}
&-2\pi \int_r^{\infty} \left(1 - \frac{1}{\left(1 + s\rho(1+x)^{-\alpha}\right)^{K'}}\right) x \, \mathrm{d}x \qquad (3.17)\\
&= \frac{-2\pi}{\alpha} \int_0^{(1+r)^{-\alpha}} \left(1 - \frac{1}{\left(1 + s\rho t\right)^{K'}}\right)\left(t^{-\frac{1}{\alpha}} - 1\right)\left(t^{-\frac{1}{\alpha}-1}\right) \mathrm{d}t\\
&= \pi(1+r)\Bigg((r-1)\\
&\qquad - (1+r)\, {}_2F_1\left(K', \frac{-2}{\alpha}; 1 - \frac{2}{\alpha}; -s\rho(1+r)^{-\alpha}\right)\\
&\qquad + 2\, {}_2F_1\left(K', \frac{-1}{\alpha}; 1 - \frac{1}{\alpha}; -s\rho(1+r)^{-\alpha}\right)\Bigg)\\
&\triangleq \mathcal{G}(s, r, \alpha, \rho, K'). \qquad (3.18)
\end{aligned}
$$

The result is derived by the change of variable $(1+x)^{-\alpha} = t$ and the use of [78, 3.194]. ${}_2F_1(a, b; c; z)$ is the Gaussian hypergeometric function .

Definition 3. *In this work, we use the notation of $c(o, R) = C_{o,R}$ to indicate the circle of radius R and center at o. Besides, we use $C^c_{o,R}$ to denote the region outside of $c(o, R)$.*

3.2.4 Main Metrics

In this subsection, we briefly explain the main metrics which will be derived in this work. First, we derive the Outage/Coverage probability of the network. By definition, the probability that the received Signal-to-Interference-plus-Noise Ratio (SINR) at a user falls below a predefined threshold is called outage probability. Moreover, in the literature, the coverage probability is defined as the complement of the outage probability [13]. Through this metric, we will show the advantage of the 2−tier PHP based networks over 2 and 3−tier HIP ones.

As the next step, we will derive the Ergodic capacity of a 2−tier MIMO HetNet with PPP MBSs and PHP active PBSs. By definition, the ergodic capacity is interpreted as the average rate that is achievable by each user [79], [80]. In this work, a lower bound for the ergodic capacity will be obtained using a PHP approximation. In addition, it will be shown that the proposed lower bound converges from above to the ergodic capacity of a typical PU in the HIP networks. Therefore, restricting the Pico tier to follow PHP does not degrade the ergodic capacity of the corresponding users.

Finally, to reach the primary goal of this chapter, we will formulate SSE and EE for the target network. To this aim, utilizing the obtained metrics such as ergodic capacity, we attain the cell throughput and then SSE and EE. Numerical evaluations show that although offloading traffic of the Macro tier to the Pico one gives higher total SSE.

3.3 Network Metrics

In this section, we will derive the metrics which are used to evaluate a cellular network and compare it with the others.

3.3.1 Coverage Probability

First, we derive the coverage probability, which is the complement of the outage probability, for a typical MU and PU. As explained before, outage occurs when the SINR becomes less than a specific threshold [13].

In this work, the SINR thresholds for MUs and PUs are denoted as τ_M, τ_P, respectively. Therefore,

$$\mathbb{P}_{\text{cov}} = 1 - \mathbb{P}_{\text{out}} = \mathbb{P}\left(\text{SINR} > \tau\right), \tag{3.19}$$

where τ is either τ_P or τ_M and SINR is

$$\text{SINR} = \frac{\hat{S}}{\hat{I} + \sigma^2}. \tag{3.20}$$

In (3.20), $\hat{S}$ denotes the power of the desired signal, whereas $\hat{I}$ and σ^2 represent the aggregate interference power and the normalized noise power, respectively.

According to (3.15), the signal and aggregate interference powers at a typical MU located at the origin[1] are given by

$$\hat{S}_M = \rho_M |\mathbf{g}_{ij}^{\mathsf{H}} \mathbf{w}_{ij}|^2 \overset{d^*}{=} \rho_M (1 + x_{ij})^{-\alpha} S_{MU}, \tag{3.21}$$

$$\begin{aligned}\hat{I}_M &= \rho_M \sum_{\eta \in \Phi_M \setminus \{j\}} \sum_{n=1}^{K'_M} |\mathbf{g}_{i\eta}^{\mathsf{H}} \mathbf{w}_{n\eta}|^2 + \rho_P \sum_{\zeta \in \tilde{\Phi}_P} \sum_{n=1}^{K'_P} |\mathbf{g}_{i\zeta}^{\mathsf{H}} \mathbf{w}_{n\zeta}|^2 \\ &\overset{d^*}{=} \rho_M \sum_{\eta \in \Phi_M \setminus \{j\}} (1 + x_\eta)^{-\alpha} I_{MM}^{\eta} + \rho_P \sum_{\zeta \in \tilde{\Phi}_P} (1 + x_\zeta)^{-\alpha} I_{MP}^{\zeta},\end{aligned} \tag{3.22}$$

where "$\overset{d^*}{=}$" yields equality in distribution. In fact, [11, 63, 81] have shown that S_{MU}, I_{MM}^{η} and I_{MP}^{ζ} are auxiliary random variables and have Gamma distributions, i.e., $S_{MU} \sim \Gamma(K_M - K'_M + 1, 1)$, $I_{MM}^{\eta} \sim \Gamma(K'_M, 1)$ and $I_{MP}^{\zeta} \sim \Gamma(K'_P, 1)$.

Additionally, based on (3.16), a typical PU receives signal power and aggregate interference power as

$$\hat{S}_P = \rho_P |\mathbf{g}_{ij}^{\mathsf{H}} \mathbf{w}_{ij}|^2 \overset{d^*}{=} \rho_P (1 + x_{ij})^{-\alpha} S_{PU}, \tag{3.23}$$

$$\hat{I}_P = \rho_M \sum_{\eta \in \Phi_M} \sum_{n=1}^{K'_M} |\mathbf{g}_{i\eta}^{\mathsf{H}} \mathbf{w}_{n\eta}|^2 + \rho_P \sum_{\zeta \in \tilde{\Phi}_P \setminus \{j\}} \sum_{n=1}^{K'_P} |\mathbf{g}_{i\zeta}^{\mathsf{H}} \mathbf{w}_{n\zeta}|^2 \tag{3.24}$$

$$\overset{d^*}{=} \rho_M \sum_{\eta \in \Phi_M} (1 + x_\eta)^{-\alpha} I_{PM}^{\eta} + \rho_P \sum_{\zeta \in \tilde{\Phi}_P \setminus \{j\}} (1 + x_\zeta)^{-\alpha} I_{PP}^{\zeta}. \tag{3.25}$$

[1] Due to PPP properties, without loss of generality we can assume that the typical user is located at the origin.

In a similar way, we have the random variables S_{PU}, I^{η}_{PM} and I^{ζ}_{PP} with Gamma distributions, i.e., $S_{PU} \sim \Gamma(K_P - K'_P + 1, 1)$, $I^{\eta}_{PM} \sim \Gamma(K'_M, 1)$ and $I^{\zeta}_{PP} \sim \Gamma(K'_P, 1)$.

As shown in [13, Appendix A], given the distance to the serving BS, r_k, finding the outage probability in networks with Rayleigh fading is equivalent to finding the Laplace transform of the signal and aggregate interference power for each user as follows

$$\mathbb{P}(\mathrm{SINR}_k > \tau_k | r_k) = e^{-\frac{\tau_k}{\rho_k}(1+r_k)^{\alpha}\sigma^2} \cdot \mathcal{L}_{\hat{I}_k | r_k}\left(\frac{\tau_k}{\rho_k}(1+r_k)^{\alpha}\right). \tag{3.26}$$

Appendix 3.7.2 provides a brief explanation toward this result. Note that since the BSs are distributed following a PPP, the PDF of the distance to the serving BS is $f_r(r_k) = 2\pi\lambda_k r_k e^{-\pi\lambda_k r_k^2}$. Moreover, in this work, we consider a fully loaded scenario, i.e., $K'_M = K_M$, $K'_P = K_P$. According to [11, Theorem 1] fully loaded MIMO networks have the lowest coverage probability compared to all scenarios with fewer users. This assumption is used to evaluate the saturation throughput, which is an important metric for network design. In this case, the distribution of S_{PU} and S_{MU} can be expressed as the Exponential distribution, i.e., $S_* \sim \Gamma(1,1) = \mathrm{Exp}(1)$. Therefore, the effective small scale channel gain would be equivalent to Rayleigh fading and (3.26) is valid in our MIMO system model, too.

Since Φ_M follows a PPP, the Laplace transform of the first term in (3.22) and (3.25) can be derived as in [76, Eq. 11]. On the other hand, finding a closed-form expression for the Laplace transform of PHP sacrifices the tractability of stochastic geometry. In this regard, along the lines of [22], to maintain tractability we derive upper and lower bounds on the Laplace transform of the interference power caused by PBSs.

It is worth mentioning that in some works, PHP has been lower bounded by the baseline PPP, i.e., ignoring the holes [71] or approximated by a PPP with the same density as PHP (3.1). Nevertheless, the bound coming from the methods in [22] is tighter, since it captures PHP's characteristics more accurately.

3.3.2 Ergodic Capacity

In this section, we derive a general expression for the ergodic capacity in terms of the Laplace transforms of the signal and interference power. In a recent work, [82] presents analytical characterizations of the ergodic spectral efficiency in MIMO cellular networks. Although the derivation of the $\mathbb{P}_{\mathrm{cov}}$ given in (3.26) is well-known, to the best of our knowledge, ergodic capacity has not been presented as a function of Laplace transform before.

By definition, the ergodic capacity per user in bit/sec/Hz is given by

$$C_{\mathrm{E}} = \mathbb{E}\left[\log_2\left(1 + \mathrm{SINR}\right)\right]. \tag{3.27}$$

***Theorem* 1.** *Given the distance to the serving BS, the Ergodic capacity of a typical user in terms of the Laplace transforms of the desired signal and*

aggregate interference power is given by

$$C_{\mathrm{E}|r} = \int_0^\infty \frac{e^{-s\sigma^2}}{s} \cdot \mathcal{L}_{\hat{I}|r}(s) \cdot \left(1 - \mathcal{L}_{\hat{S}|r}(s)\right) \mathrm{d}s \tag{3.28}$$

Proof. See Appendix 3.7.3. □

Theorem 1 gives a general expression, however the following corollary provides the ergodic capacity under effective Rayleigh fading channel.

***Corollary* 1.** *Given the distance to the serving BS, the Ergodic capacity of a typical user in a fully loaded MIMO network,*

$$C_{\mathrm{E}|r} = \rho(1+r)^{-\alpha} \int_0^\infty \frac{e^{-s\sigma^2}}{1 + s\rho(1+r)^{-\alpha}} \cdot \mathcal{L}_{\hat{I}|r}(s)\ \mathrm{d}s \tag{3.29}$$

Proof. Directly obtained by substitution of Laplace transform of Exponential distribution. □

Corollary 1 is applicable to the case of a fully loaded scenario in which $\hat{S}$ has Exponential distribution. To unbind the proposed Ergodic capacity expression, it is sufficient to take the expectation with respect to the distance to the nearest point in a PPP.

3.3.3 SSE and EE

In the last part of this section, we use the results obtained in the previous subsections to find spatial spectral and energy efficiency.

The throughput of each kind of cell with bandwidth W is given by

$$T_{\mathrm{cell}} = \mathbb{P}_{\mathrm{cov}} \cdot W \cdot C_{\mathrm{E}}, \tag{3.30}$$

where $\mathbb{P}_{\mathrm{cov}}$ and C_{E} denote respectively the coverage probability and the ergodic capacity obtained in the previous sections.

Therefore, the last step to find SSE is to multiply T_{cell} by the cell density, λ_M or λ_P. Moreover, EE is obtained as the ratio of the lifetime cell throughput, T_{LT}, and total energy consumption including the transmission and non-transmission related consumed energy [53]:

$$\mathrm{EE} = \frac{T_{LT}}{E_{\mathrm{non-trans}} + E_{\mathrm{trans}}}. \tag{3.31}$$

where $T_{LT} = T_{\mathrm{cell}} \cdot t_{LT}$ in which t_{LT} represents the lifetime of the BS. Also, $E_{\mathrm{non-trans}}$ is assumed to be constant and independent of the traffic load and comes from maintenance and hardware power consumption inside a BS site, like air-conditioning. Moreover, E_{trans} is a function of number of served users, K, and given by

$$E_{\mathrm{trans}} = (h \cdot \rho K + k) \cdot t_{LT}, \tag{3.32}$$

where, h and k are the scaling coefficients of the total transmission power, ρ.

Therefore, EE in (3.31) is given by

$$\mathrm{EE} = \frac{T_{\mathrm{cell}} \cdot t_{LT}}{E_{\mathrm{non-trans}} + (h \cdot \rho K + k) \cdot t_{LT}}. \tag{3.33}$$

3.4 Laplace Transform of Interference Power

As shown in the previous sections, finding the Laplace transform of the interference is the key to obtain the network's main metrics.

In this section, we aim to compute the Laplace transform of the aggregate interference in 2−tier HetNets while the PBSs are distributed following a PHP model. Although considering an exclusion region around the high-power BSs seems a simple strategy to manage the interference, it brings a high level of complexity to analysis. Therefore, instead of deriving the exact expression we will propose lower and upper bounds for the Laplace transform of the aggregate interference power in PHP model. In the numerical evaluation section, we show the tightness of the proposed bounds for the coverage probability and ergodic capacity.

3.4.1 Lower Bound

In this subsection, we propose a lower bound for the Laplace transform of the aggregate interference power which captures the effect of PHP at short distances, while maintaining the intrinsic tractability of PPP using stochastic geometry. To this aim, the interference caused by the Pico tier is overestimated by carving out only the closest hole to the typical user, either PU or MU.

In Lemma 3, we propose the lower bound of the aggregate interference at the typical PU. For this purpose, we first assume that the center of the closest hole is known, and then obtain the bound by taking the expectation with respect to this parameter.

***Lemma* 3.** *Let $C_{y,D} = c(y, D)$ represent a hole of radius D centered at a known $y \in \Phi_M$. The Laplace transform of the aggregate interference at a Pico User is lower bounded by*

$$\mathcal{L}_{\hat{I}_P|r_P,y}(s) \geq \left(1 + s\rho_M(1+y)^{-\alpha}\right)^{-K'_M} \cdot \exp\left[2\lambda_P g(s,y)\right] \cdot \exp\left[\lambda_M \cdot \mathcal{G}\left(s, y, \alpha, \rho_M, K'_M\right) + \lambda_P \cdot \mathcal{G}\left(s, r_P, \alpha, \rho_P, K'_P\right)\right]. \tag{3.34}$$

where

$$g(s,y) = \int_{\max\{0,y-D\}}^{y+D} \cos^{-1}\left(\max\left\{-1, \frac{t^2+y^2-D^2}{2yt}\right\}\right) \cdot \left(1 - \left(1 + s\rho_P(1+t)^{-\alpha}\right)^{-K'_P}\right) t \, \mathrm{d}t. \tag{3.35}$$

Proof. See Appendix 3.7.4. □

It can be observed that the first term is similar to the result obtained for a homogeneous random MIMO network.

As mentioned, to complete the lower bound of the Laplace transform, the condition in (3.34) should be unconditioned with respect to y.

***Proposition* 1.** *The Laplace transform of the interference power at the typical PU is lower bounded by*

$$\mathcal{L}_{\hat{I}_P|r_P}(s) \geq \int_{\max\{r_P, D-r_P\}}^{\infty} \mathcal{L}_{\hat{I}|r_P,y}(s) f_Y(y|r_P) \mathrm{d}y \tag{3.36}$$

where $f_Y(y|r_P)$ *is given in* (3.2).

Proof. Similar to the previous lemma, here we have the expectation over the closest distance between the typical PU and the hole center. Based on the cell association model, a typical PU is at distance further than r_P from the closest MBS, i.e., the closest hole center. □

In the following Lemma, we will derive the lower bound for the Laplace transform of the aggregate interference power experienced by the typical MU located at the origin.

***Lemma* 4.** *The Laplace transform of the aggregate interference power at the typical MU is lower bounded by*

$$\begin{aligned}\mathcal{L}_{\hat{I}_M|r_M}(s) &\geq \exp\left[2\lambda_P g(s, r_M)\right] \\ &\cdot \exp\left[\lambda_M \cdot \mathcal{G}\left(s, r_M, \alpha, \rho_M, K'_M\right) + \lambda_P \cdot \mathcal{G}\left(s, r_M, \alpha, \rho_P, K'_P\right)\right].\end{aligned} \tag{3.37}$$

Proof. See Appendix 3.7.5. □

3.4.2 Upper Bound

To derive the upper bound for the Laplace transform of the interference power in PHP network, similar to [22], we suppose that all the holes are carved out one by one ignoring the possible overlaps. Accordingly, the interference power is underestimated because some points of the baseline PPP may be removed multiple times due to the PPP distribution of the holes center locations. In [22], it is shown that any attempt which aims to model more accurately overlapping holes in PHP compromises the tractability of the results.

***Lemma* 5.** *Let* $\mathcal{B} \triangleq \bigcup_{y\in\Phi_M} \mathcal{C}_{y,D}$. *The Laplace transform of the aggregate interference power at a typical PU is upper bounded by*

$$\begin{aligned}\mathcal{L}_{\hat{I}_P|r_P}(s) &\leq \exp\left[\lambda_P \cdot \mathcal{G}\left(s, r_P, \alpha, \rho_P, K'_P\right)\right] \\ &\cdot \exp\left[-2\lambda_M \int_{\max\{r_P, D-r_P\}}^{\infty} \cos^{-1}\left(\max\left\{-1, -\frac{t^2 + r_P^2 - D^2}{2t r_P}\right\}\right)\right. \\ &\left. \cdot \left(1 - \left(1 + s\rho_M (1+t)^{-\alpha}\right)^{-K'_M} \cdot \exp\left[2\lambda_P g(s,t)\right]\right) t \mathrm{d}t\right],\end{aligned} \tag{3.38}$$

where $g(s, y)$ *is defined in* (3.35).

Proof. See Appendix 3.7.6. □

Note that, in the previous Lemma, the intersection of each two circles counts twice, and thus the interference is overestimated.

***Lemma* 6.** *Given the distance to the serving MBS, r_M, the Laplace transform of the aggregate interference power at a typical MU is upper bounded by*

$$\mathcal{L}_{\hat{I}_M|r_M}(s) \leq \exp\left[\lambda_P \cdot \mathcal{G}\left(s, r_M, \alpha, \rho_P, K'_P\right) + 2\lambda_P g(s, r_M)\right] \cdot \exp\left[-2\pi\lambda_M \int_{r_M}^{\infty} \left(1-(1+s\rho_M(1+t)^{-\alpha})^{-K'_M} \cdot \exp\left[2\lambda_P g(s,t)\right]\right) t\mathrm{d}t\right]. \tag{3.39}$$

Proof. See Appendix 3.7.7. □

3.4.3 HIP Network Analysis

To provide a benchmark for comparison, in this subsection we derive the Laplace transform of the interference power in a $K-$tier Homogeneous Independent Poisson (HIP) network.

To this aim, we focus on the typical user, U_i, which is served by BS_j of the k^{th} tier, $k = 1, \ldots, K$. The received signal at the typical user is given by

$$y_i = \mathbf{g}_{ikj}^{\mathsf{H}} \mathbf{u}_{kj} + \sum_{\eta \in \Phi_k \setminus \{j\}} \mathbf{g}_{ik\eta}^{\mathsf{H}} \mathbf{u}_{k\eta} + \sum_{\substack{l=1 \\ l \neq k}}^{K} \sum_{\zeta \in \Phi_l} \mathbf{g}_{il\zeta}^{\mathsf{H}} \mathbf{u}_{l\zeta} + n, \tag{3.40}$$

where $n \sim \mathcal{N}(0, \sigma^2)$ and

$$\mathbf{u}_{kj} = \sqrt{\rho_k} \sum_{n=1}^{K'_k} s_{nkj} \mathbf{w}_{nkj} \qquad \forall k = 1, 2, \ldots, K. \tag{3.41}$$

Therefore,

$$\text{SINR} = \frac{\rho_k |\mathbf{g}_{ikj}^{\mathsf{H}} \mathbf{w}_{ikj}|^2}{\rho_k \sum\limits_{\substack{\eta \in \Phi_k \\ \setminus \{j\}}} \sum\limits_{n=1}^{K'_k} |\mathbf{g}_{ik\eta}^{\mathsf{H}} \mathbf{w}_{nk\eta}|^2 + \sum\limits_{\substack{l=1 \\ l \neq k}}^{K} \rho_l \sum\limits_{\zeta \in \Phi_l} \sum\limits_{n=1}^{K'_l} |\mathbf{g}_{il\zeta}^{\mathsf{H}} \mathbf{w}_{nl\zeta}|^2 + \sigma^2}, \tag{3.42}$$

in which the aggregate interference power term is

$$\begin{aligned} \hat{I}_{ikj} &= \rho_k \sum_{\substack{\eta \in \Phi_k \\ \setminus \{j\}}} \sum_{n=1}^{K'_k} |\mathbf{g}_{ik\eta}^{\mathsf{H}} \mathbf{w}_{nk\eta}|^2 + \sum_{\substack{l=1 \\ l \neq k}}^{K} \rho_l \sum_{\zeta \in \Phi_l} \sum_{n=1}^{K'_l} |\mathbf{g}_{il\zeta}^{\mathsf{H}} \mathbf{w}_{nl\zeta}|^2 \\ &\overset{d^*}{=} \rho_k \sum_{\substack{\eta \in \Phi_k \\ \setminus \{j\}}} (1+x_\eta)^{-\alpha} I_{k\eta} + \sum_{\substack{l=1 \\ l \neq k}}^{K} \rho_l \sum_{\zeta \in \Phi_l} (1+x_\zeta)^{-\alpha} I_{l\zeta}, \end{aligned} \tag{3.43}$$

where $I_{k\eta}$ denotes the interference from BS_η of the k^{th} tier. Since we focus on a typical user located at the origin, x_η and x_ζ represent $x_{i\eta}$ and $x_{i\zeta}$, respectively. For notational simplicity $\hat{I}_{ikj}$ will be denoted by $\hat{I}_k$ which is the interference experienced by the typical user served by the k^{th} tier.

Similar to the explanation in Subsection 3.3.1, we also have an effective Rayleigh fading channel in this model. Along the lines of Appendix 3.7.2, we will present the Laplace transform of the interference power at HIP network, given the distance to the serving BS belonging the k^{th} tier, as follows

$$\begin{aligned}\mathcal{L}_{\hat{I}_k|r_k}(s) &= \mathbb{E}\left[\exp\left[-s\hat{I}_k\right]\Big|r_k\right] \\ &= \exp\left[\sum_{\ell=1}^{K}\lambda_\ell \mathcal{G}\left(s, r_k, \alpha, \rho_\ell, K'_\ell\right)\right], \end{aligned} \tag{3.44}$$

where r_k is a random variable that corresponds to the distance to the serving BS, i.e., the nearest BS in the k^{th} tier. Besides, K'_ℓ denotes the number of users served by each BS in the ℓ^{th} tier and $\mathcal{G}$-function has been given in Definition 2.

As will be shown in the following subsection, the Laplace transform of the interference power at HIP network is exactly equal to the PHP network in case of $D = 0$.

3.4.4 Special Case

In this subsection, first we find the lower and upper bounds of the Laplace transforms of PHP interference obtained in this section for the special case of $D = 0$ and then compare it with the HIP networks.

In the special case of $D = 0$, $g(s, y)$ given in (3.35) is equal to zero. Besides, we have $f_Y(y|r) = 2\pi\lambda y \exp\left[-\pi\lambda\left(y^2 - r^2\right)\right]$. Therefore in this case, Proposition 1 gives

$$\begin{aligned}\mathcal{L}_{\hat{I}_P|r_P} &\geq \exp\left[\lambda_P \cdot \mathcal{G}\left(s, r_P, \alpha, \rho_P, K'_P\right)\right] \\ &\cdot \int_{r_P}^{\infty} 2\pi\lambda y \exp\left[-\pi\lambda_M\left(y^2 - r_P^2\right)\right]\left(1 + s\rho_M(1+y)^{-\alpha}\right)^{-K'_M} \\ &\cdot \exp\left[\lambda_M \cdot \mathcal{G}\left(s, y, \alpha, \rho_M, K'_M\right)\right]\mathrm{d}y \qquad (3.45) \\ &= \exp\left[\lambda_P \cdot \mathcal{G}\left(s, r_P, \alpha, \rho_P, K'_P\right)\right] \\ &\cdot \left(-\exp\left[-\pi\lambda_M\left(y^2 - r_P^2\right) + \lambda_M \cdot \mathcal{G}\left(s, y, \alpha, \rho_M, K'_M\right)\right]\right)\Big|_{r_P}^{\infty} \qquad (3.46) \\ &= \exp\left[\lambda_P \cdot \mathcal{G}\left(s, r_P, \alpha, \rho_P, K'_P\right) + \lambda_M \cdot \mathcal{G}\left(s, r_P, \alpha, \rho_M, K'_M\right)\right] \qquad (3.47)\end{aligned}$$

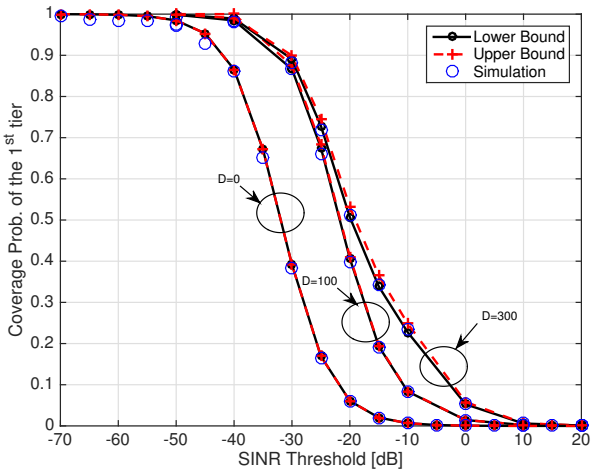

Figure 3.2: Lower and upper bounds for the coverage probability of the Macro tier in PHP model networks for different values of D

Table 3.2: Network Parameters

	1^{st} (Macro) tier	2^{nd} (Pico) tier	3^{rd} (femto) tier
λ	10^{-6} $[1/m^2]$	10^{-4} $[1/m^2]$	10^{-2} $[1/m^2]$
ρ	30 W	1 W	0.1 W
K'	64	4	1

On the other hand, Lemma 5 for $D = 0$ is

$$\mathcal{L}_{\hat{I}_P|r_P}(s) \leq \exp\left[\lambda_P \cdot \mathcal{G}\left(s, r_P, \alpha, \rho_P, K'_P\right)\right] \cdot \exp\left[-2\pi\lambda_M \int_{r_P}^{\infty} \cdot \left(1-\left(1+s\rho_M(1+t)^{-\alpha}\right)^{-K'_M}\right) t\mathrm{d}t\right] \tag{3.48}$$

$$= \exp\left[\lambda_P \cdot \mathcal{G}\left(s, r_P, \alpha, \rho_P, K'_P\right) + \lambda_M \cdot \mathcal{G}\left(s, r_P, \alpha, \rho_M, K'_M\right)\right] \tag{3.49}$$

Therefore, the lower bound in (3.47) matches the upper bound of (3.49) and both are equal to the result for 2−tier HIP as given in (3.44). Similarly, we can show that the results of Lemmas 5 and 6 for the case of $D = 0$ is

$$\mathcal{L}_{\hat{I}_M|r_M}(s) = \exp\left[\lambda_M \cdot \mathcal{G}\left(s, r_M, \alpha, \rho_M, K'_M\right) + \lambda_P \cdot \mathcal{G}\left(s, r_M, \alpha, \rho_P, K'_P\right)\right]. \tag{3.50}$$

which is equal to (3.44) for $K = 2$ and $r_k = r_M$.

3.5 Numerical Evaluation

In this section, we provide some figures to illustrate the results obtained according to the analysis of the previous sections. Table 3.2 summarizes the network parameters.

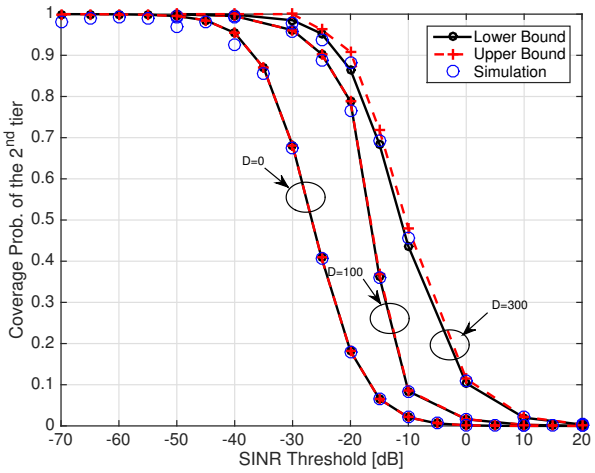

Figure 3.3: Lower and upper bounds for the coverage probability of the Pico tier in PHP model networks for different values of D

Numerous researchers in 5G assume an ultra dense network deployment and Massive MIMO as valid alternatives to fulfill the requirements. In this work, the system parameters mostly came from other references such as [53, 81]. In addition, for example, 3GPP TR36.942 reports 46 dBm maximum BS power for a 10 MHz channel bandwidth and LTE-A supports 8Tx×8Rx MIMO.

Figs. 3.2 and 3.3 illustrate the lower and upper bounds of the coverage probability of PHP model for different values of D in the Macro and Pico tiers, respectively. As provided in Subsection 3.4.4, for $D = 0$ the bounds exactly match. As expected, by increasing D the gap between the bounds grows slightly. Nevertheless, the bounds are properly matched, which means that even by carving out all the holes around MBSs, just a slight number of PBSs are ignored multiple times, making the approximation very good. Besides, these tight bounds show that we can simply but accurately estimate the coverage probability of the Pico tier using either of them. Therefore, according to the tightness and close performance of the bounds, in order to avoid untidiness and to focus on the other features, only the lower bounds are plotted in the following figures. Moreover, the simulation results justify the accuracy of the analytical derivations in this work.

In Fig. 3.4, the coverage probability in 2 and 3−tier HIP networks and its lower bound in a 2−tier PHP network are depicted. Clearly, the PHP model outperforms HIP in both tiers. Therefore, the PHP network achieves higher gain in terms of coverage probability without any need to change the network infrastructure or spend time and money to add a new tier of BSs. Note that, even if the PHP model has not been considered in the network planning phase, it is sufficient to turn off the Pico BSs located in the exclusion regions around Macro BSs to achieve approximately the same results. The slight difference comes from the BS density, which changes according to (3.1).

In order to numerically evaluate the ergodic capacity of the PHP model, we depict its lower and upper bounds for different values of D. Figs. 3.5

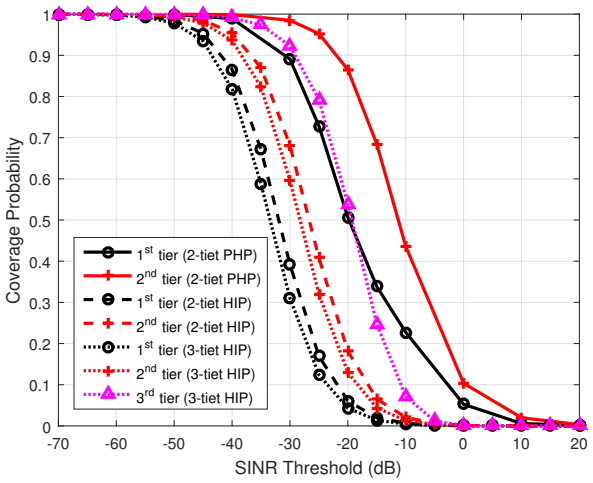

Figure 3.4: Coverage probability of 2−tier PHP with D = 300, 2 and 3−tier HIP networks

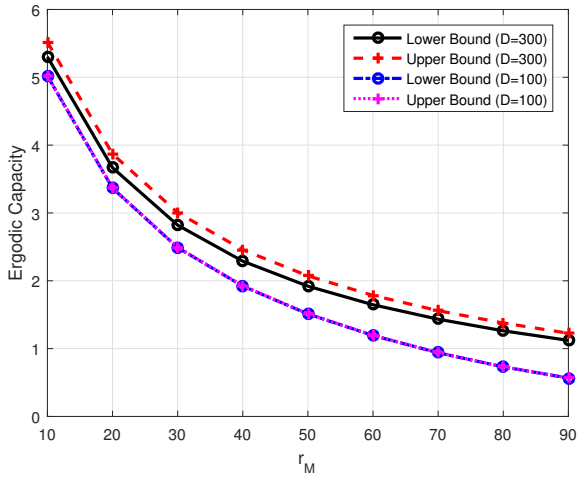

Figure 3.5: Lower and upper bounds for the Ergodic Capacity at the Macro User in PHP networks for different values of D

and 3.6 give the bounds for the Macro tier and Figs. 3.7 and 3.8 present them for the Pico tier of a PHP model. In order to provide more visibility, we use two different serving distance regimes. On the one hand, increasing the distance, r_M or r_P, degrades the ergodic capacity. On the other hand, the gaps between the bounds and the different scenarios, regarding different values of D, reduce as the serving distance grows.

Finally, in Figs. 3.9 and Fig. 3.10, SSE and EE for the 2−tier PHP and HIP networks is displayed as a function of SINR threshold, respectively. As observed in both figures, PHP outperforms the HIP model with identical network parameters.

To sum up, we summarize the main results of this section as follows:

- Tight bounds for the coverage probability in the PHP model can be derived (Figs. 3.2 and 3.3).

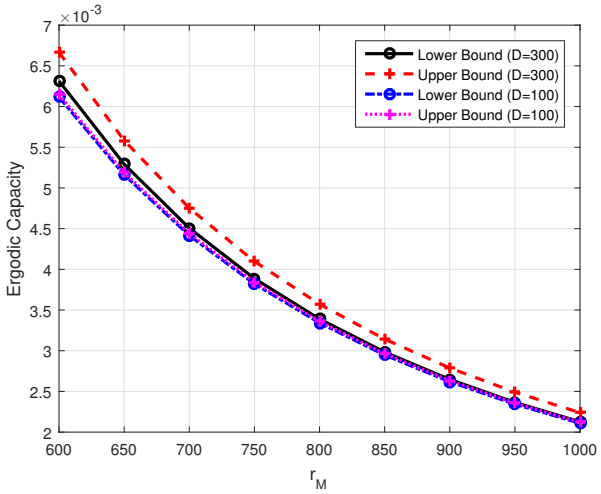

Figure 3.6: Lower and upper bounds for the Ergodic Capacity at the Macro User in PHP networks for different values of D

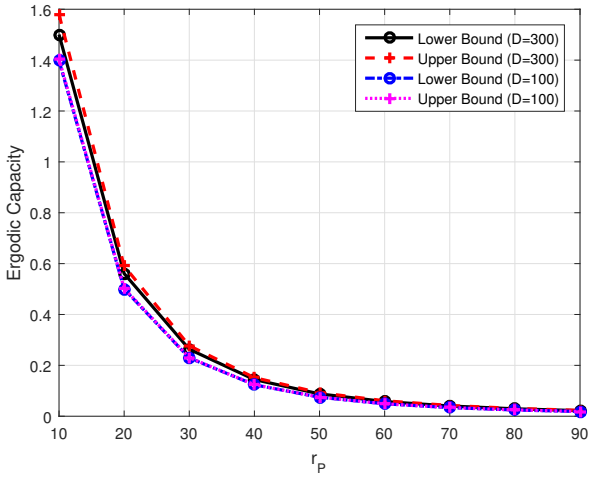

Figure 3.7: Lower and upper bounds for the Ergodic Capacity at the Pico User in PHP networks for different values of D

- The 2−tier PHP model outperforms 2 and 3−tier HIP networks (Fig. 3.4).
- Tight bounds for the ergodic capacity in the PHP model can be derived (Figs. 3.5, 3.6, 3.7 and 3.8).
- The PHP model outperforms HIP networks regarding both SSE and EE.

3.6 Conclusion

In this chapter, we investigated the performance of 2−tier MIMO HetNets in two BS deployment scenarios, namely, using HIP and PHP network models.

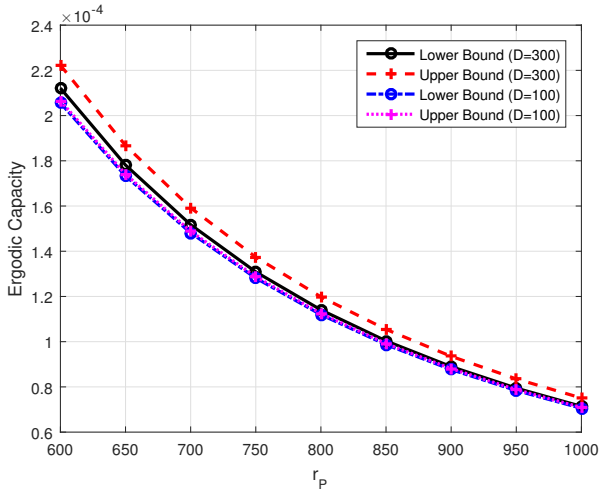

Figure 3.8: Lower and upper bounds for the Ergodic Capacity at the Pico User in PHP networks for different values of D

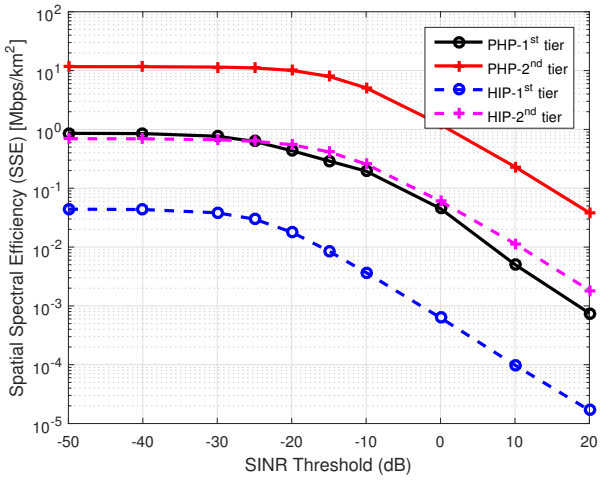

Figure 3.9: Spatial Spectral Efficiency vs. SINR Threshold in the PHP and HIP networks

We showed that the PHP model outperforms HIP, which means that this model can be considered as a theoretical guideline for BS deployment. In fact, PHP can be applied either in network planning or in current HIP networks by making the active BSs follow PHP. Moreover, Ergodic capacity, SSE and EE were derived. Numerical evaluations were presented based on the analytical results, showing better SSE and EE in the Pico tier than in the Macro tier.

Although in general this study encourages to offload traffic from MBSs to the PBSs, this should be cautiously applied because of the effect of the call arrival rate on EE. As depicted in the numerical evaluation section, the EE of the Pico tier falls below that of the Macro tier as the call arrival rate exceeds a certain threshold. This observation reveals that offloading traffic to the PBSs to achieve higher SSE should be done more carefully, especially in energy-constrained networks.

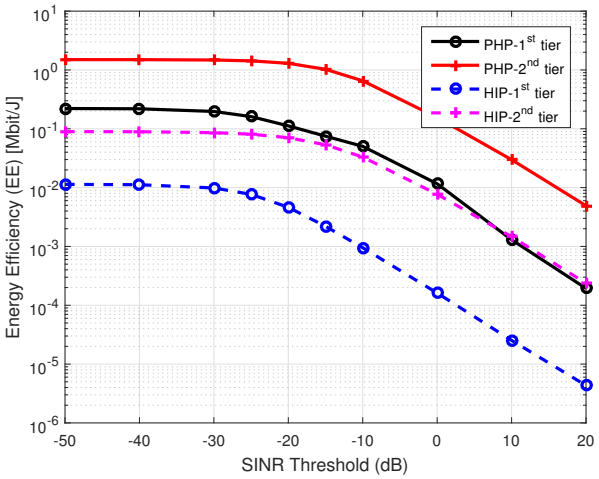

Figure 3.10: Energy Efficiency vs. SINR Threshold in the PHP and HIP networks

Finally, considering different cell association models and investigating their effects on the coverage probability and the other metrics in PHP networks is an interesting open topic for further research.

3.7 Appendices

3.7.1 Proof of Lemma 2

Consider a virtual hole of radius D around serving BS and let $\bar{F}_Y$ be the CCDF of the nearest distance to the cross tier interferer BS. By definition,

$$\begin{aligned}\bar{F}_Y(y|r_*) &= 1 - F_Y(y|r_*) = \mathbb{P}(Y > y|r_*) \\ &= \mathbb{P}(\#\text{ of cross tier interferer BS in } \mathcal{A} = 0|r_*)\end{aligned} \tag{3.51}$$

where $\mathcal{A}$ is the area at distance at least r_* and at most y from the typical user and farther than D from the serving BS. A sketch of area $\mathcal{A}$ in the PHP network is depicted in Fig. 3.11.

To find $\mathcal{A}$, we need to consider both cases, $D \leq 2r_*$ and $D > 2r_*$. Accordingly, we have

$$\begin{aligned}\mathcal{A} =& y^2 \cos^{-1}(a_1) - D^2 \cos^{-1}(a_2) + (D^2 - 2r^{*2}) \cos^{-1}(a_3) \\ &- \frac{D}{2}\sqrt{a_4} + \frac{1}{2}\sqrt{a_5},\end{aligned} \tag{3.52}$$

where a_1 to a_5 are defined in (3.4) through (3.8), respectively. Finally, the PDF is obtained as $f_Y(y|r_*) = -\frac{\partial}{\partial y}\bar{F}_Y(y|r_*)$.

3.7.2 Fully Loaded Networks

By definition, the coverage probability in the k^{th} tier is given by

$$\mathbb{P}(\text{SINR}_k > \tau_k) = \mathbb{P}\left(\frac{\rho_k (1 + r_k)^{-\alpha} S_k}{\hat{I}_k + \sigma^2} > \tau_k\right), \tag{3.53}$$

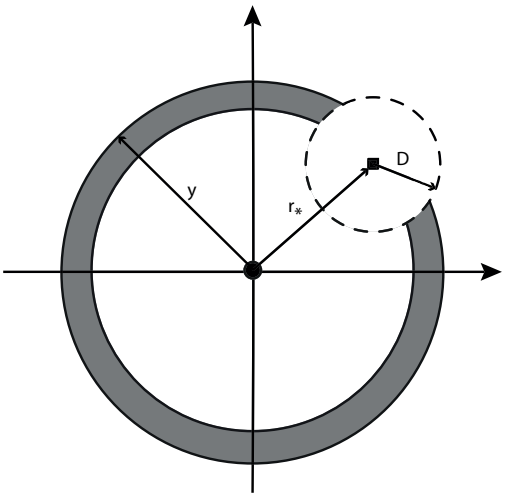

Figure 3.11: A Sketch of area $\mathcal{A}$ in the PHP network

where $S_k \sim \Gamma(K_k - K'_k + 1, 1)$, and r_k represents the distance to the serving BS, i.e., the nearest one in the k^{th} tier.

In fully loaded networks, i.e., $K'_k = K_k$, the distribution of S_k simplifies to the Exponential distribution, i.e., $S_k \sim \text{Exp}(1)$. Therefore,

$$\begin{aligned}
&\mathbb{P}\left(S_k > \frac{\tau_k}{\rho_k}(1+r_k)^{\alpha}\left(\hat{I}_k + \sigma^2\right)\Big| r_k\right) \\
&\quad = \mathbb{E}_{\hat{I}}\left[\mathbb{P}\left(S_k > \frac{\tau_k}{\rho_k}(1+r_k)^{\alpha}\left(\hat{I}_k + \sigma^2\right)\Big| r_k, \hat{I}_k\right)\right] \\
&\quad = \mathbb{E}_{\hat{I}}\left[\exp\left[-\frac{\tau_k}{\rho_k}(1+r_k)^{\alpha}\left(\hat{I}_k + \sigma^2\right)\right]\Big| r_k\right] \qquad (3.54) \\
&\quad = \exp\left[-\frac{\tau_k}{\rho_k}(1+r_k)^{\alpha}\sigma^2\right] \\
&\qquad \cdot \mathbb{E}_{\hat{I}}\left[\exp\left[-\frac{\tau_k}{\rho_k}(1+r_k)^{\alpha}\hat{I}_k\right]\Big| r_k\right] \qquad (3.55) \\
&\quad = \exp\left[-\frac{\tau_k}{\rho_k}(1+r_k)^{\alpha}\sigma^2\right] \cdot \mathcal{L}_{\hat{I}_k|r_k}\left(\frac{\tau_k}{\rho_k}(1+r_k)^{\alpha}\right). \qquad (3.56)
\end{aligned}$$

Since r_k is defined as the distance to the nearest BS of k^{th} tier, we have

$$\begin{aligned}
\mathbb{P}(\text{SINR}_k > \tau_k) = \int_{r_k>0} &2\pi\lambda_k r_k e^{-\pi\lambda_k r_k^2} \\
&\cdot e^{-\frac{\tau_k}{\rho_k}(1+r_k)^{\alpha}\sigma^2} \cdot \mathcal{L}_{\hat{I}_k|r_k}\left(\frac{\tau_k}{\rho_k}(1+r_k)^{\alpha}\right) \mathrm{d}r_k. \qquad (3.57)
\end{aligned}$$

3.7.3 Proof of Theorem 1

By expanding the ergodic capacity definition in (3.27) we have,

$$C_{\text{E}|r} = \mathbb{E}\left[\log_2\left(1 + \frac{\hat{S}}{\sigma^2 + \hat{I}}\right)\Big| r\right]$$

$$\overset{(a)}{=}\mathbb{E}\left[\int_0^\infty \frac{e^{-z}}{z}\left(1-\exp\left[-z\cdot\frac{\hat{S}}{\sigma^2+\hat{I}}\right]\right)\mathrm{d}z\middle|r\right] \tag{3.58}$$

$$\overset{(b)}{=}\mathbb{E}\left[\int_0^\infty \frac{e^{-s\left(\sigma^2+\hat{I}\right)}}{s}\cdot\left(1-\exp\left[-s\hat{S}\right]\right)\mathrm{d}s\middle|r\right] \tag{3.59}$$

$$=\mathbb{E}\left[\int_0^\infty \frac{e^{-s\sigma^2}}{s}\cdot\exp\left[-s\hat{I}\right]\cdot\left(1-\exp\left[-s\hat{S}\right]\right)\mathrm{d}s\middle|r\right] \tag{3.60}$$

$$\overset{(c)}{=}\int_0^\infty \frac{e^{-s\sigma^2}}{s}\cdot\mathbb{E}\left[\exp\left[-s\hat{I}\right]\middle|r\right]\cdot\left(1-\mathbb{E}\left[\exp\left[-s\hat{S}\right]\middle|r\right]\right)\mathrm{d}s, \tag{3.61}$$

where (a) is given by [83, Lemma 1] as $\log(1+x)=\int_0^\infty \frac{e^{-z}}{z}(1-e^{-xz})\mathrm{d}z$; (b) is the result of the change of variable $s = z\left(\sigma^2+\hat{I}\right)^{-1}$. Also, (c) comes from taking advantage of signal and interference power independence and of non-negativity of the integrand, the expectation is switched with the integral operation and factorized. Finally, the proof is completed by substitution of the Laplace transform definition.

3.7.4 Proof of Lemma 3

Given the distances to the serving PBS and the nearest MBS, which represents the nearest hole center, the Laplace transform of the aggregate interference experienced by the typical PU is obtained by substituting (3.24) in the Laplace transform definition. Therefore, we have

$$\mathcal{L}_{\hat{I}_P|r_P,y}(s)=\mathbb{E}\left[\exp\left[-s\Big(\rho_M\sum_{\eta\in\Phi_M}\sum_{n=1}^{K'_M}|\mathbf{g}_{i\eta}^{\mathsf{H}}\mathbf{w}_{n\eta}|^2 + \rho_P\sum_{\zeta\in\tilde{\Phi}_P\setminus r_P}\sum_{n=1}^{K'_P}|\mathbf{g}_{i\zeta}^{\mathsf{H}}\mathbf{w}_{n\zeta}|^2\Big)\right]\right] \tag{3.62}$$

$$\overset{(a)}{=}\mathbb{E}_{\Phi_M,\tilde{\Phi}_P}\left[\mathbb{E}_{I_{PM}^{\eta},I_{PP}^{\zeta}}\left[\prod_{\eta\in\Phi_M}\exp\left[-s\rho_M(1+x_\eta)^{-\alpha}I_{PM}^{\eta}\right]\cdot\prod_{\zeta\in\tilde{\Phi}_P\setminus r_P}\exp\left[-s\rho_P(1+x_\zeta)^{-\alpha}I_{PP}^{\zeta}\right]\right]\right] \tag{3.63}$$

$$\overset{(b)}{\geq}\mathbb{E}_{\Phi_M}\left[\prod_{\eta\in\Phi_M}\mathbb{E}_{I_{PM}^{\eta}}\left[\exp\left[-s\rho_M(1+x_\eta)^{-\alpha}I_{PM}^{\eta}\right]\right]\right]\cdot\mathbb{E}_{\Phi_P}\left[\prod_{\zeta\in\Phi_P\setminus r_P\setminus C_{y,D}}\mathbb{E}_{I_{PP}^{\zeta}}\left[\exp\left[-s\rho_P(1+x_\zeta)^{-\alpha}I_{PP}^{\zeta}\right]\right]\right] \tag{3.64}$$

$$\overset{(c)}{=}\mathbb{E}_{\Phi_M}\left[\prod_{\eta\in\Phi_M}\left(1+s\rho_M(1+x_\eta)^{-\alpha}\right)^{-K'_M}\right]$$

$$\cdot \mathbb{E}_{\Phi_P}\left[\prod_{\zeta\in\Phi_P\setminus r_P\setminus C_{y,D}}\left(1+s\rho_P(1+x_\zeta)^{-\alpha}\right)^{-K'_P}\right] \tag{3.65}$$

$$\stackrel{(e)}{=} \left(1+s\rho_M(1+y)^{-\alpha}\right)^{-K'_M}$$
$$\cdot \mathbb{E}_{\Phi_M}\left[\prod_{\eta\in\Phi_M\setminus y}\left(1+s\rho_M(1+x_\eta)^{-\alpha}\right)^{-K'_M}\right]$$
$$\cdot \mathbb{E}_{\Phi_P}\left[\prod_{\zeta\in\Phi_P\setminus r_P\setminus C_{y,D}}\left(1+s\rho_P(1+x_\zeta)^{-\alpha}\right)^{-K'_P}\right] \tag{3.66}$$

$$\stackrel{(f)}{=} \left(1+s\rho_M(1+y)^{-\alpha}\right)^{-K'_M}$$
$$\cdot \exp\left[-\lambda_M\int_{\mathbb{R}^2\setminus C_{0,y}}\left(1-\left(1+s\rho_M(1+x_\eta)^{-\alpha}\right)^{-K'_M}\right)\mathrm{d}x_\eta\right]$$
$$\cdot \exp\left[-\lambda_P\int_{\substack{\mathbb{R}^2\setminus C_{0,r_P}\\ \setminus C_{y,D}}}\left(1-\left(1+s\rho_P(1+x_\zeta)^{-\alpha}\right)^{-K'_P}\right)\mathrm{d}x_\zeta\right] \tag{3.67}$$

$$= \left(1+s\rho_M(1+y)^{-\alpha}\right)^{-K'_M}$$
$$\cdot \exp\left[\lambda_M\cdot\mathcal{G}\left(s,y,\alpha,\rho_M,K'_M\right)\right]$$
$$\cdot \exp\left[-\lambda_P\left(\int_{\mathbb{R}^2\setminus C_{0,r_P}}\left(1-\left(1+s\rho_P(1+x_\zeta)^{-\alpha}\right)^{-K'_P}\right)\mathrm{d}x_\zeta\right.\right.$$
$$\left.\left.-\int_{C_{y,D}}\left(1-\left(1+s\rho_P(1+x_\zeta)^{-\alpha}\right)^{-K'_P}\right)\mathrm{d}x_\zeta\right)\right] \tag{3.68}$$

$$= \left(1+s\rho_M(1+y)^{-\alpha}\right)^{-K'_M}$$
$$\cdot \exp\left[\lambda_M\cdot\mathcal{G}\left(s,y,\alpha,\rho_M,K'_M\right)+\lambda_P\cdot\mathcal{G}\left(s,r_P,\alpha,\rho_P,K'_P\right)\right]$$
$$\cdot \exp\left[\lambda_P\int_{C_{y,D}}\left(1-\left(1+s\rho_P(1+x_\zeta)^{-\alpha}\right)^{-K'_P}\right)\mathrm{d}x_\zeta\right]. \tag{3.69}$$

Where (a) comes from (3.25) and (b) is the result of modeling PHP by carving out just the nearest hole and overestimating the interference. Besides, (c) is obtained from the definition of the Laplace transform for Gamma distribution. In (e), we extract the interference term caused by the MBS located at the known distance of y. Moreover, (f) follows the generating functional of PPP, Φ_M, Φ_P. The proof is completed by substitution of $g(s,y)$ in (3.69).

3.7.5 Proof of Lemma 4

In this Lemma, the location of the serving BS is exactly the center of the closest hole to the typical user. Therefore, given the distance to the nearest

MBS, similar to the previous proof we have

$$\mathcal{L}_{\hat{I}_M|r_M}(s) = \mathbb{E}\left[\exp\left[-s\Big(\rho_M \sum_{\eta\in\Phi_M\setminus r_M}\sum_{n=1}^{K'_M}|\mathbf{g}_{i\eta}^{\mathsf{H}}\mathbf{w}_{n\eta}|^2 + \rho_P \sum_{\zeta\in\tilde{\Phi}_P}\sum_{n=1}^{K'_P}|\mathbf{g}_{i\zeta}^{\mathsf{H}}\mathbf{w}_{n\zeta}|^2\Big)\right]\right] \tag{3.70}$$

$$= \mathbb{E}_{\Phi_M,\tilde{\Phi}_P}\left[\mathbb{E}_{I^{\eta}_{MM},I^{\zeta}_{MP}}\left[\prod_{\eta\in\Phi_M\setminus r_M}\exp\left[-s\rho_M(1+x_\eta)^{-\alpha}I^{\eta}_{MM}\right] \cdot \prod_{\zeta\in\tilde{\Phi}_P}\exp\left[-s\rho_P(1+x_\zeta)^{-\alpha}I^{\zeta}_{MP}\right]\right]\right] \tag{3.71}$$

$$\geq \mathbb{E}_{\Phi_M}\left[\prod_{\eta\in\Phi_M\setminus r_M}\mathbb{E}_{I_{MM}}\left[\exp\left[-s\rho_M(1+x_\eta)^{-\alpha}I_{MM}\right]\right]\right] \cdot \mathbb{E}_{\Phi_P}\left[\prod_{\zeta\in\Phi_P\setminus C_{r_M,D}}\mathbb{E}_{I^{\zeta}_{MP}}\left[\exp\left[-s\rho_P(1+x_\zeta)^{-\alpha}I^{\zeta}_{MP}\right]\right]\right] \tag{3.72}$$

$$= \mathbb{E}_{\Phi_M}\left[\prod_{\eta\in\Phi_M\setminus r_M}\left(1+s\rho_M(1+x_\eta)^{-\alpha}\right)^{-K'_M}\right] \cdot \mathbb{E}_{\Phi_P}\left[\prod_{\zeta\in\Phi_P\setminus C_{y,D}}\left(1+s\rho_P(1+x_\zeta)^{-\alpha}\right)^{-K'_P}\right] \tag{3.73}$$

$$= \exp\left[-\lambda_M\int_{\mathbb{R}^2\setminus C_{0,r_M}}\left(1-\left(1+s\rho_M(1+x_\eta)^{-\alpha}\right)^{-K'_M}\right)\mathrm{d}x_\eta\right] \cdot \exp\left[-\lambda_P\int_{\mathbb{R}^2\setminus C_{0,r_M}\setminus C_{r_M,D}}\left(1-\left(1+s\rho_P(1+x_\zeta)^{-\alpha}\right)^{-K'_P}\right)\mathrm{d}x_\zeta\right] \tag{3.74}$$

$$= \exp\left[\lambda_M\cdot\mathcal{G}\left(s,r_M,\alpha,\rho_M,K'_M\right)\right] \cdot \exp\left[-\lambda_P\left(\int_{\mathbb{R}^2\setminus C_{0,r_M}}\left(1-\left(1+s\rho_P(1+x_\zeta)^{-\alpha}\right)^{-K'_P}\right)\mathrm{d}x_\zeta - \int_{C_{r_M,D}}\left(1-\left(1+s\rho_P(1+x_\zeta)^{-\alpha}\right)^{-K'_P}\right)\mathrm{d}x_\zeta\right)\right]$$

$$= \exp\left[\lambda_M\cdot\mathcal{G}\Big(s,r_M,\alpha,\rho_M,K'_M\Big)+\lambda_P\cdot\mathcal{G}\Big(s,r_M,\alpha,\rho_P,K'_P\Big)\right] \cdot \exp\left[2\lambda_P\int_{\max\{0,r_M-D\}}^{r_M+D}\cos^{-1}\left(\max\left\{-1,\frac{t^2+r_M^2-D^2}{2r_Mt}\right\}\right)\cdot\left(1-\left(1+s\rho_P(1+t)^{-\alpha}\right)^{-K'_P}\right)t\,\mathrm{d}t\right] \tag{3.75}$$

3.7.6 Proof of Lemma 5

In this Lemma, the interference power is underestimated by carving out each hole separately inattentive to possible overlaps. Thus, given the distance to the serving PBS, r_P, the Laplace transform of the aggregate interference experienced by the typical PU is

$$\mathcal{L}_{\hat{I}_P|r_P}(s) = \mathbb{E}\left[\exp\left[-s\left(\rho_M \sum_{\eta\in\Phi_M}\sum_{n=1}^{K'_M}|\mathbf{g}_{i\eta}^{\mathsf{H}}\mathbf{w}_{n\eta}|^2 + \rho_P \sum_{\zeta\in\tilde{\Phi}_P\setminus r_P}\sum_{n=1}^{K'_P}|\mathbf{g}_{i\zeta}^{\mathsf{H}}\mathbf{w}_{n\zeta}|^2\right)\right]\right] \tag{3.76}$$

$$= \mathbb{E}\left[\prod_{\eta\in\Phi_M}\mathbb{E}_{I_{PM}}\left[\exp\left[-s\rho_M(1+x_\eta)^{-\alpha}I_{PM}^{\eta}\right]\right]\right] \cdot \mathbb{E}\left[\prod_{\zeta\in\tilde{\Phi}_P\setminus r_P}\mathbb{E}_{I_{PP}^{\zeta}}\left[\exp\left[-s\rho_P(1+x_\zeta)^{-\alpha}I_{PP}^{\zeta}\right]\right]\right] \tag{3.77}$$

$$= \mathbb{E}_{\Phi_M}\left[\prod_{\eta\in\Phi_M}\left(1+s\rho_M(1+x_\eta)^{-\alpha}\right)^{-K'_M}\right] \cdot \mathbb{E}_{\Phi_M,\Phi_P}\left[\prod_{\zeta\in\Phi_P\setminus r_P\setminus\mathcal{B}}\left(1+s\rho_P(1+x_\zeta)^{-\alpha}\right)^{-K'_P}\right] \tag{3.78}$$

$$= \mathbb{E}_{\Phi_M}\left[\prod_{\eta\in\Phi_M}\left(1+s\rho_M(1+x_\eta)^{-\alpha}\right)^{-K'_M}\right] \cdot \mathbb{E}_{\Phi_M}\left[\exp\left[-\lambda_P\left(\int_{\mathbb{R}^2\setminus C_{0,r_P}}\left(1-\left(1+s\rho_P(1+x_\zeta)^{-\alpha}\right)^{-K'_P}\right)\mathrm{d}x_\zeta - \int_{\mathcal{B}}\left(1-\left(1+s\rho_P(1+x_\zeta)^{-\alpha}\right)^{-K'_P}\right)\mathrm{d}x_\zeta\right)\right]\right] \tag{3.79}$$

$$= \mathbb{E}_{\Phi_M}\left[\prod_{\eta\in\Phi_M}\left(1+s\rho_M(1+x_\eta)^{-\alpha}\right)^{-K'_M}\right] \cdot \exp\left[\lambda_P\cdot\mathcal{G}\left(s,r_P,\alpha,\rho_P,K'_P\right)\right] \cdot \mathbb{E}_{\Phi_M}\left[\exp\left[\lambda_P\left(\int_{\mathcal{B}}\left(1-\left(1+s\rho_P(1+x_\zeta)^{-\alpha}\right)^{-K'_P}\right)\mathrm{d}x_\zeta\right)\right]\right] \tag{3.80}$$

$$\overset{(a)}{\leq} \mathbb{E}_{\Phi_M}\left[\prod_{\eta\in\Phi_M}\left(1+s\rho_M(1+x_\eta)^{-\alpha}\right)^{-K'_M}\right] \cdot \exp\left[\lambda_P\cdot\mathcal{G}\left(s,r_P,\alpha,\rho_P,K'_P\right)\right] \cdot \mathbb{E}_{\Phi_M}\left[\prod_{y\in\Phi_M}\exp\left[\lambda_P\left(\int_{C_{y,D}}\left(1-\left(1+s\rho_P(1+x_\zeta)^{-\alpha}\right)^{-K'_P}\right)\mathrm{d}x_\zeta\right)\right]\right] \tag{3.81}$$

$$
\begin{aligned}
&= \mathbb{E}_{\Phi_M}\left[\prod_{\eta\in\Phi_M}\left(1+s\rho_M(1+x_\eta)^{-\alpha}\right)^{-K'_M}\right] \\
&\cdot\ \exp\left[\lambda_P\cdot\mathcal{G}\left(s,r_P,\alpha,\rho_P,K'_P\right)\right] \\
&\cdot\mathbb{E}_{\Phi_M}\left[\prod_{y\in\Phi_M}\exp\left[2\lambda_P g(s,y)\right]\right] \qquad (3.82)\\
&= \exp\left[\lambda_P\cdot\mathcal{G}\left(s,r_P,\alpha,\rho_P,K'_P\right)\right] \\
&\cdot\mathbb{E}_{\Phi_M}\left[\prod_{y\in\Phi_M}\left(1+s\rho_M(1+y)^{-\alpha}\right)^{-K'_M}\cdot\exp\left[2\lambda_P g(s,y)\right]\right] \qquad (3.83)\\
&= \exp\left[\lambda_P\cdot\mathcal{G}\left(s,r_P,\alpha,\rho_P,K'_P\right)\right] \\
&\cdot\exp\left[-2\lambda_M\int_{\max\{r_P,D-r_P\}}^{\infty}\cos^{-1}\left(\max\left\{-1,-\frac{t^2+r_P^2-D^2}{2tr_P}\right\}\right)\right. \\
&\left.\cdot\left(1-\left(1+s\rho_M(1+t)^{-\alpha}\right)^{-K'_M}\cdot\exp\left[2\lambda_P g(s,t)\right]\right)t\mathrm{d}t\right]. \qquad (3.84)
\end{aligned}
$$

Where the inequality in (a) holds since the union of the holes is substituted by the aggregation of the holes.

3.7.7 Proof of Lemma 6

Similar to the previous proof, here we have

$$
\begin{aligned}
\mathcal{L}_{\hat{I}_M|r_M}(s) &= \mathbb{E}\left[\exp\left[-s\left(\rho_M\sum_{\eta\in\Phi_M\setminus r_M}\sum_{n=1}^{K'_M}|\mathbf{g}_{i\eta}^{\mathsf{H}}\mathbf{w}_{n\eta}|^2\right.\right.\right. \\
&\qquad\left.\left.\left.+\rho_P\sum_{\zeta\in\tilde{\Phi}_P}\sum_{n=1}^{K'_P}|\mathbf{g}_{i\zeta}^{\mathsf{H}}\mathbf{w}_{n\zeta}|^2\right)\right]\right] \qquad (3.85)\\
&= \mathbb{E}\left[\prod_{\eta\in\Phi_M\setminus r_M}\mathbb{E}_{I_{PM}}\left[\exp\left[-s\rho_M(1+x_\eta)^{-\alpha}I_{PM}\right]\right]\right] \\
&\cdot\mathbb{E}\left[\prod_{\zeta\in\tilde{\Phi}_P}\mathbb{E}_{I_{PP}^{\zeta}}\left[\exp\left[-s\rho_P(1+x_\zeta)^{-\alpha}\ I_{PP}^{\zeta}\right]\right]\right] \qquad (3.86)\\
&= \mathbb{E}_{\Phi_M}\left[\prod_{\eta\in\Phi_M\setminus r_M}\left(1+s\rho_M(1+x_\eta)^{-\alpha}\right)^{-K'_M}\right] \\
&\cdot\mathbb{E}_{\Phi_M,\Phi_P}\left[\prod_{\zeta\in\Phi_P\setminus\mathcal{B}}\left(1+s\rho_P(1+x_\zeta)^{-\alpha}\right)^{-K'_P}\right] \qquad (3.87)\\
&= \mathbb{E}_{\Phi_M}\left[\prod_{\eta\in\Phi_M\setminus r_M}\left(1+s\rho_M(1+x_\eta)^{-\alpha}\right)^{-K'_M}\right]
\end{aligned}
$$

$$\cdot \mathbb{E}_{\Phi_M}\left[\exp\left[-\lambda_P\left(\int_{\mathbb{R}^2\setminus C_{0,r_M}}\left(1-\left(1+s\rho_P(1+x_\zeta)^{-\alpha}\right)^{-K'_P}\right)\mathrm{d}x_\zeta - \int_{\mathcal{B}}\left(1-\left(1+s\rho_P(1+x_\zeta)^{-\alpha}\right)^{-K'_P}\right)\mathrm{d}x_\zeta\right)\right]\right] \tag{3.88}$$

$$= \mathbb{E}_{\Phi_M}\left[\prod_{\eta\in\Phi_M\setminus r_M}\left(1+s\rho_M(1+x_\eta)^{-\alpha}\right)^{-K'_M}\right] \cdot \exp\left[\lambda_P\cdot\mathcal{G}\left(s,r_M,\alpha,\rho_P,K'_P\right)\right] \cdot \mathbb{E}_{\Phi_M}\left[\exp\left[\lambda_P\left(\int_{\mathcal{B}}\left(1-\left(1+s\rho_P(1+x_\zeta)^{-\alpha}\right)^{-K'_P}\right)\mathrm{d}x_\zeta\right)\right]\right] \tag{3.89}$$

$$\leq \mathbb{E}_{\Phi_M}\left[\prod_{\eta\in\Phi_M\setminus r_M}\left(1+s\rho_M(1+x_\eta)^{-\alpha}\right)^{-K'_M}\right] \cdot \exp\left[\lambda_P\cdot\mathcal{G}\left(s,r_M,\alpha,\rho_P,K'_P\right)\right] \cdot \mathbb{E}_{\Phi_M}\left[\prod_{y\in\Phi_M}\exp\left[\lambda_P\left(\int_{C_{y,D}}\left(1-\left(1+s\rho_P(1+x_\zeta)^{-\alpha}\right)^{-K'_P}\right)\mathrm{d}x_\zeta\right)\right]\right] \tag{3.90}$$

$$= \mathbb{E}_{\Phi_M}\left[\prod_{\eta\in\Phi_M\setminus r_M}\left(1+s\rho_M(1+x_\eta)^{-\alpha}\right)^{-K'_M}\right] \cdot \exp\left[\lambda_P\cdot\mathcal{G}\left(s,r_M,\alpha,\rho_P,K'_P\right)\right] \cdot \mathbb{E}_{\Phi_M}\left[\prod_{y\in\Phi_M}\exp\left[2\lambda_P g(s,y)\right]\right] \tag{3.91}$$

$$= \mathbb{E}_{\Phi_M}\left[\prod_{\eta\in\Phi_M\setminus r_M}\left(1+s\rho_M(1+x_\eta)^{-\alpha}\right)^{-K'_M}\right] \cdot \exp\left[\lambda_P\cdot\mathcal{G}\left(s,r_M,\alpha,\rho_P,K'_P\right)\right] \cdot \mathbb{E}_{\Phi_M}\left[\prod_{y\in\Phi_M\setminus r_M}\exp\left[2\lambda_P g(s,y)\right]\right]\cdot\exp\left[2\lambda_P g(s,r_M)\right] \tag{3.92}$$

$$= \exp\left[\lambda_P\cdot\mathcal{G}\left(s,r_M,\alpha,\rho_P,K'_P\right)+2\lambda_P g(s,r_M)\right] \cdot \exp\left[-2\pi\lambda_M\int_{r_M}^{\infty}\left(1-(1+s\rho_M(1+t)^{-\alpha})^{-K'_M}\cdot\exp\left[2\lambda_P g(s,t)\right]\right)t\,\mathrm{d}t\right]. \tag{3.93}$$

Chapter 4

Cell Zooming in PVT Random Cellular Networks

In this chapter, we study the Energy Efficiency (EE) and Area Spectral Efficiency (ASE) of green random cellular networks which utilize the Cell Zooming (CZ) techniques. To this aim, using stochastic geometry, we derive a tractable expression for the Ergodic Capacity in a Poisson Voronoi Tessellation (PVT) random cellular network in which both Base Station (BS) and Mobile User (MU) locations are drawn randomly from two independent Poisson Point Processes (PPPs). The performance of this network is examined under different MU densities and two CZ algorithms. Numerical evaluations show that there is an optimum transmission power, which maximizes EE in PVT random cellular networks. On the other hand, increasing the transmission power and the cell size does not improve ASE much more after passing a threshold. The tradeoff between EE and ASE is also presented.

4.1 Introduction

The next generation of mobile communication systems, namely *5G*, intends to improve some characteristics of the previous mobile generations, e.g., data rate, delay and cost in addition to addressing new features, such as ubiquitous coverage, device-to-device (D2D) communications, etc. Besides achieving these goals, realization of *green* 5G is essential for both environmental concerns, such as air pollution and carbon dioxide footprint, and also energy-related costs in the mobile communication industry, which are important for end-users and telecommunication companies as well [26].

In addition, the concept of small cells and random deployment of Base Stations (BSs) in LTE and 5G, e.g., Heterogeneous Network (HetNet), introduced a new area in cellular network planning, named random cellular networks. In this regard, stochastic geometry came up as a novel and helpful technique to deal with these random structures [58].

Recently, random networks have been studied through several aspects in the literature. In [13], stochastic geometry is exploited to propose a useful approach to deal with random cellular networks. Besides, [53] studied spatial spectrum and Energy Efficiency (EE) in a Poisson Voronoi Tessellation

(PVT) random cellular network using a Markov Chain (MC) channel access model. In another work [76], EE and Spatial Spectral Efficiency (SSE) in random MIMO cellular networks have been analyzed.

The approach followed in this work is different from what has been done before, and provides a new expression for ergodic capacity which is less complex to compute and also to simulate.

Cell Zooming (CZ) was introduced in [26] as a technique to reduce energy consumption in cellular networks by fine-tuning the cell size via adaptation of the coverage radius of a BS. Nowadays in the network planning phase, capacity and cell size are assigned statically based on the maximum transmission power corresponding to the estimated peak traffic load. However, the traffic pattern in cellular networks exhibits large fluctuations in both time and space. This characteristic of mobile networks can be used for energy saving purposes through range adaptation techniques [84].

More precisely, CZ is a technique to adjust the BS's coverage area dynamically according to the network traffic load. [85] reported that CZ can decrease total power consumption by approximately 20%. CZ is achieved differently in different scenarios. For instance, when the traffic is low or the users are concentrated around the BS, the transmission power can be reduced without any loss in expected Quality of Services (QoS). As another example, in a low traffic scenario some BSs can be switched off, while the others compensate the coverage holes by increasing their power, a technique called zooming out.

In order to address CZ, techniques such as Coverage Extension Technology (CET) need to be adopted. In fact, CET is not only limited to increasing transmit power, it can also be obtained by relay and cooperative multi-point (CoMP) transmission [26]. Reference [86] gives an overview of the CZ concept.

In another work [87], three algorithms were proposed to implement CZ and their performance in a single cell scenario was studied. The three proposed methods, namely *Continuous*, *discrete* and *fuzzy* CZ algorithms, aim to dynamically adjust the BS transmission power in order to avoid constantly working with maximum power emission. It was shown that all the proposed techniques outperform the traditional approaches, assuming that the location of the users are known or can be obtained by a location detection scheme.

Moreover, up to 57% of the total power in wireless mobile communication is consumed by BSs [88]. Therefore, it seems crucial to find a strategy to reduce the BS power consumption or the number of active BSs. To this aim, turning off the serving macrocells is one of the techniques to improve the power saving efficiency without loss of throughput [89].

To the best of our knowledge, the concept of CZ in random cellular networks, which is the main scope of this work, has not yet been studied. In addition, in this chapter we consider a random distribution of Mobile Users (MUs). To this aim, first we derive an expression for the ergodic capacity and then use it to formulate EE and Area Spectral Efficiency (ASE) in this setting. We finally evaluate our results by numerical methods.

The rest of the chapter is organized as follows. In Section 4.2 the system

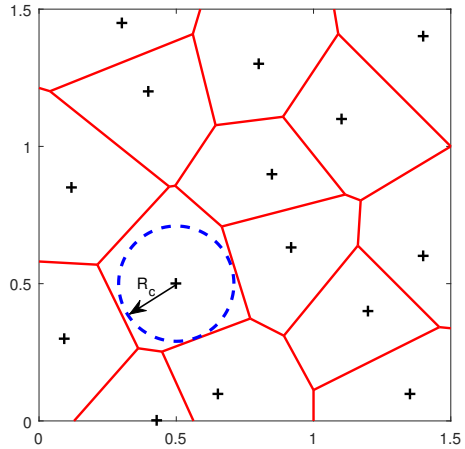

Figure 4.1: An example of PVT Random Cellular Network

model and two CZ algorithms are introduced. Sections 4.3 and 4.4 provide the ergodic capacity and EE and ASE in PVT random cellular networks, respectively. The numerical evaluations are reported in Section 4.5. Finally, Section 4.6 concludes the chapter and discusses some future works.

4.2 System Model

In this work, we focus on downlink transmission in which each MU is associated with its nearest BS. The channel between the transmitter and the receiver is modeled by $\sqrt{(1+r)^{-\alpha}}h$, where $h \sim \mathcal{CN}(0,1)$ is an i.i.d. Rayleigh fading channel coefficient and $(1+r)^{-\alpha}$ represents a non-singular path-loss model; where r and α are the transmission distance and the path-loss exponent, respectively. At the receiver side, there is also AWGN with normalized power σ^2.

Moreover, in our model a PVT random cellular network is considered, where the BSs are located based on a Poisson Point Processes (PPP), called Φ_B, with density λ_B. Each BS forms a circular coverage area of radius $R_c \in \mathcal{R}_c$ around itself. Fig. 4.1 sketches an example of PVT random cellular network with the circular coverage area of radius R_c. $\mathcal{R}_c$ and equivalently $\mathcal{P}_t$, the set of allowed transmission powers, will be defined later based on the CZ scenarios. Also, we assume that MUs are randomly located based on Φ_M, which is a PPP with density λ_M.

In this work, two CZ scenarios will be discussed. In the first case, a discrete CZ is adopted where each cell is divided into N concentric circular zones. Cell partitioning can be done in different ways, for example based on equal distance partition, so that

$$\mathcal{R}_c = \left\{ \frac{D}{N}, \frac{2D}{N}, \ldots, \frac{(N-1)D}{N}, D \right\},$$

where D is the maximum cell radius imposed by the maximum transmitted power of a BS, $P_{\max}$ and the BS density [90]. In this scenario, the set of

allowed transmission powers is

$$\mathcal{P}_t = \left\{ P_{\max}\left(\frac{1}{N}\right)^{\alpha}, P_{\max}\left(\frac{2}{N}\right)^{\alpha}, \ldots, P_{\max} \right\},$$

which satisfies the QoS requirement of the MUs located at the cell edge by keeping the received power at the prescribed level. Alternatively, cell partitioning can also be determined according to an equal power split.

In the second scenario, a general CZ method is considered. In this case, under a low traffic situation, i.e., small MU density, only a subset of the BSs remain active, while the others turn to sleep mode. In this case, we apply the thinning operation to the PPP of the BS distribution [77], which results in a *p-thinned point process* $\tilde{\Phi}_B$ with density

$$\tilde{\lambda}_B = p \cdot \lambda_B, \tag{4.1}$$

where p is the retention probability, i.e., each BS switches off with probability $(1-p)$, independently of the location and of the possibility that any other BS$\in \Phi_B$ switches off or remains active. p can be determined based on the network parameters and the traffic profile.

4.3 Ergodic Capacity

Without loss of generality, by exploiting the PPP characteristics of the BS and MU locations, we can just focus and analyze the behavior of a typical MU located at the origin and its typical BS. Then the obtained results will be generalized to the whole network.

To this aim, the Signal-to-Interference-plus-Noise Ratio, SINR, experienced by the typical MU associated with its nearest BS, BS$_i$, is given by

$$\text{SINR} = \frac{P_t(1+r_i)^{-\alpha}|h_i|^2}{\sum\limits_{j\in\Phi_B\setminus\{i\}} P_t(1+r_j)^{-\alpha}|h_j|^2 + \sigma^2}, \tag{4.2}$$

where the channel coefficient between the typical MU and BS$_\ell$ is denoted by h_ℓ. Note that r_ℓ, which denotes the distance from the typical MU to BS$_\ell$, is a random variable due to the random location of BSs. Besides, it is assumed that all BSs transmit with the same power P_t.

The ergodic capacity is the average rate that is achievable by each user and is given by [79, 80]

$$C = \mathbb{E}\left[\log_2\left(1+\text{SINR}\right)\right]. \tag{4.3}$$

Lemma 7. *The ergodic capacity per user in a PVT random cellular network is given by*

$$\begin{aligned} C = &\int_0^{\infty} \frac{e^{-t\sigma^2}}{t} \\ &\cdot \left(\exp\left[-2\pi\lambda_B \int_{R_c}^{\infty} \left[1 - \frac{1}{1+tP_t(1+r)^{-\alpha}} \right] r\mathrm{d}r \right] \right. \\ &\left. - \exp\left[-2\pi\lambda_B \int_{0}^{\infty} \left[1 - \frac{1}{1+tP_t(1+r)^{-\alpha}} \right] r\mathrm{d}r \right] \right) \mathrm{d}t, \end{aligned} \tag{4.4}$$

where σ^2 is the noise power. Besides, λ_B, R_c and P_t are the BS density, the cell radius and the transmission power, respectively.

Proof. By substitution of Eq. (4.2) in Eq. (4.3), we have

$$
\begin{aligned}
C =& \mathbb{E}_{\Phi_B,\mathbf{h}}\left[\log_2\left(1+\frac{P_t(1+r_i)^{-\alpha}|h_i|^2}{\sum\limits_{j\in\Phi_B\setminus\{i\}} P_t(1+r_j)^{-\alpha}|h_j|^2+\sigma^2}\right)\right] \\
\overset{(a)}{=}& \mathbb{E}_{\Phi_B,\mathbf{h}}\left[\int_0^\infty \frac{e^{-z}}{z}\left(1-\right.\right. \\
& \left.\left.\exp\left(-z\frac{P_t(1+r_i)^{-\alpha}|h_i|^2}{\sum\limits_{j\in\Phi_B\setminus\{i\}} P_t(1+r_j)^{-\alpha}|h_j|^2+\sigma^2}\right)\right)\mathrm{d}z\right] \qquad (4.5) \\
\overset{(b)}{=}& \mathbb{E}_{\Phi_B,\mathbf{h}}\left[\int_0^\infty \frac{e^{-t\sigma^2}}{t}\right. \\
& \cdot\exp\left(-t\sum_{j\in\Phi_B\setminus\{i\}} P_t(1+r_j)^{-\alpha}|h_j|^2\right) \\
& \left.\cdot\left(1-\exp\left(-tP_t(1+r_i)^{-\alpha}|h_i|^2\right)\right)\mathrm{d}t\right] \qquad (4.6) \\
=& \mathbb{E}_{\Phi_B,\mathbf{h}}\left[\int_0^\infty \frac{e^{-t\sigma^2}}{t}\right. \\
& \cdot\left(\exp\left(-t\sum_{j\in\Phi_B\setminus\{i\}} P_t(1+r_j)^{-\alpha}|h_j|^2\right)\right. \\
& \left.\left.-\exp\left(-t\sum_{j\in\Phi_B} P_t(1+r_j)^{-\alpha}|h_j|^2\right)\right)\mathrm{d}t\right] \qquad (4.7) \\
\overset{(c)}{=}& \int_0^\infty \frac{e^{-t\sigma^2}}{t} \\
& \cdot\left(\mathbb{E}_{\Phi_B,\mathbf{h}}\left[\exp\left(-t\sum_{j\in\Phi_B\setminus\{i\}} P_t(1+r_j)^{-\alpha}|h_j|^2\right)\right]\right. \\
& \left.-\mathbb{E}_{\Phi_B,\mathbf{h}}\left[\exp\left(-t\sum_{j\in\Phi_B} P_t(1+r_j)^{-\alpha}|h_j|^2\right)\right]\right)\mathrm{d}t \qquad (4.8) \\
\overset{(d)}{=}& \int_0^\infty \frac{e^{-t\sigma^2}}{t} \\
& \cdot\left(\mathbb{E}_{\Phi_B}\left[\prod_{j\in\Phi_B\setminus\{i\}}\mathbb{E}_{\mathbf{h}}\left[\exp\left(-tP_t(1+r_j)^{-\alpha}|h_j|^2\right)\right]\right]\right. \\
& \left.-\mathbb{E}_{\Phi_B}\left[\prod_{j\in\Phi_B}\mathbb{E}_{\mathbf{h}}\left[\exp\left(-tP_t(1+r_j)^{-\alpha}|h_j|^2\right)\right]\right]\right)\mathrm{d}t \qquad (4.9)
\end{aligned}
$$

$$\overset{(e)}{=} \int_0^\infty \frac{e^{-t\sigma^2}}{t} \cdot \left(\mathbb{E}_{\Phi_B} \left[\prod_{j \in \Phi_B \setminus \{i\}} \frac{1}{1 + tP_t(1 + r_j)^{-\alpha}} \right] - \mathbb{E}_{\Phi_B} \left[\prod_{j \in \Phi_B} \frac{1}{1 + tP_t(1 + r_j)^{-\alpha}} \right] \right) \mathrm{d}t. \tag{4.10}$$

Where (a) comes from Lemma 1 of [83], which states that $\log(1 + x) = \int_0^\infty \frac{e^{-z}}{z}(1 - e^{-xz})\mathrm{d}z$. The change of variable $t = z \left(\sum_{j \in \Phi_B \setminus \{i\}} P_t (1 + r_j)^{-\alpha} |h_j|^2 + \sigma^2 \right)^{-1}$ gives (b). In (c), the expectation and integral can be interchanged since the integrand is non-negative. Then, (d) and (e) follow from independence of the PPP Φ_B and Rayleigh channel fading property. The final result is obtained by using the probability generating functional of a PPP Φ with density λ, given by

$$\mathbb{E}_\Phi \left[\prod_{x \in \Phi} f(x) \right] = \exp \left(-\lambda \iint_{\mathbb{R}^2} (1 - f(x)) \, \mathrm{d}x \right).$$

□

To use the result of the previous lemma in the CZ framework, we just need to substitute the proper BS density, λ_B, transmission power, $P_t \in \mathcal{P}_t$, and cell radius, $R_c \in \mathcal{R}_c$.

Compared to the other works [13]- [53] which derived the ergodic capacity in random networks, the approach and final expression in Eq. (4.4) is more tractable and less complex to simulate in MATLAB and Mathematica. This result also takes advantage of stochastic geometry to reduce the simulation time compared to the conventional Monte-Carlo method.

4.4 Energy and Area Spectral Efficiency (EE & ASE)

In this section, we investigate the performance of the CZ scenarios in random cellular networks in terms of EE and ASE.

Along the lines of [80, 91], ASE is formulated as

$$\mathrm{ASE} = \lambda_M \cdot C, \tag{4.11}$$

where λ_M and C are the MU density and the ergodic capacity of each user, respectively. Note that since we consider a random distribution for the users, we substitute the ratio of the total number of active users over the cell area with the MU density.

Additionally, the EE of an active BS can be expressed as

$$\mathrm{EE} = \frac{WLC}{aP_t + P_c}, \tag{4.12}$$

where W, L account for the spectral bandwidth and the total number of active users in a cell. Besides, in the denominator of Eq. (4.12), P_c denotes the non-transmission related power consumption, which corresponds to the hardware

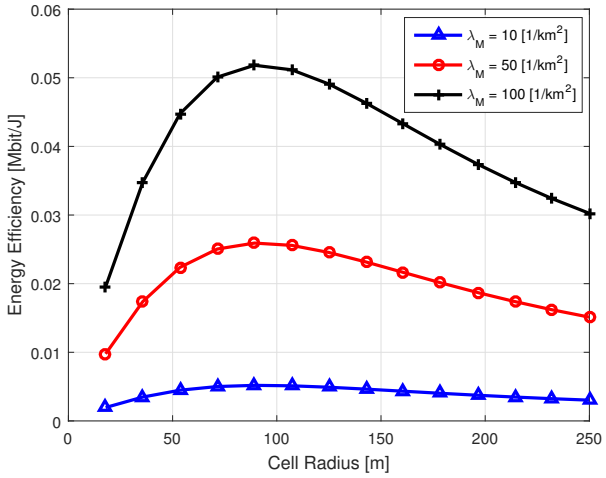

Figure 4.2: Energy efficiency of a PVT random cellular network for different user densities

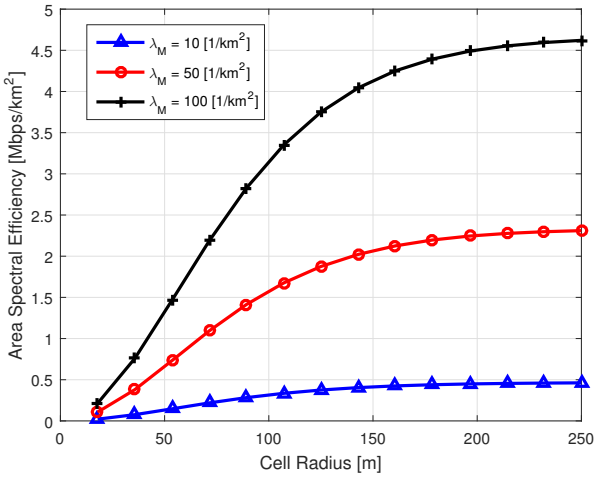

Figure 4.3: Area spectral efficiency of a PVT random cellular network for different user densities

power consumption such as electronic circuits, processors, air-conditioners, rectifiers and backup batteries [80]. Also, $a \geq 1$ represents a scaling factor to compensate for the difference between consumed and radiated power, which is caused by internal losses, like the feeders.

4.5 Performance Evaluation and Numerical Results

In this section, we evaluate the performance of a green PVT random cellular network in terms of EE and ASE while adopting the CZ techniques. The system parameters are summarized in Table 4.1. Note that considering EE or ASE individually does not give a comprehensive overview about the network

Table 4.1: Network Parameters

N	15
α	3
a	1.5
σ^2	−50 [dBm]
$P_{\max}$	44.77 [dBm]
W	0.1 [MHz]
λ_B	1 [/km^2]
λ_M	10 [/km^2]

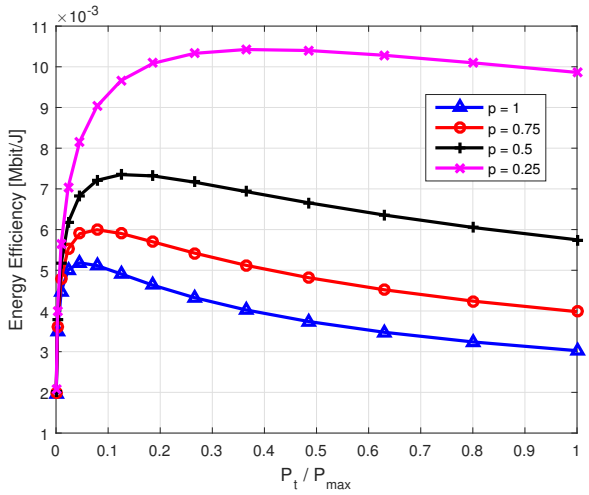

Figure 4.4: Energy efficiency of a PVT random cellular network for different retention probabilities

performance, since there is a tradeoff between the two metrics.

First, the EE of the network for different MU densities is depicted in Fig. 4.2. As shown, in general the EE improves by increasing the number of active users, since more MUs can be served with the same power transmission level. However, for a fixed λ_M, there is an optimum cell radius which maximizes EE. The reason is that, although a larger cell size causes higher ergodic capacity, on the other hand more transmission power is needed in this case to satisfy the QoS requirements for the MUs located at the cell edge.

Furthermore, Fig. 4.3 shows that ASE grows monotonically with the MU density and the cell radius, however, it almost saturates when the transmission power approaches its maximum value.

Figs. 4.4 and 4.5 illustrate the effect of the second CZ scenario for a PVT random cellular network. Note that we assumed that there are enough resources to serve the MUs even when decreasing the number of active BSs. As mentioned in Eq. (4.1), $\tilde{\lambda}_B$ is proportional to the retention probability, i.e., decreasing p reduces the number of active BSs which serve the specific num-

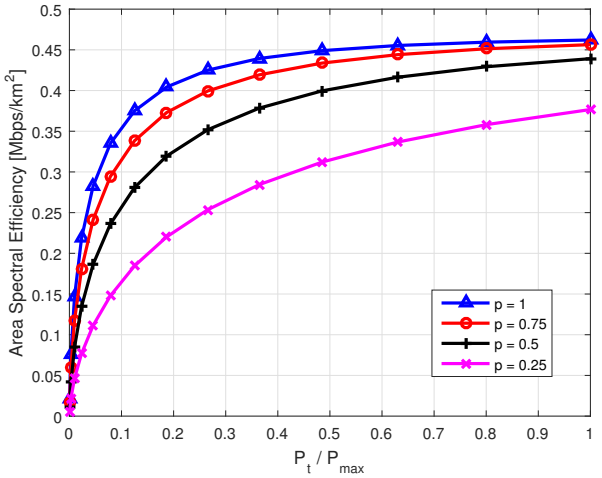

Figure 4.5: Area spectral efficiency of a PVT random cellular network for different retention probabilities

ber of users. Therefore, EE improves as p decreases. Note that in this work we consider a constant retention probability in order to study the performance in a simple scenario. Obviously, more elaborated thinning operation can enhance the results and opens a new direction for future works.

Although reducing the BS density improves EE, it degrades ASE as presented in Fig. 4.5. It is also shown that the higher the BS density the faster the saturation of ASE.

As a significant result of this chapter, Figs. 4.6 and 4.7 illustrate the tradeoff between EE and ASE, revealing that improving ASE does not always accompany with an EE enhancement. In fact, concavity of the curves proves the existence of an optimum point in tradeoff between EE and ASE. In other words, after passing through the curve's peaks, increasing ASE degrades EE. Besides, it can be observed that this happens approximately when ASE approaches its saturation region. The result of this figure gives a useful perspective for network planning. In addition, Figs. 4.6 and 4.7 demonstrate that as long as there are enough resources to serve the active users, it is worth reducing the number of working BSs, a result that could not have been obtained easily by individual analysis of the ASE and the EE.

4.6 Conclusion

In this work, we investigated the energy and area spectral efficiency in a PVT random cellular network which utilizes cell zooming techniques in transmission strategy. To this aim, using stochastic geometry, we derived a novel expression for the ergodic capacity in random networks, which is less complex and faster to simulate compared to the ones proposed before. Two CZ algorithms have been considered in this work.

Numerical evaluations showed that there is an optimum cell radius, and equivalently a transmission power, which maximizes EE. Besides, they re-

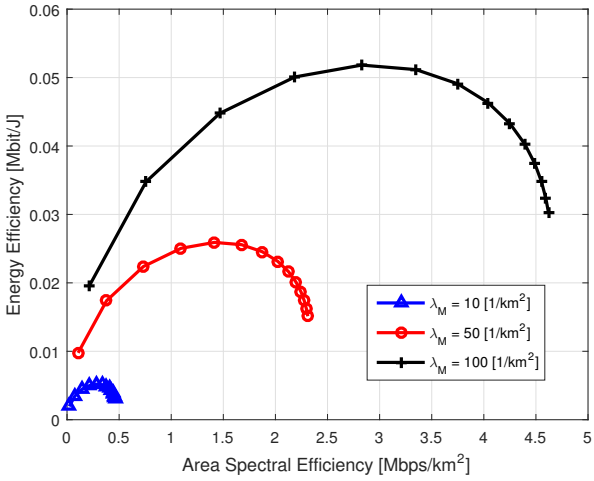

Figure 4.6: Tradeoff between energy and area spectral efficiency of a PVT random cellular network for different BS Densities

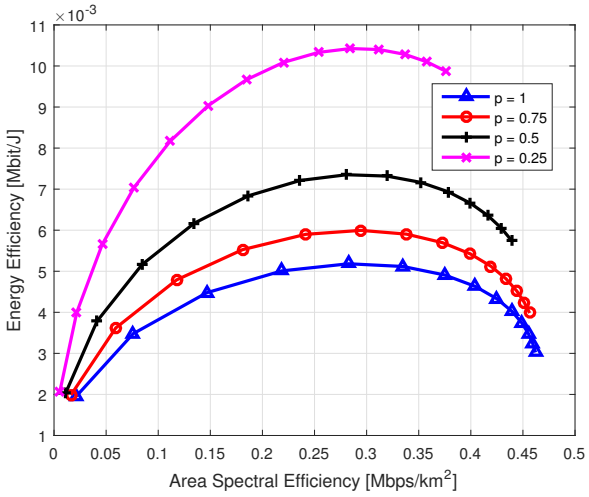

Figure 4.7: Tradeoff between energy and area spectral efficiency of a PVT random cellular network for different retention probabilities

vealed that by adopting the CZ algorithm based on the thinned point process, as the number of active BSs decreases EE increases and ASE degrades. Also, the tradeoff between EE and ASE was demonstrated and the results showed that as long as there are enough resources to serve the MUs, the CZ technique based on the thinned point process provides some gains.

As future work, the effect of other CZ techniques in random cellular networks can be investigated. Also, the concept of random MIMO cellular network and different types of infrastructures are interesting items for future investigation. In addition, more precise thinning and retention probability models are an interesting topic for future works.

Chapter 5

Cell Zooming and Energy Harvesting

In this chapter, we study the performance of $K-$tier heterogeneous random cellular networks (HetNets) in terms of Energy Efficiency (EE) and Spectral Efficiency (SE). In order to improve efficiency, two Cell Zooming (CZ) techniques, namely telescopic and ON/OFF schemes, are applied to these networks. Accordingly, we investigate multi-tier HetNets in which the Base Stations gather their required energy from the environment. Therefore, two important concepts in green cellular networks, namely CZ and Energy Harvesting (EH), are addressed in this work. Subsequently, numerical results show the performance improvement in terms of the coverage and blocking probabilities in addition to EE and SE.

5.1 Introduction

The notions of random cellular networks and small cell networks (SCNs) have emerged as a viable solution to fulfill the requirements of fifth generation mobile communication systems, *5G*, such as high capacity and ubiquitous coverage. Besides, some other new features in 5G such as machine-to-machine (M2M) and device-to-device (D2D) communications are intrinsically based on random networks. In this regard, random network studies have recently become a hot research topic and are usually investigated through a powerful mathematical tool, named Stochastic Geometry [10, 12, 42, 58].

In such networks, low power Base Stations (BSs) play an important role. As a matter of fact, in small cell BSs (SCBSs) short communication distances and simpler baseband processing require lower transmission power and less circuit (and processing) power consumption, respectively [38]. Therefore, energy consumption of a BS in dense SCNs is much less than in present Macro-cell BSs (MBSs). Reportedly, about 10% of the total power in a MBS is consumed for air conditioning or cooling, which can be significantly reduced in SCBSs [38, 92].

Notice that, to fulfill the capacity and coverage requirements, dense deployment of the SCBSs is inevitable. Consequently, the total power consumption of the network would still be high. Hence, investigating efficient

ways to control and possibly reduce power consumption in such networks is essential.

In particular, green communications addresses environmental concerns, for instance, carbon dioxide footprint. Therefore, gathering energy from renewable, clean and free resources such as sun, wind and geo-thermal heat or ambient Radio Frequency (RF) signals in both BSs and Mobile Users (MUs) is a promising technique in this regard [93]. Although there are several reasons which may prevent the practical use of Energy Harvesting (EH) in current high-power MBSs (e.g., the low efficiency of the harvesting devices and the innate uncertainties of the EH sources), its ability to run low-power BSs, e.g., Pico-BSs (PBSs) or Femto-BSs (FBSs), has been recently demonstrated in the literature [38, 94], where it was shown that a 20% reduction of the CO2 emissions of the communication industry may be obtained by using EH techniques [95]. In addition, in a random deployment of SCBSs, e.g., according to a Poisson Point Process (PPP), it might happen that some SCBSs have no easy access to the power grid and in this case EH is a practical solution to feed these BSs.

In [38], a hybrid solar-wind EH technique was studied. Note that, in practice, EH is implementable only if the harvested energy is sufficient and cost-effective. For example, the Center for White Space Communications designed a renewable energy wireless BS, called WindFi, which is able to achieve 99.98% reliability in rural communities using only harvested solar and/or wind power [96].

Although the high level of co-channel interference is one of the major constraints in ultra-dense SCNs, it can be exploited for EH purposes. Hence, the feasibility of ambient RF energy harvesting in such networks was investigated in [94]. A mixture of on-grid SCBSs, powered by the electrical grid, and off-grid SCBSs, powered by EH, was considered in that work. Besides, validation of the proposed model and optimization of the corresponding portion of on-grid and off-grid SCBSs were demonstrated through numerical results.

Particularly, [42] studied a $K-$tier Heterogeneous Cellular Network (HetNet) where the BSs are powered by EH modules only. Considering the stochastic energy arrival process and using other parameters of the network, an achievable *Availability region* has been characterized, so that lying in this region guarantees no performance degradation due to unreliable energy sources.

Similarly, in the current study we assume that all the required energy in the network is supplied by EH from the environment. Besides, we suppose that the BSs are equipped with finite size batteries. Although, to improve reliability, one can suggest that some tiers should be connected to the power grid and serve the users without any EH constraint, this assumption degrades the Energy Efficiency (EE) of the network and is beyond the scope of this work. Furthermore, we will demonstrate the reliability of the proposed model through numerical evaluations based on the availability proof [42].

Recently, Cell Zooming (CZ) techniques have been proposed to achieve cost-effectiveness and EE in green cellular networks [**?**, 26, 80, 97]. Although

the traffic pattern reveals an intense fluctuation in the spatial and temporal domains, in present cellular networks the size and capacity of each cell are fixed and determined based on the peak traffic load. Therefore, CZ can be fulfilled, for example, by adjusting the coverage area of a BS or fine-tuning the cell size and transmission power based on the traffic pattern or other constraints in the network. It has been reported that about 20% power consumption reduction is achieved by CZ [85]. For example, in a low traffic scenario, a BS can shrink the coverage area by reducing its transmission power or offload the traffic to the nearby BSs and then shut off.

In [87], CZ is implemented through different techniques, namely *continuous*, *discrete* and *fuzzy* CZ algorithms which proposed special transmission policies in order to avoid transmitting with maximum power corresponding to the peak traffic load. Conditioned on the given user locations, the advantage of the proposed schemes over the traditional approach has been shown.

Another CZ technique is known as ON/OFF scheme which has been shown to improve the power saving efficiency without loss of throughput [89]. As a matter of fact, BSs consume up to 57% of the total power in cellular networks [88]. Therefore, the ON/OFF scheme is conjectured to have a strong impact on reducing the total power consumption.

To the best of our knowledge, the concept of CZ was mostly studied in traditional hexagonal cellular networks. However, in [97], CZ in a Poisson Voronoi Tessellation (PVT) random cellular network has been investigated. As an extension of [97], in this work we study EE and Spatial Spectral Efficiency (SSE) in $K-$tier HetNets. Besides, we propose an EH framework and investigate the effect of CZ on these networks.

5.1.1 Contributions and Remarks

In this subsection, we highlight the main goals and summarize the contributions and the results achieved in this work.

The original novelty of this chapter is to introduce Cell Zooming (CZ) as a viable approach toward Green communication in randomly structured cellular networks, known as HetNets. Our primary purpose is to investigate EE and SE in a green communication framework, thereby addressing one of the major concerns in 5G. Consequently, we aim to propose a technique which keeps the network efficient despite the changing nature of wireless networks, e.g., fluctuation in traffic pattern or weather changes in EH-based networks. To this aim, we adopt two CZ schemes, namely telescopic and ON/OFF schemes, and study their effects on a $K-$tier network scenario.

First, we study $K-$tier HetNets in which BSs are only powered by EH. In fact, this scenario justifies the assumption of independent thinning process proposed in the previous chapter. Although a general model for such networks has been developed in [42], in this work we focus on SSE and EE and provide performance comparison between this model and a non-EH unbiased network. Derivations of coverage, retention and blocking probabilities with respect to the telescopic CZ scheme, are the other interesting intermediate results obtained towards the final expression for the SSE and EE.

In the best case, in past studies it was shown that under specific conditions, no performance loss would occur in EH-based HetNets [42]. We will show that, in addition, the network functionality improves in terms of coverage and blocking probabilities, EE and SSE. In fact, the network performance can be enhanced while reducing the energy consumption, by applying joint telescopic and ON/OFF CZ schemes in EH-based HetNets, which is the most significant achievement of this work and has not been considered before.

The rest of this chapter is organized as follows. In Section 5.2, the system model will be introduced. The $K-$tier HetNet with EH modules, will be investigated in Section 5.3. Then, Section 5.4 evaluates the performance of the proposed model and discusses numerical results, and Section 5.5 concludes the chapter.

5.2 System Model

In this piece of work, which is the extension of the previous chapter and the work reported in [97], we investigate $K-$tier Heterogeneous Random Cellular Networks (HetNets) which leverage Energy Harvesting (EH) to feed Base Stations (BSs). Moreover, each scenario utilizes two Cell Zooming (CZ) techniques.

In these networks, the locations of the BSs in each tier follow an independent homogeneous Poisson Point Process (PPP), called Φ_k, of density λ_k for $k = 1, 2, \ldots, K$. Besides, the Mobile Users (MUs) locations are drawn from another independent PPP, Φ_u, with density λ_u.

As mentioned, two CZ techniques are adopted in this work. In the first case, namely the telescopic scheme, the coverage area of the cells is adjustable. To this aim, different techniques can be applied, for instance, tuning the cell radius by controlling the power emission or adjusting a bias factor for the received power [12].

In the second technique, called ON/OFF scheme, only a portion of the BSs remain active. For example, those BSs that only have a light traffic demand and are able to offload their traffic to the nearby BSs, switch off. To model the active BS locations in the k^{th} tier, we exploit the *$p-$thinned point process*, $\Phi_k^{(a)}$, of density [10, 77]

$$\lambda_k^{(a)} = \rho_k \cdot \lambda_k, \tag{5.1}$$

where ρ_k is called the retention probability, i.e., each BS in the k^{th} tier switches off with probability $(1 - \rho_k)$, independently of the location and of the possibility that any other BS$\in \Phi_k$, for $k = 1, 2, \ldots, K$, switches off or remains active. ρ_k can be determined based on the network parameters and the traffic profile. This parameter is also named as *availability* in [42].

Note that, since we focus on downlink transmission, according to Slivnyak's theorem [77] and without loss of generality, we study a typical MU located at the origin and then generalize the results to the whole network.

To model propagation, in this work we consider Rayleigh fading along with the path-loss model. Therefore, the received Signal-to-Interference-plus-

Noise Ratio (SINR) at the typical MU served by BS_j located at $x_j \in \Phi_k^{(a)}$ is given by

$$\mathrm{SINR}_k = \frac{P_k |h_j|^2 \|x_j\|^{-\alpha}}{\sum_{\ell=1}^{K} \sum_{x_z \in \Phi_\ell^{(a)} \setminus x_j} P_\ell |h_z|^2 \|x_z\|^{-\alpha} + \sigma^2}\,, \tag{5.2}$$

where $h_{(\cdot)} \sim \mathcal{CN}(0,1)$ is the fading channel coefficient between $\mathrm{BS}_{(\cdot)}$ and the typical MU located at the origin, and $\alpha > 2$ and σ^2 are the path-loss exponent and the normalized power of AWGN at the receiver, respectively.

In this work, network operation is studied on two time scales, namely *short* and *long time scales*. The former deals with the instantaneous transmission and scheduling, which takes in the order of a block duration. On the other hand, long time scale is related to the BS operational mode (ON or OFF), and cell association, and takes a longer time in order to avoid the "ping-pong effect" due to unnecessary handovers [12]. Therefore, we simply assume that a BS mode remains unchanged during the short time scale.

5.3 Network Metrics

In order to apply the telescopic CZ scheme, as in [12] we assume a specific bias multiplier for the received signal power from the BSs of each tier, called CZ factor, $B_k \geq 1$, for $k = 1, 2, \ldots, K$. The advantage of using the CZ factor technique is that a user may connect to a lower power (but denser) tier of the BSs although it may receive a stronger signal from a higher power (but less dense) BS tier. Therefore, some traffic of the high-power BSs can be off-loaded to the low-power BSs, so that the lower transmission power does not result in lower traffic load due to the smaller coverage area.

In addition, the energy arrival in each tier of BSs is modeled by a Poisson process. This assumption has been validated in the literature, for example [42, 98]. In general, the BSs in a specific tier, say the k^{th} tier, have equal EH rate, γ_k, maximum battery size, N_k, and transmit power, P_k, which are varied across the tiers.

In this work, the temporal dynamics of the energy level at the BSs of each tier are modeled as a birth-death process. We assume that serving a user at each time unit requires one energy quantum. Accordingly, the maximum number of available energy quanta at each BS of the k^{th} tier is equal to its battery capacity, N_k.

Moreover, the energy utilization in each BS is modeled by a Poisson process whose rate is a function of the BS densities, transmission powers and CZ factors. [42, Corollary 1] gives the energy utilization rate as $\frac{\mathbb{P}^{\mathrm{cov}} \lambda_u (P_k B_k)^{2/\alpha}}{\sum_{\ell=1}^{K} \rho_\ell \lambda_\ell (P_\ell B_\ell)^{2/\alpha}}$, which can be interpreted as the average number of serving users by each BS in the k^{th} tier.

Note that, due to the limited storage capacity and uncertain nature of the harvested energy, it may happen that some BSs do not have enough energy to serve any user. Accordingly, a general CZ technique, also known as ON/OFF scheme [26, 97], has been utilized in this network scenario. In other words, only a portion of BSs in each tier remain active, as imposed by

the network parameters and the EH related constraints.

Furthermore, the SINR at the typical MU served by BS_j, belonging to the k^{th} tier and located at $x_j \in \Phi_k^{(a)}$, is given by

$$\mathrm{SINR}_k = \frac{P_k |h_j|^2 \|x_j\|^{-\alpha}}{\sum_{\ell=1}^{K} \sum_{x_z \in \Phi_\ell^{(a)} \setminus x_j} P_\ell |h_z|^2 \|x_z\|^{-\alpha} + \sigma^2}\,, \tag{5.3}$$

We assume that a user is associated to the BS that provides the highest Biased Received Power (BRP) on the long time scale [12]. Accordingly, the typical MU is connected to BS_j located at

$$x_j = \arg \max_{x \in \{x_\ell^*\}} P_\ell B_\ell \|x\|^{-\alpha}, \tag{5.4}$$

where

$$x_\ell^* = \arg \max_{x \in \Phi_\ell^{(a)}} P_\ell B_\ell \|x\|^{-\alpha} \quad \text{for } \ell = 1, \ldots, K. \tag{5.5}$$

As a matter of fact, a higher bias or CZ factor, $B_k > 1$, results in an extension of the cell coverage and enables us to control the traffic load on the lower power tiers.

5.3.1 Coverage, Retention and Blocking Probabilities

To derive the total coverage probability expression, first we obtain the per-tier association probability, which is the probability that a typical user is associated with a BS in a specific tier, say the k^{th} tier. The per-tier association probability is given by [12, Lemma 1]

$$\mathcal{A}_k = \frac{\lambda_k^{(a)} (P_k B_k)^{2/\alpha}}{\sum_{\ell=1}^{K} \lambda_\ell^{(a)} (P_\ell B_\ell)^{2/\alpha}} = \frac{\rho_k \lambda_k (P_k B_k)^{2/\alpha}}{\sum_{\ell=1}^{K} \rho_\ell \lambda_\ell (P_\ell B_\ell)^{2/\alpha}}. \tag{5.6}$$

Note that due to the EH constraints and applying joint CZ schemes, in this system unlike [12] the association probability is a function of $\boldsymbol{\rho}$ as well.

Furthermore, the coverage probability of the k^{th} tier of BSs is given by

$$\begin{aligned} \mathbb{P}_k^{\text{cov}} &= \mathbb{P}\left(\mathrm{SINR}_k > \tau_k\right) \\ &= \frac{\sum_{\ell=1}^{K} \rho_\ell \lambda_\ell (P_\ell B_\ell)^{2/\alpha}}{\sum_{\ell=1}^{K} \rho_\ell \lambda_\ell (P_\ell)^{2/\alpha} \left(B_\ell^{2/\alpha} + \frac{2\tau}{\alpha - 2} B_k B_\ell^{2/\alpha - 1} \mathcal{F}_{k,\ell} \right)}, \end{aligned} \tag{5.7}$$

where τ_k is the SINR threshold in the k^{th} tier and $\mathcal{F}_{k,\ell}$ is a Gaussian hypergeometric function, defined as

$$\mathcal{F}_{k,\ell} = {}_2F_1 \left[1, 1 - 2/\alpha; 2 - 2/\alpha; \frac{-\tau_k B_k}{B_\ell} \right]. \tag{5.8}$$

Thus, the total coverage probability is given by

$$\mathbb{P}^{\text{cov}} = \sum_{k=1}^{K} \mathcal{A}_k \cdot \mathbb{P}_k^{\text{cov}}. \tag{5.9}$$

Along the lines of [42], the retention probability with respect to the system model in this work and under the BRP cell association, is formulated as follows]

$$\rho_k = 1 - \left(\frac{1 - \frac{\gamma_k \sum_{\ell=1}^{K} \rho_\ell \lambda_\ell (P_\ell B_\ell)^{2/\alpha}}{\mathbb{P}^{\text{cov}} \lambda_u (P_k B_k)^{2/\alpha}}}{1 - \left(\frac{\gamma_k \sum_{\ell=1}^{K} \rho_\ell \lambda_\ell (P_\ell B_\ell)^{2/\alpha}}{\mathbb{P}^{\text{cov}} \lambda_u (P_k B_k)^{2/\alpha}} \right)^{N_k+1}} \right). \tag{5.10}$$

Accordingly, [42, Theorem 2] provided a necessary and sufficient condition for the existence of a solution for the system of equations given by Eq. (5.10), for $k = 1, 2, \ldots, K$, as

$$\sum_{k=1}^{K} \gamma_k \lambda_k > \mathbb{P}^{\text{cov}} \lambda_u. \tag{5.11}$$

Note that the energy conservation principle given in Eq. (5.11) captures some network parameters such as battery size, CZ factor and so on. For the next step, the blocking condition and its probability will be introduced. A channel is assumed to be available if it is not in outage, i.e., if the SINR of the link is greater than a threshold. An available channel can also be free or occupied in each time slot. Therefore, an arriving call will be blocked if the total number of available channels, n, is equal to the number of occupied ones, m. Note that we define V as the total number of channels, so that $m \leq n \leq V$.

Using a Markov Chain (MC) model, (m, n) represents the network state for the transition between available and unavailable, free and occupied channel. In this respect, the steady state probability of a typical cell in the k^{th} tier is [76]

$$\pi_k(m, n) = \frac{1}{\chi} \left(\frac{\mu}{\eta} \right)^m \frac{1}{m!} \binom{V}{n} \left(\frac{\mathbb{P}_k^{\text{cov}}}{1 - \mathbb{P}_k^{\text{cov}}} \right)^n, \tag{5.12}$$

where χ is a normalization factor, and μ and η are the call arrival rate and mean channel holding time, respectively.

Based on the mentioned definition, the Blocking probability, $\mathbb{P}^{\text{b}}$, is obtained through summation over all cases in which the number of available channels, n, is equal to the number of occupied ones, m. Thus, using Eq. (5.12), we have

$$\begin{aligned} \mathbb{P}_k^{\text{b}} &= \sum_{m=n \leq V} \pi_k(m, n) \\ &= \sum_{m=n \leq V} \frac{1}{\chi} \left(\frac{\mu}{\eta} \right)^m \frac{1}{m!} \binom{V}{n} \left(\frac{\mathbb{P}_k^{\text{cov}}}{1 - \mathbb{P}_k^{\text{cov}}} \right)^n. \end{aligned} \tag{5.13}$$

In order to evaluate the spectral efficiency in a multi-tier scenario, we derive the Spatial Spectral Efficiency (SSE) in the following subsection. This expression gives per tier measure and enables us to have a comparison among different tiers. To this aim, first we introduce the cell throughput and then provide the SSE in $K-$tier HetNets.

5.3.2 Spatial Spectral Efficiency

Along the lines of [76], the throughput of a typical cell belonging to the k^{th} tier is given by

$$T_k = (1 - \mathbb{P}_k^{\text{b}}) \cdot W \cdot C_k^{\text{E}} \cdot \sum_{0 \le m \le n \le V} m \cdot \pi_k(m, n), \tag{5.14}$$

where W is the bandwidth and C_k^{E} is the ergodic capacity of the k^{th} tier BSs, derived as

$$\begin{aligned} C_k^{\text{E}} &= \mathbb{E}\left[\log_2(1 + \text{SINR}_k)\right] \\ &= \int_0^{+\infty} \mathbb{P}\left(\log_2(1 + \text{SINR}_k) > \tau\right) \mathrm{d}\tau \\ &= \int_0^{+\infty} \mathbb{P}\left(\text{SINR}_k > 2^{\tau} - 1\right) \mathrm{d}\tau \end{aligned} \tag{5.15}$$

where the integrand of Eq. (5.15) follows the definition of the coverage probability in Eq. (5.7).

Finally, to obtain the SSE of the k^{th} tier, we have

$$\text{SSE}_k = \rho_k \cdot \lambda_k \cdot T_k. \tag{5.16}$$

5.3.3 Energy Efficiency

In order to obtain EE, we adopt a model which considers both the operation energy and the so-called "embodied" energy, which includes the initial energy consumed during the manufacturing [99]. Accordingly, EE is defined as the ratio of the lifetime throughput and the total energy consumption during the lifetime of a BS. Therefore, the EE of the typical cell belonging to the k^{th} tier is given by

$$\text{EE}_k = \frac{T_k \cdot t_{LT}}{E_k^{\text{tot}}}, \tag{5.17}$$

where t_{LT} denotes the BS lifetime, and E_k^{tot} is the total energy of a BS in the k^{th} tier, which includes the energy consumed in the factories to manufacture the BS, E_k^{e}, the energy required for maintenance, E_k^{m}, and the transmission energy, E_k^{t}.

The transmission energy is obtained by

$$E_k^{\text{t}} = \left(a \cdot P_k \sum_{0 \le m \le n \le C} m \cdot \pi_k(m, n) + b\right) \cdot t_{LT} \tag{5.18}$$

where a and b are the scaling coefficients.Therefore, EE in Eq. (5.17) is given by

$$\text{EE}_k = \frac{T_k \cdot t_{LT}}{E_k^{\text{e}} + E_k^{\text{m}} + (a \cdot P_k \sum_{0 \le m \le n \le C} m \cdot \pi(m, n) + b) \cdot t_{LT}}. \tag{5.19}$$

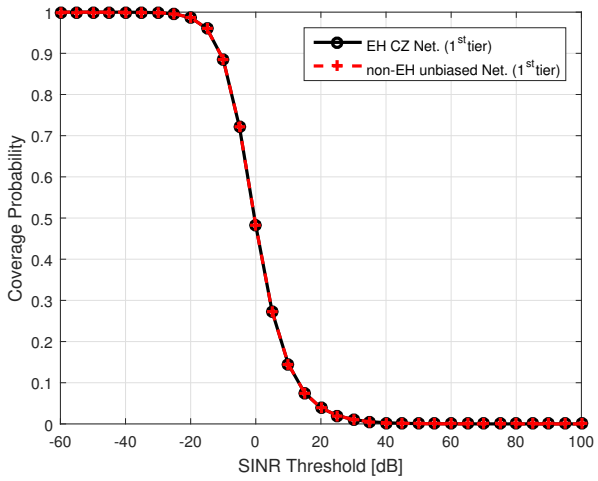

Figure 5.1: Coverage probability of a $K = 1-$tier HetNet

Table 5.1: Network Parameters

	1^{st} tier	2^{nd} tier	3^{rd} tier
λ_k $[1/m^2]$	10^{-6}	10^{-4}	10^{-2}
P_k [dBm]	44.77	30	20
B_k [dB]	0	10	17
N_k	30	15	5

Note that, in this chapter, we adopt a model of the $K-$tier EH HetNets in which the BSs are powered only by the self-contained EH modules. Accordingly, all the required energy for maintenance and transmission purposes is earned from the ambient environment and this part of the consumed energy is not taken into account for EE computation. Therefore, in this system we just have the first term in the denominator of Eq. (5.19).

5.4 Performance Evaluation and Numerical Results

In the following, we will provide some numerical results in order to evaluate the performance of $K-$tier EH HetNets which utilize CZ. To show reliability and the advantages of our proposed model, we compare it with a non-EH unbiased network with identical parameters for $K = 1, 2, 3$. The network parameters are provided in Table 5.1. Moreover, for simplicity we assume that the energy arrival rate is equal to the battery size of the BSs in each tier i.e., $\gamma_k = N_k$ energy quanta per time unit for $k = 1, 2, \ldots, K$.

In Figs. 5.1, 5.2 and 5.3, the coverage probabilities of the $K = 1, 2, 3-$tier networks are illustrated, respectively. With reference to Table 5.1, the bias factor of the 1^{st} tier is equal to one, which is equivalent to an unbiased

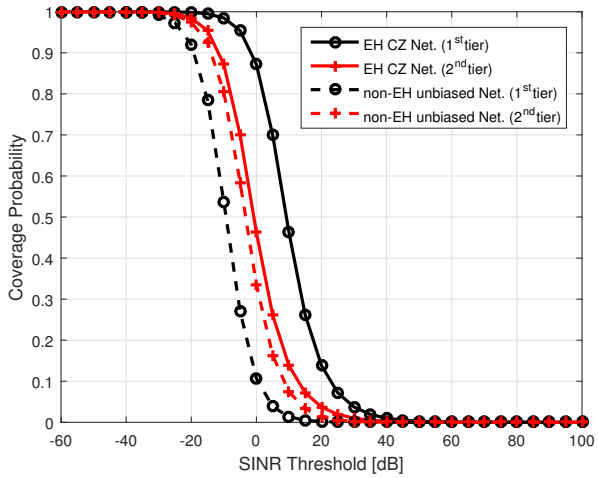

Figure 5.2: Coverage probability of a $K = 2-$tier HetNet

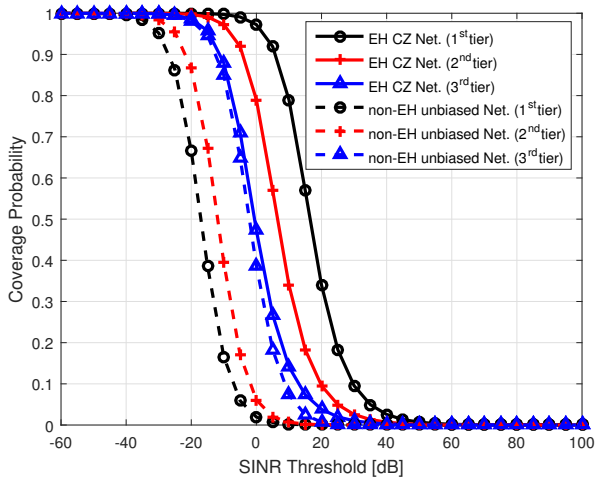

Figure 5.3: Coverage probability of a $K = 3-$tier HetNet

scenario. Therefore, in Fig. 5.1, the two curves are matched, which implies that using EH with proper considerations does not degrade the performance of such networks. Moreover, in $K = 2, 3-$tier networks, corresponding to Figs. 5.2 and 5.3 respectively, the coverage probability of EH CZ networks is higher than for the non-EH unbiased ones.

Moreover, compared to non-EH networks, the order of curves corresponding to different tiers is reversed in EH CZ networks. The reason is that in these networks, we assume a smaller BS, smaller battery size and less energy arrival rate for denser tiers due to the considered system model, which obviously degrades the performance of such tiers. However, under these constraints, limited battery size and uncertain nature of the energy harvesting, EH CZ networks outperform the non-EH ones in all tiers.

A similar description is valid for the blocking probabilities of the $K = 1, 2, 3-$tier networks in Figs. 5.4, 5.5 and 5.6, respectively. As shown in Fig. 5.4, a single tier EH CZ network has the same blocking probability as the

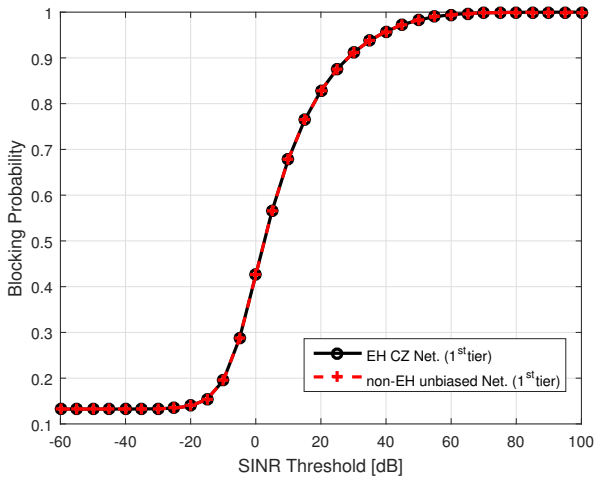

Figure 5.4: Blocking probability of a $K = 1-$tier HetNet

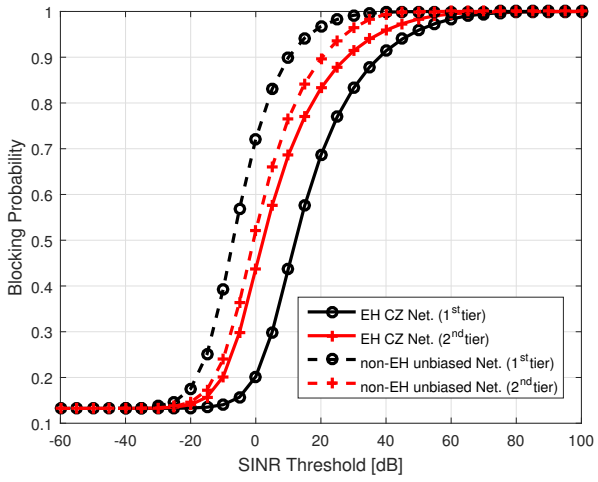

Figure 5.5: Blocking probability of a $K = 2-$tier HetNet

non-EH unbiased network. Moreover, in 2 and 3−tier networks, a new call would be blocked with lower probability in EH CZ networks. Therefore, also in this case, our numerical evaluations show that the energy obtained from the environment thanks to EH has the potential to sustain the network with no performance degradation compared to the case in which a reliable energy source (e.g., the power grid) is available. Note that, for the same reason here we have a reversed order for the curves corresponding to different tiers in 2 and 3−tier networks .

Figs. 5.7, 5.8 and 5.9 depict the SSE of the $K = 1, 2, 3-$tier networks, respectively. As observed in Fig. 5.7, the SSE of the non-EH unbiased network is slightly better than the $K = 1-$tier EH CZ network because, according to Eq. (5.16), SSE is proportional to the retention probability, ρ, which is equal to 0.9 in the EH CZ network according to the system parameters. On the other hand, in the $K = 2, 3-$tier networks, the SSE of the EH CZ networks outperforms the non-EH unbiased networks.

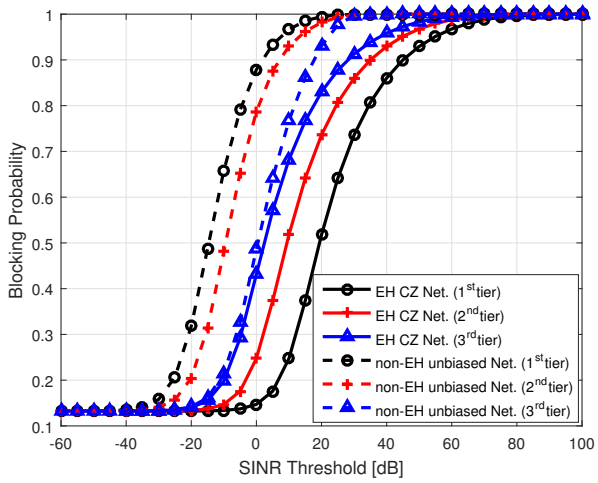

Figure 5.6: Blocking probability of a $K = 3-$tier HetNet

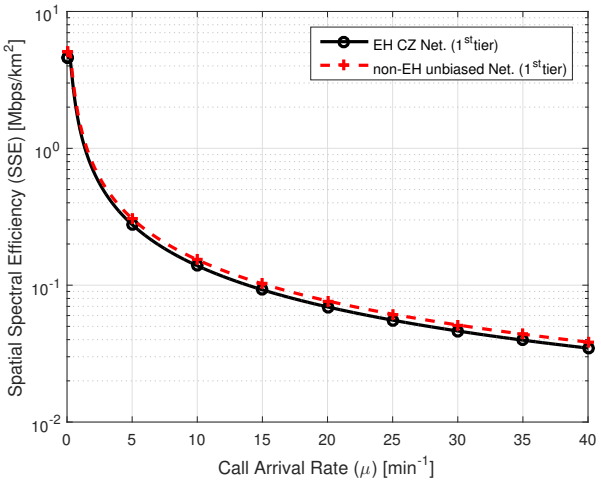

Figure 5.7: Spatial spectral efficiency of a $K = 1-$tier HetNet

Finally, Figs. 5.10, 5.11 and 5.12 illustrate the EE of the $K = 1, 2, 3-$tier networks, respectively. As expected, the EE of the EH CZ networks significantly outperforms those of non-EH unbiased networks. Unlike the other metrics which have a close performance in the case of the single tier HetNets, Figs. 5.1, 5.4 and 5.7, the EE of the EH CZ scenario is higher than the EE in non-EH unbiased networks, depicted in Fig. 5.10. According to Fig. 5.11, in 2−tier HetNets, there is only a slight gap between the EE of the 1st tier of the EH CZ networks and the EE of the 2nd tier of the non-EH unbiased networks. Moreover, Fig. 5.12 properly shows the advantage of the EH CZ networks over non-EH unbiased ones in 3−tier HetNets, where the EE of the 1st tier of the EH CZ networks outperforms the EE of both the 1st and 2nd tiers of the non-EH unbiased networks. In addition, the EE of the 2nd tier of the EH CZ networks has a slight gap to the EE of the 3rd tier of the non-EH biased networks.

Based on the results presented in this section, we can conclude the ad-

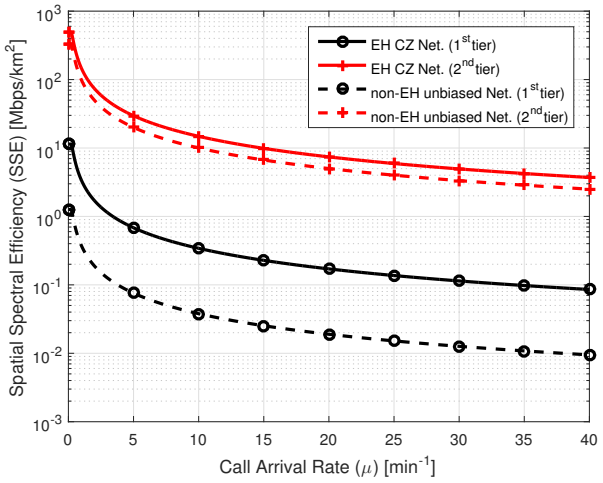

Figure 5.8: Spatial spectral efficiency of a $K = 2-$tier HetNet

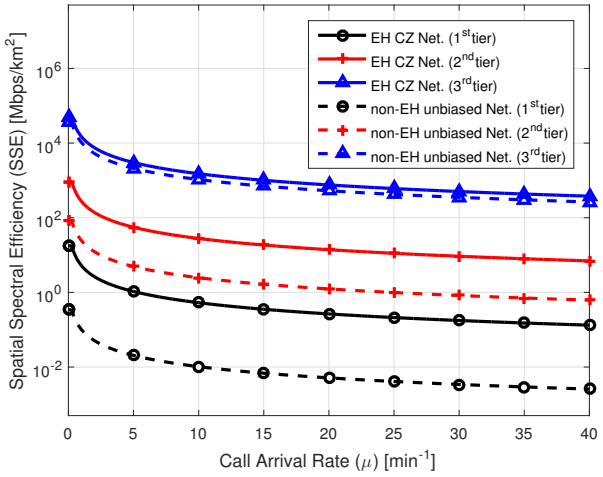

Figure 5.9: Spatial spectral efficiency of a $K = 3-$tier HetNet

vantage of using EH and CZ techniques in HetNet in terms of the EE while the performance of the networks in other aspects is guaranteed.

5.5 Conclusion

In this work, we investigated two CZ techniques, namely telescopic and ON/OFF schemes, in $K-$tier energy harvesting HetNets. We showed that although using EH in cellular networks comprises several constraints, such as uncertainty in energy harvesting and finite size of the batteries, the system performance does not degrade and even improves using the CZ techniques. In this respect, the coverage and blocking probabilities of $K = 1, 2, 3-$tier networks in two different scenarios, namely EH-CZ and non-EH unbiased networks, are compared. Furthermore, SSE and EE in this scenario have been derived and the advantage of this model over the non-EH unbiased

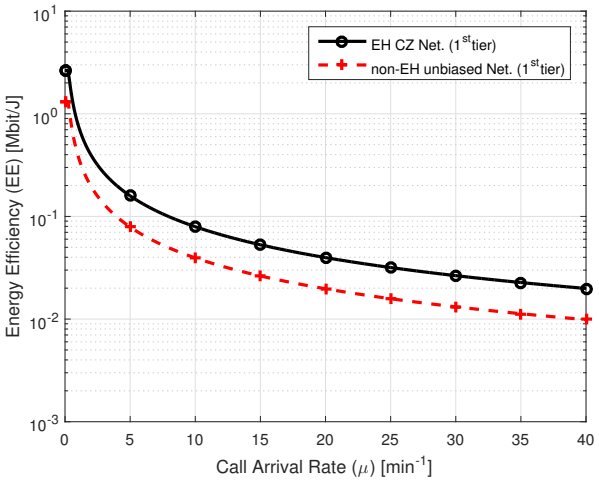

Figure 5.10: Energy efficiency of a $K = 1-$tier HetNet

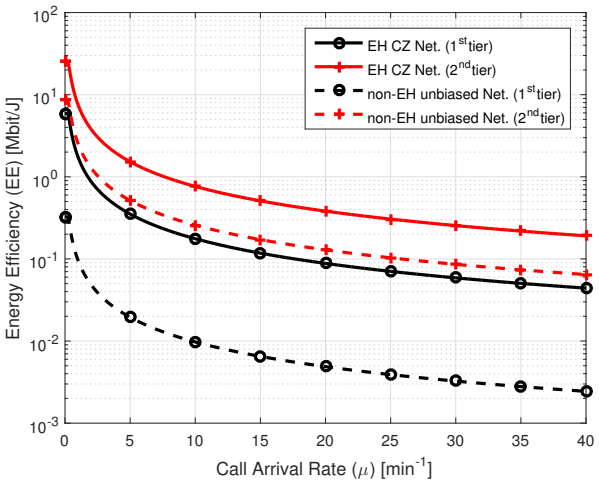

Figure 5.11: Energy efficiency of a $K = 2-$tier HetNet

for $K = 1, 2, 3-$tier networks was highlighted through numerical evaluations. Based on these results, an interesting item for future work is to increase our understanding of the effects of EH technologies on green communications and efficient cellular networks.

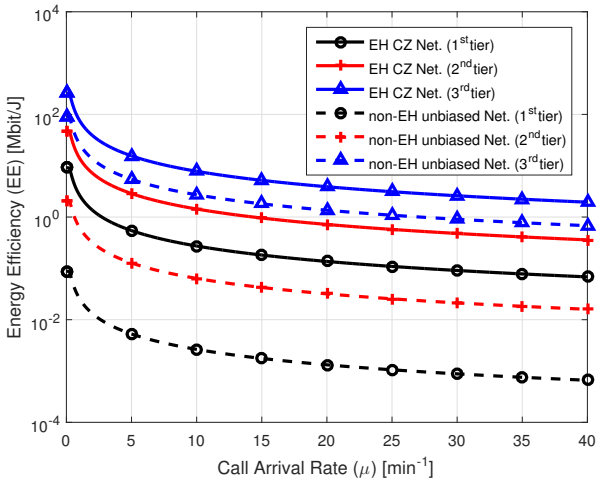

Figure 5.12: Energy efficiency of a $K = 3-$tier HetNet

Chapter 6

Conclusion

In this dissertation, we investigated two main approaches towards green communications in 5G using stochastic geometry. For each approach, we first studied a simple scenario of single tier PVT random cellular networks, while in the next step, we extended our works to more accurate or general network models.

In Chapters 2 and 3, we focused on the efficiency of MIMO technology in HetNets. Despite higher circuit power consumption of MIMO due to multiple RF chains and requirements for more signal processing, comparing the obtained results with the SISO scenario in PVT random cellular networks shows the gain of MIMO systems in terms of SSE and EE.

Unlike most works on HetNets which assume no correlation between the locations of different BS tiers, we adopt a model in which the locations of lower power BSs, PBSs, follow a PHP. Although PHP generalizes the PPP where equality holds in the case of $D = 0$, working with this process is not as straightforward as with PPP. Accordingly, we used two approximations which respectively underestimate and overestimate the interference experienced by the typical user. Tightness of the bounds has been shown through numerical results. Moreover, the advantage of PHP based networks over commonly-used HIP model has been indicated in terms of EE and SSE.

To overcome the sharp increase of total power consumption in HetNets due to dense deployment of small cells (although they consume less energy individually), we adopt two CZ techniques, namely telescopic and ON/OFF methods, in Chapters 4 and 5.

For different CZ parameters, we have derived the tradeoff between EE and ASE in PVT random cellular networks which revealed that improving ASE does not always accompany with an EE enhancement. Therefore, this tradeoff presented a network working region which is necessary to consider for network design.

In the last technical part, we studied $K-$tier HetNets in which BSs are only powered by energy harvesting. Although EH has attracted extensive attention in recent years, the uncertain and intermittent nature of energy arrivals makes it challenging to be practically used in cellular networks. However, combining the two mentioned CZ techniques enables us to achieve higher network performance in terms of the coverage and blocking probabil-

ities while reducing the total power consumption and increasing the energy and spectral efficiencies.

To sum up, we have focused on green 5G where heterogeneous networks seem to be a promising structure to fulfill high capacity demand. However, power consumption in HetNets is another important challenge facing 5G. Thus, we have studied two techniques, namely MIMO and CZ, in order to achieve energy and spectral efficiencies in HetNets where in both methods we have shown their positive impacts on network performance.

Some interesting research directions for future works are listed below.

- Exact characterization of PHP in modeling wireless networks.
- Extend the concept of PHP in order to model more than 2−tier HetNets and study the network performance accordingly.
- Develop smart CZ techniques like traffic-based or proximity-based methods in order to achieve higher efficiency.
- Study CZ scenarios for more realistic user distributions, such as non-uniform and cluster-based user location.

Chapter 7

Appendix

In order to increase the network capacity and fulfill the Quality of Service (QoS) requirements in multi-user wireless networks, Interference Alignment (IA) has been proposed. Subsequently, Ergodic IA was introduced as a promising scheme to achieve a Degrees of Freedom (DoF) metric equal to $\frac{1}{2}$, at the expense of additional delay. In this work, we study the delay-rate trade-off in Ergodic IA and exactly compute the best Delay Exponent of JAP-B, a state-of-the-art Ergodic IA scheme. Moreover, we derive lower and upper bounds for the best delay exponent and show the much better tightness of the proposed bounds compared to those available in the state of the art.

7.1 Introduction

Interference Alignment (IA) was proposed and shown to be able to improve the capacity of multi-user interference networks [100]. In IA literature, to measure the multi-user performance of an interference network a metric named Degrees of Freedom (DoFs) was defined as

$$\mathrm{DoF} = \lim_{P\to\infty} \frac{C(P)}{\log_2(P)},$$

where C is the sum rate of the network, and P represents the per-node transmit power [101]. Hence, DoF indicates the number of interference-free transmitted data streams in a multi-user interference network and is a capacity pre-log factor [102].

However, most of the IA schemes are only feasible in the high Signal-to-Noise ratio (SNR) regime. Ergodic IA, on the other hand, works in any SNR regime [103]. ?Along with these positive features, namely network size and SNR independence, the main drawbacks of Ergodic IA are the intrinsic time delay and global channel state information (CSI) requirement. In fact, this scheme achieves high capacity by pairing time slots with specific channel conditions, in which to transmit the same data stream. Therefore, Ergodic IA may suffer a long time delay waiting for the desired channel state to occur.

To deal with global CSI requirement, authors in [104] showed that with proper power control or rate adaptation strategies, performance of the Er-

godic IA scheme can still outperform conventional orthogonal transmission approaches with limited feedback. Moreover, [105] studies the available interference alignment testbed implementations and explores the applications of IA in the next generation wireless systems.

Inspired by Ergodic IA, some schemes were proposed to control delay [106]- [107]. In [106], two schemes (JAP and JAP-B) were proposed to control the trade-off between transmission rate and delay, and analytical bounds on the delay exponent were provided. In this work, along the line of [103, 106], we consider a time varying (or equivalently frequency selective) Gaussian interference channel. Channel coefficients are quantized and form a finite field of size q. Note that, as mentioned in [100], there is no difference between time and frequency dimension, however the varying nature of the channel coefficients from one channel-use to another one is an important assumption.

By definition, the expected delay is the average time needed before a single codeword symbol from each transmitter is successfully retrieved by the receivers. In Ergodic IA, the expected delay is exponentially scaled with the number of users however, JAP-B scheme reduces the delay exponent without sacrificing rate.

In [108], using the Viterbi algorithm, the optimum user allocation to achieve the lowest delay exponent was obtained numerically. However, the complexity of this method grows with the network size.

Compared to the original Ergodic IA scheme which decodes all users simultaneously, JAP reduces the time delay by successively canceling the interference matching more than two channel matrices. To this aim, in the K-user interference network, users are placed in n groups represented by the user allocation vector $\mathbf{a} = (a_1, a_2, \ldots, a_i, \ldots, a_n)$ of length n and weight K. At the i-th retransmission, a_i users decode their data, $i = 1, \ldots, n$, where n is the total number of retransmissions. Using the JAP scheme, DoF $= 1/(n+1)$ is achievable [106], with Ergodic IA as a special case for $n = 1$ and DoF $= 1/2$.

As an evolution of JAP, JAP-B takes advantage of beamforming to improve the performance. To this aim, instead of repeating the same message, i.e., w_i, in each retransmission, transmitter i sends $\left(H_{\ell i}[t_m]\right)^{-1} H_{\ell i}[t_0] w_i$, where $m \in \{1, 2, \ldots, n\}$ denotes the retransmission step and $\ell = \left(\sum_{i=1}^{m-1} a_i\right) + 1$. Besides, $H_{\ell i}[t_m]$ represents the channel coefficient from transmitter i to user ℓ at time t_m. Therefore, the interference suffered by the first user of each set is canceled by using beamforming, while for all other users JAP is used. Note that JAP-B always outperforms JAP although both adopt the same user allocation vector[1].

In this work, we derive the exact analytical expression of the lowest delay exponent of JAP-B, which until now could only be evaluated numerically [106, 108]. As this involves an integer truncation operation, we also derive continuous analytical expressions of a lower bound and two upper bounds for the delay exponent and compare them with the bounds provided in [106]. The numerical results show the much better tightness of our proposed bounds.

[1]Full details about JAP and JAP-B can be found in [106].

7.2 Exact Evaluation of the Delay Exponent

In this section we find all solutions to the problem [106]

$$\min_{\mathbf{a}} T_B(\mathbf{a}) = \min_{\mathbf{a}} \max_{i\in\{1,\ldots,n\}} (a_i - 1)(K - i - 1) \tag{7.1}$$

$$\text{s.t.:} \quad \mathbf{a} = (a_1, \ldots, a_n) \quad \sum_{i=1}^{n} a_i = K \quad a_i > 0 \; \forall \; i$$

where $T_B(\mathbf{a})$ is the delay exponent of JAP-B when the user allocation vector $\mathbf{a}$ is used, which we want to minimize with respect to $\mathbf{a}$. The problem can be recast as follows. Consider n bins in which we need to fit K users. The metric associated to bin i when j users have been placed in it is $c_{ij} = (j-1)(K-i-1)$.

Consider a grid of $K \times n$ cells, arranged in K rows and n columns. We need to fill the columns (the bins) from the bottom up by placing $a_i > 0$ users (one per cell) in column i, with $\sum_{i=1}^{n} a_i = K$, so that the resulting value of $T_B(\mathbf{a})$ is minimized. (Note that each column will be filled without gaps since each cell is strictly dominated by those below, i.e., $c_{ij} > c_{ik}$ for $j > k$.)

In order to do so, we can use the following algorithm. Starting from an empty grid, we add one user at a time to the proper bin, so that the corresponding cell being added is the one with the lowest metric among those not yet filled. If there are multiple cells with that property, we pick one of them at random. Once K cells have been selected, the number of users in the different bins provide an optimal solution to problem (7.1), since the way cells are added, choosing the bin with the lowest metric in each step, guarantees that there is no other way which returns a lower value of $T_B(\mathbf{a})$.

We now characterize the solution of the problem, by studying the outcome of the above algorithm. Note that if $K \leq n$ the problem is trivially solved by any of the $\binom{n}{K}$ solutions in which each user is in a bin by itself, for which $T_B(\mathbf{a}) = 0$. In addition, $K = n + 1$ also leads to $T_B(\mathbf{a}) = 0$ for $a_i = 1, i = 1, \ldots, K-1, a_K = 2$. Therefore, in the following we assume $K > n + 1$.

Lemma 1: The only possible assignment of the first $m < K$ users fills completely an integer number of rows $\left\lfloor \frac{m}{n} \right\rfloor$ plus the rightmost $m - n \left\lfloor \frac{m}{n} \right\rfloor$ cells of the next highest row.

Proof: We prove this result by induction. Obviously, first users up to number n are assigned one per bin which result $T_B(\mathbf{a}) = 0$. So we focus on the case $m > n$. After assignment of first n users, the $n + 1$-st user must be added to bin n because a given cell strictly dominates all those to its left, i.e., $c_{ij} > c_{kj}$ for $i < k, j > 1$. Note that this is true not only after the first row has been completely filled, but also after completing each row.

Now suppose $m - 1$ users have been assigned so that $j - 1$ rows are completely filled, with $j - 1 = \left\lfloor \frac{m-1}{n} \right\rfloor$, and the rightmost $n - i = m - 1 - (j-1)n$ cells of the j-th row are filled. If $m - 1$ is an integer multiple of n, the assignment corresponds to $j - 1$ complete rows, and the next assignment necessarily fills cell n, j, starting a new row.

If instead $n - i = m - 1 - (j - 1)n > 0$, we have that row j is partially filled. Since each cell strictly dominates all those to its left, the only possible candidate cells for the assignment of the m-th user are cell i, j (i.e., one more

in row j) and cell $n, j+1$ (i.e., the rightmost cell of row $j+1$). To see which one is to be chosen, we evaluate

$$\begin{aligned} c_{ij} - c_{n,j+1} &= (j-1)(K-i-1) - j(K-n-1) \\ &= j(K-1) - ji - (K-i-1) - j(K-1) + jn \\ &= jn - ji - K + i + 1 = (jn - i + 1) - K - (j-2)i \end{aligned} \tag{7.2}$$

Note that in (7.2) we have $jn - i + 1 = m < K$, so that $(jn - i + 1) - K < 0$, and $-(j-2)i \leq 0$ (note that $m > n$ implies $j > 1$), and therefore

$$c_{ij} - c_{n,j+1} = (jn - i + 1) - K - (j-2)i < 0 \tag{7.3}$$

so that cell ij strictly dominates cell $n, j+1$, and the assignment of user m is unique.

From the above argument, and using the induction principle, we can conclude that the only assignment that minimizes $\max_{i\in\{1,\ldots,n\}}(a_i - 1)(K - i - 1)$, $\sum_{i=1}^{n} a_i = m < K$ is obtained by filling successive rows right to left, moving to row j only after row $j-1$ has been completely filled. The lemma is thus proved. ■

Theorem 1: Problem (7.1) has a unique solution if $K > 2n$, whereas it has exactly two solutions if $n + 1 < K \leq 2n$. These solutions are:

$$\mathbf{a} = \begin{cases} (t, \ldots, t, t+1, \ldots, t+1) & \text{if } K > 2n \\ (t, \ldots, t, t+1, \ldots, t+1) \text{ and} & \\ (t, \ldots, t, t+1, \ldots, t+1, t+2) & \text{if } n+1 < K \leq 2n \end{cases} \tag{7.4}$$

where $t = \left\lfloor \frac{K-1}{n} \right\rfloor$, and the number of elements equal to $t, t+1$ and $t+2$ is uniquely determined by the total number of users K and by the number of bins n.

Proof: From Lemma 1, we have that the first $K-1$ users are assigned to fill t rows plus the $K - 1 - tn \geq 0$ rightmost cells of row $t+1$. If $K-1$ is an integer multiple of n, i.e., $K - 1 - tn = 0$, then the only possible assignment for the K-th user is in cell $n, t+1$ and the lemma is proved. (Note that this case can only occur when $K > 2n$, since our assumption that $K > n+1$ implies that the smallest K for which $K-1$ is an integer multiple of n is $K = 2n+1$.)

If instead $K - 1 - tn > 0$, we have two possibilities to assign user K, namely cells ij and $n, j+1$, with $i = (t+1)n - (K-1)$ and $j = t+1$. As before, we have that

$$c_{ij} - c_{n,j+1} = (jn - i + 1) - K - (j-2)i = -(j-2)i \tag{7.5}$$

where the last equality derives from the fact that, when assigning the last user, $jn - i + 1 = K$. Therefore, if $j > 2$ (i.e., $K > 2n$), $c_{ij} - c_{n,j+1} < 0$ and the solution is unique, whereas if $j = 2$ (i.e., $n + 1 < K \leq 2n$), $c_{ij} - c_{n,j+1} = 0$ and problem (7.1) admits two equivalent solutions. This concludes the proof of the theorem. ■

Remark: More specifically, the optimal solutions are as follows. If $K > 2n$, the unique solution contains $(t+1)n - K \geq 0$ elements equal to t, followed

by $K - tn > 0$ elements equal to $t+1$. If $n+1 < K \leq 2n$, one optimal solution contains $2n - K \geq 0$ elements equal to 1 and $K - n > 0$ elements equal to 2, and the other contains $2n - K + 1 > 0$ elements equal to 1, $K - n - 2 \geq 0$ elements equal to 2, and one element equal to 3.

Note that the optimal value of the delay exponent corresponds to the last cell being filled, which is

$$\begin{aligned} T(K,n) &= c_{(t+1)n-K+1,t+1} \\ &= t(K-1-((t+1)n-K+1)) \\ &= (2K-2-(t+1)n)t, \qquad t = \left\lfloor \frac{K-1}{n} \right\rfloor \end{aligned} \tag{7.6}$$

The expression in (7.6) involves the use of $t = \left\lfloor \frac{K-1}{n} \right\rfloor$, which is not always easy to handle analytically because of the truncation. For this reason, in the following we provide some useful and tight upper and lower bounds expressed as continuous and (infinitely) differentiable functions of K and n.

7.3 Bounds

Lemma 2:

$$\frac{(K-1)^2}{n} - (K-1) \leq T(K,n) \leq \frac{(K-1)^2}{n} - (K-1) + \frac{n}{4} \tag{7.7}$$

Proof:

$$\begin{aligned} & T(K,n) - \left(\frac{(K-1)^2}{n} - (K-1) \right) \\ &= (2K-2-(t+1)n)t - \frac{(K-1)^2}{n} + (K-1) \\ &= n\left[2t\left(\frac{K-1}{n}\right) - t^2 - t - \left(\frac{K-1}{n}\right)^2 + \frac{K-1}{n} \right] \\ &= n\left[\left(\frac{K-1}{n} - t\right) - \left(\frac{K-1}{n} - t\right)^2 \right] = n(\xi - \xi^2) \end{aligned} \tag{7.8}$$

where $\xi = \left(\frac{K-1}{n} - t\right) \in [0,1]$ and we have $0 \leq (\xi - \xi^2) \leq \frac{1}{4}$ which concludes the proof. ■

Remark: As a refinement of the previous result, note that since $\xi = \left(\frac{K-1}{n} - t\right) \in \{0, \frac{1}{n}, \frac{2}{n}, \ldots, \frac{n-1}{n}\}$, we have that

$$0 \leq (\xi - \xi^2) \leq \begin{cases} \frac{1}{4} & \text{for } n \text{ even} \\ \frac{n^2-1}{4n^2} = \frac{1}{4} - \frac{1}{4n^2} & \text{for } n \text{ odd} \end{cases} \tag{7.9}$$

The following lemma provides an alternative upper bound.

Lemma 3:

$$T(K,n) \leq \frac{(K-1)^2}{n} - n \tag{7.10}$$

Proof:

$$\begin{aligned} T(K,n) &= c_{(t+1)n-K+1,t+1} \leq c_{n,t+2} \\ &= (t+1)(K-n-1) \leq \left(\frac{K-1}{n}+1\right)(K-n-1) \\ &= \frac{(K-1+n)(K-n-1)}{n} = \frac{(K-1)^2-n^2}{n} \end{aligned} \tag{7.11}$$

where we used the fact that all cells in row $t+2$ are empty and $T(K,n)$ is less than or equal to the value of any empty cell, and the fact that $t = \left\lfloor \frac{K-1}{n} \right\rfloor \leq \frac{K-1}{n}$. ■

Remark: The bounds given above are always better than the bounds provided in [106, Theorem 5]:

$$\frac{K(K-2)}{n} - (2K-n-2) \leq T(K,n) \leq \frac{K(K-2)}{n} \tag{7.12}$$

The lower bound in (7.7) is always better (i.e., higher) that the one in (7.12) since

$$\begin{aligned} &\frac{(K-1)^2}{n} - (K-1) - \frac{K(K-2)}{n} + (2K-n-2) \\ &\qquad = (K-1-n) + \frac{1}{n} > 0 \end{aligned} \tag{7.13}$$

because $K \geq n+1$.

The upper bound in (7.7) is always better (i.e., lower) that the one in (7.12) since, for $n \geq 2$,

$$\begin{aligned} &\frac{K(K-2)}{n} - \left(\frac{(K-1)^2}{n} - (K-1) + \frac{n}{4}\right) \\ = \;& K-1-\frac{n}{4}-\frac{1}{n} \geq \frac{3}{4}n - 1 > 0 \end{aligned} \tag{7.14}$$

because $K \geq n+1$. For $n = 1$, the delay exponent can be trivially computed as $(K-1)(K-2)$, and the bound in (7.12) is $K(K-2)$, which is strictly greater than the actual value, whereas our (refined) bound is exact.

Similarly, comparing the upper bound in (7.10) with that in (7.12) we have the inequality

$$\frac{K(K-2)}{n} - \left(\frac{(K-1)^2}{n} - n\right) = n - \frac{1}{n} \geq 0 \tag{7.15}$$

which is strict if we again exclude the trivial case $n = 1$.

As will be shown in the results section, not only are our new bounds always guaranteed to be better than those in [106], but they often provide a very significant improvement.

7.4 Asymptotic regimes

As in [106], we study the asymptotic regimes for fixed single-user rate (Regime I – the number of DoFs is fixed to some number $\alpha \in (0, 1/2]$) and for fixed sum-rate (Regime II – the number of DoFs is β/K, for $\beta > 1$, and goes to zero as the number of users grows). We have the following results.

Lemma 4: In Regime I, for fixed α and as $K \to \infty$, the delay exponent obeys

$$0 \leq T(K,n) - \frac{K^2 - \left\lfloor \frac{1}{\alpha} + 1 \right\rfloor K + \left\lfloor \frac{1}{\alpha} \right\rfloor}{\left\lfloor \frac{1}{\alpha} - 1 \right\rfloor} \leq \frac{1}{4} \left\lfloor \frac{1}{\alpha} - 1 \right\rfloor \tag{7.16}$$

Proof: Trivially obtained from (7.7). ∎

Remark: As in [106], $T(K,n)$ scales as $\left(\left\lfloor \frac{1}{\alpha} - 1 \right\rfloor\right)^{-1} K^2$. However, (7.16) provides bounds with guaranteed distance $\frac{1}{4}\left\lfloor \frac{1}{\alpha} - 1 \right\rfloor, \forall K$.

Lemma 5: In Regime II, for fixed β and as $K \to \infty$, the delay exponent obeys

$$\begin{aligned} (\beta-1)K \leq T(K,n) &\leq \min\left\{\beta - 1 + \frac{1}{4\beta}, \beta - \frac{1}{\beta}\right\} K \\ &\leq \left(\beta - \frac{4}{5}\right) K \end{aligned} \tag{7.17}$$

Proof: For the lower bound, since $n = \left\lfloor \frac{K}{\beta} - 1 \right\rfloor \leq \frac{K}{\beta} - 1$, we have for any K

$$T(K,n) \geq \frac{(K-1)^2}{n} - (K-1) \geq \frac{(K-1)^2}{\frac{K}{\beta}-1} - (K-1) \tag{7.18}$$

$$= (K-1)\left[\frac{\beta(K-1)-(K-\beta)}{K-\beta}\right] \tag{7.19}$$

$$= \frac{(K-1)(\beta-1)K}{K-\beta} \geq (\beta-1)K \tag{7.20}$$

For the upper bound, for $K \to \infty$ we know from (7.7)

$$\begin{aligned} \frac{(K-1)^2}{n} - (K-1) + \frac{n}{4} &\sim \frac{\beta(K-1)^2}{K} - (K-1) + \frac{K}{4\beta} \\ &\sim \left(\beta - 1 + \frac{1}{4\beta}\right) K \end{aligned} \tag{7.21}$$

and from (7.10)

$$\frac{(K-1)^2}{n} - n \sim \frac{\beta(K-1)^2}{K} - \frac{K}{\beta} \sim \left(\beta - \frac{1}{\beta}\right) K \tag{7.22}$$

and since both upper bounds apply we get the first result. The last inequality is obtained by observing that

$$\begin{aligned} \beta - 1 + \frac{1}{4\beta} \leq \beta - \frac{4}{5} \quad &\text{for } \beta \leq \tfrac{5}{4} \\ \beta - \frac{1}{\beta} \leq \beta - \frac{4}{5} \quad &\text{for } \beta \geq \tfrac{5}{4} \end{aligned} \tag{7.23}$$

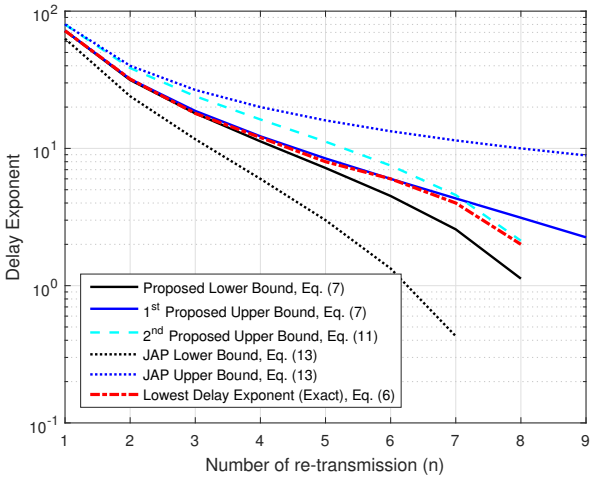

Figure 7.1: Delay Exponent in a 10-user Interference Network

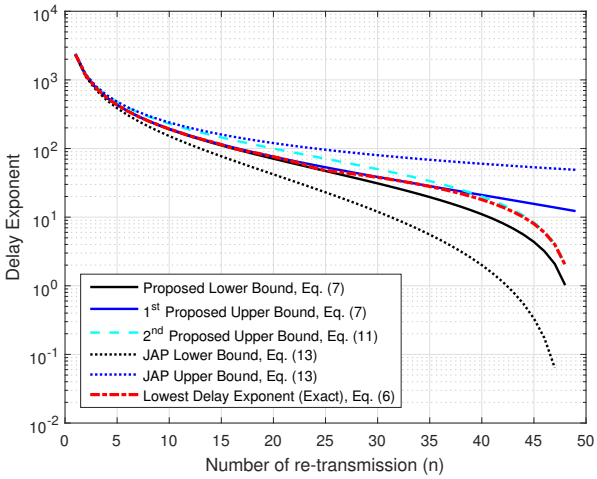

Figure 7.2: Delay Exponent in a 50-user Interference Network

which completes the proof. ■

Remark: Note that in [106], the asymptotic bounds are given as $(\beta - 2)K \leq T(K,n) \leq \beta K$ which diverge at a rate $2K$, whereas in (7.17) the maximum rate of divergence of the two bounds is $K/5$, i.e., ten times smaller.

7.5 Numerical Results and Conclusion

In Figs. 7.1 through 7.3, the exact delay exponent in (7.6) and the proposed bounds in (7.7) and (7.10) are illustrated and compared with the bounds in (7.12) previously proposed in [106], for $K = 10, 50, 1000$. As observed, in all cases our proposed bounds are much tighter than those given in [106].

Looking closely at these figures, we observe that the better (i.e., the lower) of the proposed upper bounds in (7.7) and (7.10) always provides a very tight approximation of the exact delay exponent. In the four cases

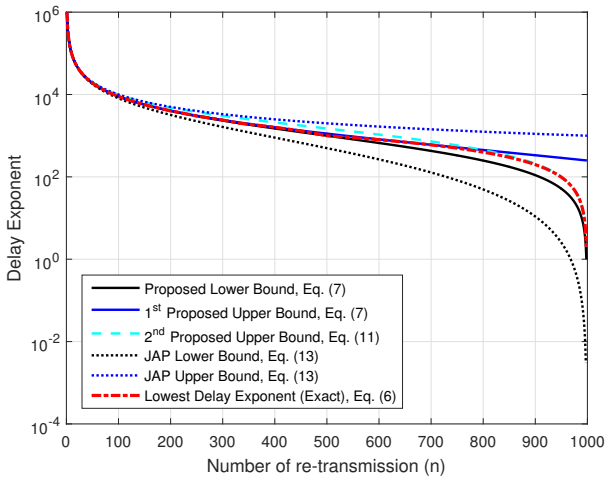

Figure 7.3: Delay Exponent in a 1000-user Interference Network

shown, the maximum errors when using such an approximation instead of the actual value are 4.2, 11, and 12.4%, respectively.

Therefore, when dealing with mathematical developments that require analytically tractable closed-form expressions (which prevents from using the exact formula given in (7.4)), an excellent approximation can be achieved using these upper bounds.

Bibliography

[1] A. Osseiran, F. Boccardi, V. Braun, K. Kusume, P. Marsch, M. Maternia, O. Queseth, M. Schellmann, H. Schotten, H. Taoka, H. Tullberg, M. A. Uusitalo, B. Timus, and M. Fallgren, "Scenarios for 5G mobile and wireless communications: the vision of the METIS project," *IEEE Communications Magazine*, vol. 52, pp. 26–35, May 2014.

[2] E. Hossain, M. Rasti, H. Tabassum, and A. Abdelnasser, "Evolution toward 5G multi-tier cellular wireless networks: An interference management perspective," *IEEE Wireless Communications*, vol. 21, pp. 118–127, June 2014.

[3] Q. Wu, G. Y. Li, W. Chen, D. W. K. Ng, and R. Schober, "An overview of sustainable green 5G networks," *IEEE Wireless Communications*, vol. 24, no. 4, pp. 72–80, 2017.

[4] D. Gunduz, K. Stamatiou, N. Michelusi, and M. Zorzi, "Designing intelligent energy harvesting communication systems," *IEEE Communications Magazine*, vol. 52, pp. 210–216, January 2014.

[5] S. Cai, Y. Che, L. Duan, J. Wang, S. Zhou, and R. Zhang, "Green 5G heterogeneous networks through dynamic small-cell operation," *IEEE Journal on Selected Areas in Communications*, vol. 34, pp. 1103–1115, May 2016.

[6] M. Deruyck, W. Vereecken, E. Tanghe, W. Joseph, M. Pickavet, L. Martens, and P. Demeester, "Power consumption in wireless access network," in *2010 European Wireless Conference (EW)*, pp. 924–931, April 2010.

[7] C. Han, T. Harrold, S. Armour, I. Krikidis, S. Videv, P. M. Grant, H. Haas, J. S. Thompson, I. Ku, C. X. Wang, T. A. Le, M. R. Nakhai, J. Zhang, and L. Hanzo, "Green radio: radio techniques to enable energy-efficient wireless networks," *IEEE Communications Magazine*, vol. 49, pp. 46–54, June 2011.

[8] J. G. Andrews, S. Buzzi, W. Choi, S. V. Hanly, A. Lozano, A. C. K. Soong, and J. C. Zhang, "What will 5G be?," *IEEE Journal on Selected Areas in Communications*, vol. 32, pp. 1065–1082, June 2014.

[9] A. Aijaz, M. Dohler, A. H. Aghvami, V. Friderikos, and M. Frodigh, "Realizing the tactile internet: Haptic communications over next generation 5G cellular networks," *IEEE Wireless Communications*, vol. 24, pp. 82–89, April 2017.

[10] M. Haenggi, *Stochastic Geometry for Wireless Networks*. New York, NY, USA: Cambridge University Press, 1st ed., 2012.

[11] H. S. Dhillon, M. Kountouris, and J. G. Andrews, "Downlink MIMO HetNets: Modeling, ordering results and performance analysis," *IEEE Transactions on Wireless Communications*, vol. 12, pp. 5208–5222, October 2013.

[12] H. S. Jo, Y. J. Sang, P. Xia, and J. G. Andrews, "Heterogeneous cellular networks with flexible cell association: A comprehensive downlink SINR analysis," *IEEE Transactions on Wireless Communications*, vol. 11, pp. 3484–3495, October 2012.

[13] J. G. Andrews, F. Baccelli, and R. K. Ganti, "A tractable approach to coverage and rate in cellular networks," *IEEE Transactions on Communications*, vol. 59, pp. 3122–3134, November 2011.

[14] T. Kwon and J. M. Cioffi, "Random deployment of data collectors for serving randomly-located sensors," *IEEE Transactions on Wireless Communications*, vol. 12, pp. 2556–2565, June 2013.

[15] T. D. Novlan, H. S. Dhillon, and J. G. Andrews, "Analytical modeling of uplink cellular networks," *IEEE Transactions on Wireless Communications*, vol. 12, pp. 2669–2679, June 2013.

[16] H. B. Kong, P. Wang, D. Niyato, and Y. Cheng, "Modeling and analysis of wireless sensor networks with/without energy harvesting using Ginibre point processes," *IEEE Transactions on Wireless Communications*, vol. 16, pp. 3700–3713, June 2017.

[17] Y. Li, F. Baccelli, H. S. Dhillon, and J. G. Andrews, "Statistical modeling and probabilistic analysis of cellular networks with determinantal point processes," *IEEE Transactions on Communications*, vol. 63, pp. 3405–3422, Sept 2015.

[18] C. h. Lee and M. Haenggi, "Interference and outage in poisson cognitive networks," *IEEE Transactions on Wireless Communications*, vol. 11, pp. 1392–1401, April 2012.

[19] N. Deng, W. Zhou, and M. Haenggi, "Heterogeneous cellular network models with dependence," *IEEE Journal on Selected Areas in Communications*, vol. 33, pp. 2167–2181, Oct 2015.

[20] H. Sun, M. Wildemeersch, M. Sheng, and T. Q. S. Quek, "D2d enhanced heterogeneous cellular networks with dynamic tdd," *IEEE Transactions on Wireless Communications*, vol. 14, pp. 4204–4218, Aug 2015.

[21] M. Afshang and H. S. Dhillon, "Spatial modeling of device-to-device networks: Poisson cluster process meets poisson hole process," in *49th Asilomar Conference on Signals, Systems and Computers*, pp. 317–321, Nov 2015.

[22] Z. Yazdanshenasan, H. S. Dhillon, M. Afshang, and P. H. J. Chong, "Poisson hole process: Theory and applications to wireless networks," *IEEE Transactions on Wireless Communications*, vol. 15, pp. 7531–7546, Nov 2016.

[23] M. A. Kishk and H. S. Dhillon, "Tight lower bounds on the contact distance distribution in poisson hole process," *IEEE Wireless Communications Letters*, vol. 6, pp. 454–457, Aug 2017.

[24] A. H. Sakr and E. Hossain, "Cognitive and energy harvesting-based d2d communication in cellular networks: Stochastic geometry modeling and analysis," *IEEE Transactions on Communications*, vol. 63, pp. 1867–1880, May 2015.

[25] T. X. Tran and K. C. Teh, "Performance analysis of two-tier hetnets with massive mimo and non-uniformly small cell deployment," *IEEE Transactions on Vehicular Technology*, vol. PP, no. 99, pp. 1–1, 2017.

[26] Z. Niu, Y. Wu, J. Gong, and Z. Yang, "Cell zooming for cost-efficient green cellular networks," *IEEE Communications Magazine*, vol. 48, pp. 74–79, November 2010.

[27] X. Weng, D. Cao, and Z. Niu, "Energy-efficient cellular network planning under insufficient cell zooming," in *Vehicular Technology Conference (VTC Spring), 2011 IEEE 73rd*, pp. 1–5, May 2011.

[28] X. Xu, C. Yuan, W. Chen, X. Tao, and Y. Sun, "Adaptive cell zooming and sleeping for green heterogeneous ultra-dense networks," *IEEE Transactions on Vehicular Technology*, vol. PP, no. 99, pp. 1–1, 2017.

[29] M. A. Marsan, L. Chiaraviglio, D. Ciullo, and M. Meo, "Optimal energy savings in cellular access networks," in *2009 IEEE International Conference on Communications Workshops*, pp. 1–5, June 2009.

[30] I. Ashraf, F. Boccardi, and L. Ho, "Sleep mode techniques for small cell deployments," *IEEE Communications Magazine*, vol. 49, pp. 72–79, August 2011.

[31] Y. L. Che, L. Duan, and R. Zhang, "Dynamic base station operation in large-scale green cellular networks," *IEEE Journal on Selected Areas in Communications*, vol. 34, pp. 3127–3141, Dec 2016.

[32] F. Han, Z. Safar, and K. J. R. Liu, "Energy-efficient base-station cooperative operation with guaranteed QoS," *IEEE Transactions on Communications*, vol. 61, pp. 3505–3517, August 2013.

[33] E. Oh, K. Son, and B. Krishnamachari, "Dynamic base station switching-on/off strategies for green cellular networks," *IEEE Transactions on Wireless Communications*, vol. 12, pp. 2126–2136, May 2013.

[34] M. F. Hossain, K. S. Munasinghe, and A. Jamalipour, "Distributed inter-bs cooperation aided energy efficient load balancing for cellular networks," *IEEE Transactions on Wireless Communications*, vol. 12, pp. 5929–5939, November 2013.

[35] J. Xu, L. Duan, and R. Zhang, "Energy group buying with loading sharing for green cellular networks," *IEEE Journal on Selected Areas in Communications*, vol. 34, pp. 786–799, April 2016.

[36] L. Silu, "The green CDMA base station," *Huawei Commun.*, Dec 2008. [Available] http://www1.huawei.com/enapp/198/hw-082748.htm.

[37] G. Piro, M. Miozzo, G. Forte, N. Baldo, L. A. Grieco, G. Boggia, and P. Dini, "Hetnets powered by renewable energy sources: Sustainable next-generation cellular networks," *IEEE Internet Computing*, vol. 17, pp. 32–39, Jan 2013.

[38] Y. Mao, Y. Luo, J. Zhang, and K. B. Letaief, "Energy harvesting small cell networks: feasibility, deployment, and operation," *IEEE Communications Magazine*, vol. 53, pp. 94–101, June 2015.

[39] J. Yang and S. Ulukus, "Optimal packet scheduling in an energy harvesting communication system," *IEEE Transactions on Communications*, vol. 60, pp. 220–230, January 2012.

[40] O. Ozel, K. Tutuncuoglu, J. Yang, S. Ulukus, and A. Yener, "Transmission with energy harvesting nodes in fading wireless channels: Optimal policies," *IEEE Journal on Selected Areas in Communications*, vol. 29, pp. 1732–1743, September 2011.

[41] J. Gong, S. Zhou, and Z. Niu, "Optimal power allocation for energy harvesting and power grid coexisting wireless communication systems," *IEEE Transactions on Communications*, vol. 61, pp. 3040–3049, July 2013.

[42] H. S. Dhillon, Y. Li, P. Nuggehalli, Z. Pi, and J. G. Andrews, "Fundamentals of heterogeneous cellular networks with energy harvesting," *IEEE Transactions on Wireless Communications*, vol. 13, pp. 2782–2797, May 2014.

[43] P. S. Yu, J. Lee, T. Q. S. Quek, and Y. W. P. Hong, "Traffic offloading in heterogeneous networks with energy harvesting personal cells-network throughput and energy efficiency," *IEEE Transactions on Wireless Communications*, vol. 15, pp. 1146–1161, Feb 2016.

[44] K. Huang and V. K. N. Lau, "Enabling wireless power transfer in cellular networks: Architecture, modeling and deployment," *IEEE Transactions on Wireless Communications*, vol. 13, pp. 902–912, February 2014.

[45] T. A. Khan, A. Alkhateeb, and R. W. Heath, "Millimeter wave energy harvesting," *IEEE Transactions on Wireless Communications*, vol. 15, pp. 6048–6062, Sept 2016.

[46] I. Krikidis, "Simultaneous information and energy transfer in large-scale networks with/without relaying," *IEEE Transactions on Communications*, vol. 62, pp. 900–912, March 2014.

[47] Z. Ding, I. Krikidis, B. Sharif, and H. V. Poor, "Wireless information and power transfer in cooperative networks with spatially random relays," *IEEE Transactions on Wireless Communications*, vol. 13, pp. 4440–4453, Aug 2014.

[48] M. A. Kishk and H. S. Dhillon, "Coexistence of rf-powered iot and a primary wireless network with secrecy guard zones," *IEEE Transactions on Wireless Communications*, vol. PP, no. 99, pp. 1–1, 2017.

[49] M. A. Kishk and H. S. Dhillon, "Joint uplink and downlink coverage analysis of cellular-based rf-powered iot network," *IEEE Transactions on Green Communications and Networking*, vol. PP, no. 99, pp. 1–1, 2017.

[50] F. Baccelli and B. Blaszczyszyn, *Stochastic Geometry and Wireless Networks, Volume I - Theory*, vol. 1 of *Foundations and Trends in Networking Vol. 3: No 3-4, pp 249-449*. NoW Publishers, 2009. Stochastic Geometry and Wireless Networks, Volume II - Applications; see http://hal.inria.fr/inria-00403040.

[51] M. Haenggi, J. G. Andrews, F. Baccelli, O. Dousse, and M. Franceschetti, "Stochastic geometry and random graphs for the analysis and design of wireless networks," *IEEE Journal on Selected Areas in Communications*, vol. 27, pp. 1029–1046, Sep 2009.

[52] J. G. Andrews, A. K. Gupta, and H. S. Dhillon, "A primer on cellular network analysis using stochastic geometry," *CoRR*, vol. abs/1604.03183, 2016.

[53] X. Ge, B. Yang, J. Ye, G. Mao, C.-X. Wang, and T. Han, "Spatial spectrum and energy efficiency of random cellular networks," *IEEE Transactions on Communications*, vol. 63, pp. 1019–1030, March 2015.

[54] S. Pattaramalai, V. A. Aalo, and G. P. Efthymoglou, "Evaluation of call performance in cellular networks with generalized cell dwell time and call-holding time distributions in the presence of channel fading," *IEEE Transactions on Vehicular Technology*, vol. 58, pp. 3002–3013, July 2009.

[55] F. P. Kelly, *Reversibility and Stochastic Networks*. New York, NY, USA: Cambridge University Press, 2011.

[56] V. Chandrasekhar, J. Andrews, and A. Gatherer, "Femtocell networks: a survey," *IEEE Communications Magazine*, vol. 46, pp. 59–67, Sep 2008.

[57] J. Andrews, "Seven ways that HetNets are a cellular paradigm shift," *IEEE Communications Magazine*, vol. 51, pp. 136–144, Mar 2013.

[58] H. ElSawy, E. Hossain, and M. Haenggi, "Stochastic geometry for modeling, analysis, and design of multi-tier and cognitive cellular wireless networks: A survey," *IEEE Communications Surveys & Tutorials*, vol. 15, pp. 996–1019, March 2013.

[59] S. Chaudhari, J. Hu, B. Daneshrad, and J. Chen, "Performance comparison between MIMO and SISO based on indoor field measurements," *CoRR*, vol. abs/1408.6587, 2014.

[60] S. C. Lam, R. Heidary, and K. Sandrasegaran, "A closed-form expression for coverage probability of random cellular network in composite Rayleigh-lognormal fading channels," in *International Telecommunication Networks and Applications Conference*, pp. 161–165, Nov 2015.

[61] Y. Wu, M. McKay, and R. Heath, "Coverage and area spectral efficiency in downlink random cellular networks with channel estimation error," in *IEEE International Conference on Acoustics, Speech and Signal Processing*, pp. 4404–4408, May 2013.

[62] A. Behnad, H. Purmehdi, and F. Lahouti, "Probability of outage in a clustered Poisson field of interfering nodes," in *IEEE 17th International Conference on Telecommunications*, pp. 784–789, Apr 2010.

[63] K. Hosseini, W. Yu, and R. Adve, "Modeling and analysis of ergodic capacity in network MIMO systems," in *IEEE Globecom Workshops*, pp. 808–814, Dec 2014.

[64] S. T. Veetil, K. Kuchi, A. K. Krishnaswamy, and R. K. Ganti, "Coverage and rate in cellular networks with multi-user spatial multiplexing," in *IEEE International Conference on Communications*, pp. 5855–5859, June 2013.

[65] C. Li, J. Zhang, J. G. Andrews, and K. B. Letaief, "Success probability and area spectral efficiency in multiuser MIMO HetNets," *IEEE Transactions on Communications*, vol. 64, pp. 1544–1556, April 2016.

[66] N. Deng, W. Zhou, and M. Haenggi, "A heterogeneous cellular network model with inter-tier dependence," in *IEEE Global Communications Conference (GLOBECOM)*, pp. 1522–1527, Dec 2014.

[67] T. E. Bogale and L. B. Le, "Massive MIMO and mmWave for 5G wireless HetNet: Potential benefits and challenges," *IEEE Vehicular Technology Magazine*, vol. 11, pp. 64–75, March 2016.

[68] H. S. Dhillon, R. K. Ganti, F. Baccelli, and J. G. Andrews, "Modeling and analysis of K-tier downlink heterogeneous cellular networks," *IEEE Journal on Selected Areas in Communications*, vol. 30, pp. 550–560, April 2012.

[69] Y. S. Soh, T. Quek, M. Kountouris, and H. Shin, "Energy efficient heterogeneous cellular networks," *IEEE Journal on Selected Areas in Communications*, vol. 31, pp. 840–850, May 2013.

[70] Z. Hasan, H. Boostanimehr, and V. Bhargava, "Green cellular networks: A survey, some research issues and challenges," *IEEE Communications Surveys & Tutorials*, vol. 13, pp. 524–540, Fourth 2011.

[71] M. Haenggi, *Stochastic Geometry for Wireless Networks*. Cambridge University Press, 2013.

[72] I. Boukhedimi, A. Kammoun, and M. S. Alouini, "Performance analysis of coordination strategies in two-tier heterogeneous networks," in *IEEE 17th International Workshop on Signal Processing Advances in Wireless Communications (SPAWC)*, pp. 1–6, July 2016.

[73] Y. Kwon, T. Hwang, and X. Wang, "Energy-efficient transmit power control for multi-tier MIMO HetNets," *IEEE Journal on Selected Areas in Communications*, vol. 33, pp. 2070–2086, Oct 2015.

[74] H. H. Yang, G. Geraci, and T. Q. S. Quek, "Energy-efficient design of MIMO heterogeneous networks with wireless backhaul," *IEEE Transactions on Wireless Communications*, vol. 15, pp. 4914–4927, July 2016.

[75] T. Zhang, J. Zhao, L. An, and D. Liu, "Energy efficiency of base station deployment in ultra dense HetNets: A stochastic geometry analysis," *IEEE Wireless Communications Letters*, vol. 5, pp. 184–187, April 2016.

[76] A. R. Khamesi, B. Yang, X. Ge, and M. Zorzi, "Energy and spatial spectral efficiency analysis of random MIMO cellular networks," in *22nd European Wireless Conference*, May 2016.

[77] D. Stoyan, W. S. Kendall, and J. Mecke, *Stochastic geometry and its applications*. 2nd ed., John Wiley and Sons, 1996.

[78] I. S. Gradshteyn and I. M. Ryzhik, *Table of integrals, series, and products*. Elsevier/Academic Press, seventh ed., 2007.

[79] A. Thornburg and R. Heath, "Ergodic capacity in mmWave ad hoc network with imperfect beam alignment," in *IEEE Military Communications Conference (MILCOM)*, pp. 1479–1484, Oct 2015.

[80] M. Aldosari and K. Hamdi, "Trade-off between energy and area spectral efficiencies of cell zooming and BSs cooperation," in *5th International Conference on Intelligent and Advanced Systems (ICIAS)*, pp. 1–6, June 2014.

[81] K. Hosseini, W. Yu, and R. S. Adve, "A stochastic analysis of network MIMO systems," *IEEE Transactions on Signal Processing*, vol. 64, pp. 4113–4126, Aug 2016.

[82] G. George, R. K. Mungara, A. Lozano, and M. Haenggi, "Ergodic spectral efficiency in MIMO cellular networks," *IEEE Transactions on Wireless Communications*, vol. 16, pp. 2835–2849, May 2017.

[83] K. A. Hamdi, "Capacity of MRC on correlated Rician fading channels," *IEEE Transactions on Communications*, vol. 56, pp. 708–711, May 2008.

[84] S. Luo, R. Zhang, and T. J. Lim, "Optimal power and range adaptation for green broadcasting," *IEEE Transactions on Wireless Communications*, vol. 12, pp. 4592–4603, September 2013.

[85] V. Prithiviraj, S. B. Venkatraman, and R. Vijayasarathi, "Cell zooming for energy efficient wireless cellular network," *Journal of Green Engineering*, vol. 3, no. 4, pp. 421–434, 2013.

[86] K. C. Tun and K. Kunavut, "Green cellular networks: A survey, some research issues and challenges," *KMUTNB: International Journal of Applied Science and Technology*, vol. 7, pp. 1–13, July 2014.

[87] R. Balasubramaniam, S. Nagaraj, M. Sarkar, C. Paolini, and P. Khaitan, "Cell zooming for power efficient base station operation," in *9th International Wireless Communications and Mobile Computing Conference (IWCMC)*, pp. 556–560, July 2013.

[88] D. Zhang, K. Yu, Z. Zhou, and T. Sato, "Energy efficiency scheme with cellular partition zooming for massive MIMO systems," in *IEEE Twelfth International Symposium on Autonomous Decentralized Systems (ISADS)*, pp. 266–271, March 2015.

[89] J. Y. Kim, J. Kim, and C. S. Kang, "A novel BS power saving scheme with virtual coverage management for green heterogeneous LTE networks," in *2015 International Conference on Computing and Network Communications (CoCoNet)*, pp. 886–891, Dec 2015.

[90] R. W. Heath, M. Kountouris, and T. Bai, "Modeling heterogeneous network interference using Poisson point processes," *IEEE Transactions on Signal Processing*, vol. 61, pp. 4114–4126, Aug 2013.

[91] M.-S. Alouini and A. Goldsmith, "Area spectral efficiency of cellular mobile radio systems," *IEEE Transactions on Vehicular Technology*, vol. 48, pp. 1047–1066, Jul 1999.

[92] G. Auer, V. Giannini, C. Desset, I. Godor, P. Skillermark, M. Olsson, M. A. Imran, D. Sabella, M. J. Gonzalez, O. Blume, and A. Fehske, "How much energy is needed to run a wireless network?," *IEEE Wireless Communications*, vol. 18, pp. 40–49, October 2011.

[93] S. Ulukus, A. Yener, E. Erkip, O. Simeone, M. Zorzi, P. Grover, and K. Huang, "Energy harvesting wireless communications: A review of recent advances," *IEEE Journal on Selected Areas in Communications*, vol. 33, pp. 360–381, March 2015.

[94] A. Ghazanfari, H. Tabassum, and E. Hossain, "Ambient RF energy harvesting in ultra-dense small cell networks: performance and tradeoffs," *IEEE Wireless Communications*, vol. 23, pp. 38–45, April 2016.

[95] G. Piro, M. Miozzo, G. Forte, N. Baldo, L. A. Grieco, G. Boggia, and P. Dini, "HetNets powered by renewable energy sources: Sustainable next-generation cellular networks," *IEEE Internet Computing*, vol. 17, pp. 32–39, Jan 2013.

[96] "Centre for White Space Communications, University of Strathclyde Glasgow, "WindFi"."

[97] A. R. Khamesi and M. Zorzi, "Energy and area spectral efficiency of cell zooming in random cellular network," in *IEEE Global Communications Conference (GLOBECOM)*, Dec 2016.

[98] O. Ozel, K. Tutuncuoglu, J. Yang, S. Ulukus, and A. Yener, "Transmission with energy harvesting nodes in fading wireless channels: Optimal policies," *IEEE Journal on Selected Areas in Communications*, vol. 29, pp. 1732–1743, September 2011.

[99] I. Humar, X. Ge, L. Xiang, M. Jo, M. Chen, and J. Zhang, "Rethinking energy efficiency models of cellular networks with embodied energy," *IEEE Network*, vol. 25, pp. 40–49, March 2011.

[100] V. Cadambe and S. Jafar, "Interference alignment and degrees of freedom of the K -user interference channel," *IEEE Transactions on Information Theory*, vol. 54, no. 8, pp. 3425–3441, 2008.

[101] F. L. Blasco, F. Rossetto, and G. Bauch, "Time interference alignment via delay offset for long delay networks," *IEEE Transactions on Communications*, vol. 62, pp. 590–599, February 2014.

[102] N. Zhao, F. R. Yu, M. Jin, Q. Yan, and V. C. M. Leung, "Interference alignment and its applications: A survey, research issues and challenges," *IEEE Communications Surveys Tutorials*, vol. PP, no. 99, pp. 1–1, 2016.

[103] B. Nazer, M. Gastpar, S. Jafar, and S. Vishwanath, "Ergodic interference alignment," *IEEE Transactions on Information Theory*, vol. 58, no. 10, pp. 6355–6371, 2012.

[104] H. Farhadi, C. Wang, and M. Skoglund, "Ergodic interference alignment with limited feedback: Power control and rate adaptation," *IEEE Transactions on Wireless Communications*, vol. 14, pp. 6679–6694, Dec 2015.

[105] C. M. Yetis, J. Fanjul, J. A. Garcia-Naya, N. N. Moghadam, and H. Farhadi, "Interference alignment testbeds," *IEEE Communications Magazine*, vol. 55, pp. 120–126, OCTOBER 2017.

[106] O. Johnson, M. Aldridge, and R. Piechocki, "Delay-rate tradeoff in ergodic interference alignment," in *IEEE International Symposium on Information Theory Proceedings (ISIT)*, pp. 2626–2630, July 2012.

[107] J. Koo, W. Wu, and J. Gill, "Delay-rate tradeoff for ergodic interference alignment in the gaussian case," in *48th Annual Allerton Conference on Communication, Control, and Computing*, pp. 1069–1075, 2010.

[108] A. R. Khamesi, F. Lahouti, and M. Zorzi, "Optimum delay-rate tradeoff in ergodic interference alignment," in *Telecommunications (IST), 2014 7th International Symposium on*, pp. 1233–1238, Sept 2014.